

ANALYSIS OF ANCIENT STORM DEPOSITS ALONG COASTAL AREAS OF ANDAMAN SEA,
THAILAND AND COASTAL AREAS OF SOUTH CHINA SEA, VIETNAM



A Dissertation Submitted in Partial Fulfillment of the Requirements
for the Degree of Doctor of Philosophy in Geology

Department of Geology

FACULTY OF SCIENCE

Chulalongkorn University

Academic Year 2021

Copyright of Chulalongkorn University

การวิเคราะห์ตะกอนพายุโบราณตามแนวชายฝั่งทะเลอันดามันของประเทศไทยและชายฝั่งทะเลจีนใต้
ของประเทศเวียดนาม



วิทยานิพนธ์นี้เป็นส่วนหนึ่งของการศึกษาตามหลักสูตรปริญญาวิทยาศาสตรดุษฎีบัณฑิต
สาขาวิชาธรณีวิทยา ภาควิชาธรณีวิทยา
คณะวิทยาศาสตร์ จุฬาลงกรณ์มหาวิทยาลัย
ปีการศึกษา 2564
ลิขสิทธิ์ของจุฬาลงกรณ์มหาวิทยาลัย

Thesis Title ANALYSIS OF ANCIENT STORM DEPOSITS ALONG
COASTAL AREAS OF ANDAMAN SEA, THAILAND AND
COASTAL AREAS OF SOUTH CHINA SEA, VIETNAM

By Mr. Stapana Kongsen

Field of Study Geology

Thesis Advisor Professor MONTRI CHOOWONG, Ph.D.

Thesis Co Advisor Sumet Phantuwongraj, Ph.D.

Accepted by the FACULTY OF SCIENCE, Chulalongkorn University in Partial
Fulfillment of the Requirement for the Doctor of Philosophy

----- Dean of the FACULTY OF SCIENCE
(Professor POLKIT SANGVANICH, Ph.D.)

DISSERTATION COMMITTEE

----- Chairman
(Professor Punya Charusiri, Ph.D.)

----- Thesis Advisor
(Professor MONTRI CHOOWONG, Ph.D.)

----- Thesis Co-Advisor
(Sumet Phantuwongraj, Ph.D.)

----- Examiner
(Professor SANTI PAILOPLEE, Ph.D.)

----- Examiner
(Assistant Professor VICHAI CHUTAKOSITKANON, Ph.D.)

----- External Examiner
(Parisa Nimnate, Ph.D.)

สถาปนา กองเซ็น : การวิเคราะห์ตะกอนพายุโบราณตามแนวชายฝั่งทะเลอันดามันของประเทศไทยและชายฝั่งทะเลจีนใต้ของประเทศเวียดนาม. (ANALYSIS OF ANCIENT STORM DEPOSITS ALONG COASTAL AREAS OF ANDAMAN SEA, THAILAND AND COASTAL AREAS OF SOUTH CHINA SEA, VIETNAM) อ.ที่ปรึกษาหลัก : ศ. ดร.มนตรี ชูวงศ์, อ.ที่ปรึกษาร่วม : อ. ดร.สุเมธ พันธุ์วงศ์ราช

ความถี่ของเหตุการณ์พายุและสึนามิที่มีความรุนแรงสูงมีความสำคัญต่อเรื่องความเปราะบางของภัยพิบัติต่อชุมชนทางด้านชายฝั่ง การระบุและการหาอายุจากหลักฐานทางตะกอนที่สะสมตัวโดยเหตุการณ์เหล่านี้สามารถช่วยในการวางแผนและการกำหนดมาตรการการป้องกันที่เหมาะสมต่อชุมชนชายฝั่งได้ ชายฝั่งทะเลอันดามันของประเทศไทยนั้นเสี่ยงต่อเหตุการณ์เหล่านี้จากการที่เคยเกิดคลื่นสึนามิในมหาสมุทรอินเดียปี 2557 และชายฝั่งทะเลจีนใต้ของประเทศเวียดนามได้รับความเสียหายที่รุนแรงของเหตุการณ์พายุในอดีต ในการศึกษาที่ผู้วิจัยได้ศึกษาตะกอนที่เกิดจากเหตุการณ์ที่มีความรุนแรงสูงในอดีตสองพื้นที่ ได้แก่ พื้นที่ชายฝั่งทะเลอันดามันของประเทศไทย คืออุทยานแห่งชาติแหลมสน จังหวัดระนอง และพื้นที่ชายฝั่งทะเลจีนใต้ของประเทศเวียดนาม คือ Hoa Duan จากจังหวัด Thua Thein Hue

ผลการศึกษาพบว่าในพื้นที่ชายฝั่งแหลมสนของประเทศไทยมีชั้นตะกอนที่เกิดจากเหตุการณ์ที่มีความรุนแรงสูงสองชั้นตะกอน ได้แก่ ชั้นตะกอนจากเหตุการณ์สึนามิในปี 2557 และชั้นตะกอนพายุที่เกิดขึ้นมาแล้วมากกว่า 350 ปีที่แล้ว สำหรับพื้นที่ชายฝั่งของ Hoa Duan มีชั้นตะกอนที่เกิดจากเหตุการณ์ที่มีความรุนแรงสูงห้าชั้นตะกอนซึ่งเป็นของชั้นตะกอนพายุสามชั้น และชั้นตะกอนน้ำท่วมสองชั้น โดยพบว่าชั้นตะกอนพายุสองชั้นและชั้นตะกอนน้ำท่วมหนึ่งชั้นเคยเกิดขึ้นในระหว่าง 130 ± 10 ปีที่แล้วถึงปัจจุบัน นอกจากนี้ยังพบว่าชั้นตะกอนพายุสองชั้นและชั้นตะกอนน้ำท่วมหนึ่งชั้นเกิดขึ้นในช่วงอายุที่มากกว่า 130 ± 10 ปีที่แล้ว

สาขาวิชา ธรณีวิทยา

ปีการศึกษา 2564

ลายมือชื่อนิสิต

ลายมือชื่อ อ.ที่ปรึกษาหลัก

ลายมือชื่อ อ.ที่ปรึกษาร่วม

6072889123 : MAJOR GEOLOGY

KEYWORD: STORM DEPOSIT, FLUVIAL FLOOD DEPOSIT, OSL DATING, BARRIER ISLAND, VIETNAM, 2004 INDIAN OCEAN TSUNAMI, ANDAMAN SEA THAILAND

Stapana Kongsen : ANALYSIS OF ANCIENT STORM DEPOSITS ALONG COASTAL AREAS OF ANDAMAN SEA, THAILAND AND COASTAL AREAS OF SOUTH CHINA SEA, VIETNAM. Advisor: Prof. MONTRI CHOOWONG, Ph.D. Co-advisor: Sumet Phantuwongraj, Ph.D.

The frequency of high energy storm and tsunami events is crucial for apprehending the vulnerability of coastal communities. Identifying and dating sedimentary evidence deposited by such high energy events can assist in the planning and installation of suitable protection measurements. The Andaman Sea coast of Thailand is particularly vulnerable to such events as illustrated by the 2004 Indian Ocean Tsunami (2004 IOT) and the South China Sea coast of Vietnam has been experienced from the past severe storm event. Here, the authors study the high energy sediments. The selected area of Andaman Sea coast Thailand is Laem Son National park, while the South China Sea coast of Vietnam is located in Hoa Duan, Thua Thein Hue.

The results indicate that in Laem Son area, two high energy sediment layers are discovered including the 2004 IOT layer and a storm layer. The depositional age of the storm event occurred more than 350 years ago. For Hoa Duan coastal area, six layers of high energy events belonged to storm and fluvial flood layers were discovered. Two layers of storm event and one layer of fluvial flood event occurred during 130 ± 10 years ago and two layers of storm event and one layer of fluvial flood event occurred more than 130 ± 10 years ago.

Field of Study: Geology

Academic Year: 2021

Student's Signature

Advisor's Signature

Co-advisor's Signature

ACKNOWLEDGEMENTS

The Royal Golden Jubilee Ph.D program (Grant No. PHD/0198/2560), (3.G.CU/60/B.1) supported SK financially. MESA Research Unit of the Department of Geology, Faculty of Science, Chulalongkorn University and the Institute of Earth and Environmental Sciences, University of Freiburg, Germany are acknowledged for logistics and laboratory works.

Special thanks also go to Professor Dr. Frank Preusser, Dr. Johannes Miocic, Dr. Sakonvan Chawchai for the constructive comments and grain size analysis. Alexander Füllung and Jenny Wolff are also thanked for support with the sample preparation and measurements.

Additionally, my special thankfulness goes to all friends, brothers and sisters who assisted me in the field investigation, especially Dr. Nikhom Chaiwongsean, Dr. Doan Thi Anh Vu, Dinh Quoc Tuan and Supawich Fuengfu for fieldwork throughout the coastline of Vietnam, and Supawich Fuengfu, Apivut Veeravinantanakul, Sirawat Udomsak, Chanista Chansom, Chanakan Ketthong and Peerasit Surakiatchai for fieldwork along the Andaman Sea coast.



จุฬาลงกรณ์มหาวิทยาลัย
CHULALONGKORN UNIVERSITY

Stapana Kongsan

TABLE OF CONTENTS

	Page
.....	iii
ABSTRACT (THAI)	iii
.....	iv
ABSTRACT (ENGLISH)	iv
ACKNOWLEDGEMENTS	v
TABLE OF CONTENTS	vi
LIST OF TABLES	ix
LIST OF FIGURES.....	xi
CHAPTER 1 INTRODUCTION	1
1.1 Rationale.....	1
1.2 Objectives.....	3
1.3 Scope and limitation	3
1.4 Outputs.....	3
CHAPTER 2 LITERATURE REVIEWS	4
2.1 Paleotempestology.....	4
2.2 Background of the study areas	6
2.2.1 Thailand	6
2.2.2 Vietnam.....	12
CHAPTER 3 METHODOLOGY	21
3.1 Pre-fieldwork.....	21
3.2 Fieldwork.....	21

3.2.1 Topographic survey and stratigraphy.....	21
3.2.1.1 Laem Son area.....	21
3.2.1.2 Hoa Duan, Thua Thien Hue, central Vietnam	23
3.2.2 Sedimentology and loss on ignition	24
3.2.3 Optically stimulated luminescence dating.....	27
3.2.3.1 Laem Son area.....	27
3.2.3.2 Hoa Duan, Thua Thien Hue, central Vietnam	28
CHAPTER 4 RESULTS	31
4.1 Laem Son area, Ranong, Thailand	31
4.1.1 Sediment characteristics of modern beach deposits and monsoon-driven storm surges sediments.....	31
4.1.2 Sedimentological characteristics of each unit.....	34
4.1.3 Comparison on grain size distribution curves.....	45
4.1.4 Optically stimulated luminescence dating.....	46
4.2 Hoa Duan area, Thua Thien Hue, central Vietnam	47
4.2.1 Sediment characteristics of modern beach deposits	49
4.2.2 Sedimentological characteristics of each unit.....	52
4.2.3 Comparison on grain size distribution curves.....	63
4.2.4 Optically stimulated luminescence dating.....	65
CHAPTER 5 DISCUSSION.....	67
5.1 Laem Son National Park, Ranong Thailand.....	67
5.1.1 Diagnostic key to identify monsoon sediments	67
5.1.2 Diagnostic key to identify a normal condition sediment deposit.....	68
5.1.3 Diagnostic key to identify high energy event sediments	71

5.1.4 Environmental reconstruction	74
5.1.5 The 2004 Indian Ocean Tsunami deposits	76
5.1.6 Grain size distribution parameters and flow energy	80
5.2 Hoa Duan area, Thua Thien Hue, central Vietnam	82
5.2.1 Identification of storm deposits	82
5.2.2 Identification of fluvial flood deposits	85
5.2.3 Flow behavior of the storm and fluvial flood deposits.....	89
5.2.4 Relevance of grain size parameter for classification.....	94
5.2.5 Age of depositional events	97
5.2.6 Dynamic and evolution of the Hoa Duan sand barrier	98
5.3 Comparison between the sedimentary characteristics of storms in Laem Son, Thailand and Hoa Duan, Vietnam.....	103
5.4 The difference of K, Th and U from OSL dating.....	105
CHAPTER 6 CONCLUSION.....	107
REFERENCES.....	112
VITA	136

LIST OF TABLES

	Page
Table 1 Range of sediment composition grain properties of the six identified units as well as the recent beach and monsoon sediments. MMS, monsoon-driven storm surges; 2004 IOT, 2004 Indian Ocean Tsunami; OSB, old surface before Indian Ocean Tsunami; UBS, upper surface sediment; UFS, upper foreshore sediment.....	32
Table 2 Range of grain size distribution parameters, sedimentary structures and marine fossil and microfossil for each stratigraphic unit. MMS, monsoon-driven storm surges; 2004 IOT, 2004 Indian Ocean Tsunami; OSB, old surface before Indian Ocean Tsunami; UBS, upper surface sediment; UFS, upper foreshore sediment.....	36
Table 3 Summary of the results of OSL dating in Laem Son area with the concentration of a dose-relevant element (K, Th, and U), measured sediment moisture, the total dose rate (D), observed overdispersion (od), the applied age model (CAM = central age model; MAM = minimum age model), mean De, and resulting OSL age.	46
Table 4 The values of sediment composition, grain properties, LOI, sphericity and roundness of various sediments (Kongsen et al., 2021b).	50
Table 5 The values of grain size distribution parameters and sedimentary structures for each stratigraphic unit (Kongsen et al., 2021b).	56
Table 6 Summary data of OSL dating in the Hoa Duan area with the concentration of dose-relevant elements (K, Th, and U), measured sediment moisture, total dose rate (D), observed overdispersion, the applied age model (CAM = central age model; MAM = minimum age model), mean De, and resulting age (Kongsen et al., 2021b).	65
Table 7 Lists of tropical storm and typhoon tracks occurred chronologically in central Vietnam during 1951 to 2019 (Kongsen et al., 2021b).	102

Table 8 Comparison of and the sedimentary characteristics of the storm sediments discovered from the area of Laem Son, Thailand and the area of Hoa Duan, Vietnam.

..... 105



LIST OF FIGURES

	Page
Figure 1 The study area at Laem Son National Park, Ranong Province, southern Thailand. (A) Map showing the overview of the southern peninsula, Thailand flanked by the Andaman Sea and the Gulf of Thailand. The study area is indicated by the black star. (B) and (C) Orthophotograph of the ridges and swales in the study site showing the locations of the previous work, the transect lines, the positions of the cores as well as sampling points for recent beach samples and location of OSL samples.	7
Figure 2 The study site at Hoa Duan, Thua Thein Hua, Central Vietnam. (A) Vietnam with tracks of major tropical storms and typhoons from 1952 to 2019, which mostly moved from east to west. Note that the tracks of tropical storms and typhoons are listed only for those in central Vietnam and are presented in Supplementary Table 2. (B) A geomorphological map of the study site showing the sand barriers, lagoons, alluvial plains, Thuan An inlet, and old Hoa Duan inlet (which was permanently closed), and (C) a close-up satellite image from Google Earth of the Hoa Duan barrier showing the sampling points of core samples, OSL dating, and recent shore-normal beach samples (Kongsen et al., 2021b).	13
Figure 3 Laem Son area, (A) the traces of the washover sedimentation and a derelict building on the beach zone by the monsoon. (B) The traces of the washover sediments and saltwater penetrated inland by the monsoon. (C) Three transects perpendicular to the shoreline where the 2004 IOT propagated and the positions of core and OSL samples. All photographs were taken on May 18, 2019. (D) and (E) Cross-sections of Laem Son area showing the detailed topography from west to east. Transect 1 with positions of core 1, 2, 3 and 4 and OSL samples (a yellow circle) of D1-1, D1-2, D1-3, D2-1, D2-2, D3-1 and D3-2, and transect 3 with the positions of core 7, 8, 9 and 10 and OSL samples of D4-1, D4-2, D5 and D6.	22

Figure 4 Hoa Duan barrier. (A, B) Beach scarps and derelict buildings resulting from wave erosion during the typhoon season that indicated the maximum wave height during the typhoon season. (C) A local villager showing a water mark level of the flood in November 1999 (2 m). (D) The VN1 and ST4 sampling points in the low topography of the Hoa Duan barrier. (E) Cross-section of Hoa Duan, measured using a total station survey camera, coupled with core locations with depth and the OSL ages (a yellow circle). A dashed red line indicates the water level of the flood in November 1999 that inundated this area (2-m depth). The OSL dating of STA4, STA5, and STA6 indicated the depositional ages as modern, modern, and 130 ± 10 years, respectively. The modern age means less than 100 years. The correlations are presented in detail in Figure 12. All photos were taken on January 12, 2019 (Kongsen et al., 2021b).....26

Figure 5 Detailed topography of Laem Son area in transect 1 showing the interpreted stratigraphy of cores 1, 2, 3 and 4. The OSL dating (a yellow circle) of D1-1, D1-2, D1-3, D2-1, D2-2, D3-1 and D3-2 indicated the depositional ages as 40 ± 5 yr, 105 ± 5 yr and 140 ± 10 yr, 235 ± 15 yr and 255 ± 10 yr, 35 ± 10 yr and 260 ± 10 yr, respectively. MMS, monsoon-driven storm surges; 2004 IOT, 2004 Indian Ocean Tsunami; OSB, old surface before Indian Ocean Tsunami; UBS, upper backshore sediment; UFS, upper foreshore sediment.33

Figure 6 Detailed topography of Laem Son area in transect 3 showing the interpreted stratigraphy of cores 7, 8, 9 and 10. The OSL dating (a yellow circle) of D4-1, D4-2, D5, D6 and D7 indicated the depositional ages as 110 ± 10 yr, 135 ± 10 yr, 295 ± 15 yr, 305 ± 15 yr and 340 ± 20 yr, respectively. 2004 IOT, 2004 Indian Ocean Tsunami; OSB, old surface before Indian Ocean Tsunami; UBS, upper backshore sediment; UFS, upper foreshore sediment.....34

Figure 7 Close-up of the six sedimentary units from cores 1, 2, 3 and 4. In core 1, monsoon sediments are identified at 4 to 62 cm depth and are characterized by grey to orange sand with slight lamination. In core 2, Unit II is identified at 0 to 29 cm depth which is characterized as dark brown to orange sand. The erosional lower contact of Unit II with Unit III in core 2 is recognized at 29 cm depth. In core 3, Unit IV

is identified at 4 to 50 cm depth and contain gradational lower contact with Unit V. In Unit V of core 3, the concretion and crab remain (*Ocypode ceratophthalmus*) are observed. In core 4, Unit VI is observed at 101 to 157 cm depth which is characterized as brown to grey sand with lamination at 123 to 133 cm depth and shell fragment layer at 149 to 157 cm depth. MMS, monsoon-driven storm surges; 2004 IOT, 2004 Indian Ocean Tsunami; OSB, old surface before Indian Ocean Tsunami; UBS, upper backshore sediment; UFS, upper foreshore sediment.37

Figure 8 Close-up of the detailed sedimentary characteristics from cores 7, 8, 9 and 10. In core 7, Unit I is classified at 0 to 6 cm depth and are characterized as brown sand overlying Unit IV. In core 8, Unit II is identified at 4 to 14 cm depth which is characterized as dark brown sand with the erosional lower contact overlying the Unit IV. In core 9, Unit II is identified is observed at 3 to 15 cm depth and is characterized as black sand overlying the darker sand layer of Unit III in range of 15 to 19 cm depth. The lamination of Unit II in core 9 is recognized at 4 to 10 cm depth and the erosional lower contact with Unit III is recognized at 15 cm depth. In core 10, Unit V is identified at 103 to 115 cm depth which contain the erosional top contact with Unit IV at 103 cm depth and the sharp erosional lower contact with Unit VI at 115 cm depth. Unit VI in core 10 is observed at 115 to 150 cm depth which contain shell fragmented and lamination at 115 to 121 cm depth. 2004 IOT, 2004 Indian Ocean Tsunami; OSB, old surface before Indian Ocean Tsunami; UBS, upper backshore sediment; UFS, upper foreshore sediment.....38

Figure 9 Stratigraphic sequence, grain size distribution and composition data of cores of transect 1. The MMS sediments are identified in core 1. The topsoil layer (Unit I) is recognized in cores 1, 3 and 4. The IOT 2004 layer (Unit II) is identified in cores 2 and 4. The OSB 2004 IOT layer (Unit III) is observed in cores 2 and 4. The UBS layer (Unit III) is recognized in cores 2, 3 and 4. The UFS layer (Unit V) is recognized in cores 2, 3 and 4. The storm layer is identified in cores 2, 3 and 4. MMS, monsoon-driven storm surges; 2004 IOT, 2004 Indian Ocean Tsunami; OSB, old surface before Indian Ocean Tsunami; UBS, upper backshore sediment; UFS, upper foreshore sediment.41

Figure 10 Stratigraphic sequence, grain size distribution and composition data of cores of transect 3. (A) core 7, (B) core 8, (C) core 9 and (D) core 10. The topsoil layer (Unit I) is recognized in cores 7, 8, 9 and 10. The IOT 2004 layer (Unit II) is identified in cores 8, 9 and 10. The OSB 2004 IOT (Unit III) is observed in cores 9 and 10. The UBS layer (Unit III) is recognized in cores 7, 8, 9 and 10. The UFS layer (Unit V) is recognized in cores 8, 9 and 10. The storm layer is identified in cores 7, 9 and 10. 2004 IOT, 2004 Indian Ocean Tsunami; OSB, old surface before Indian Ocean Tsunami; UBS, upper backshore sediment; UFS, upper foreshore sediment.....43

Figure 11 Comparison on grain size distribution curves of the recent beach sediments and various sediments from the study area. (A) Recent beach sediment (n=4) and MSS sediments (n=58), (B) Recent beach sediment (n=4) and Unit I: topsoil sediments (n=29), (C) Recent beach sediment (n=4) and Unit II: 2004 IOT sediments (n=86), (D) Recent beach sediment (n=4) and Unit III: OSB 2004 IOT sediments (n=20), (E) Recent beach sediment (n=4) and Unit IV: UBS (n=458), (F) UFS (n=4) and Unit V: paleo-beach sediments(n=172), (G) Recent beach sediment (n=4) and Unit VI: storm sediments (n=169). Grain size distributions of the monsoon sediments, Unit IV, V, and VI are similar to the distribution of grain sizes at the present day beach. In contrast, the grain size distribution of Unit I and II show a shift towards coarser grain sizes. MMS, monsoon-driven storm surges; 2004 IOT, 2004 Indian Ocean Tsunami; OSB, old surface before Indian Ocean Tsunami; UBS, upper backshore sediment; UFS, upper foreshore sediment.....44

Figure 12 Cores VN1, VN2, and VN3 and pits of VN1, VN2. and VN3 represent the units of deposition between the storm and fluvial flood layers with the dominant sedimentary structures. Units II, IV, VI, and VII, which were considered to be the storm layers, mostly contained sharp basal contact and inclined and parallel lamination, whereas Units III and V, classified as the fluvial flood layers, were characterized as a mud grain layer with sharp, erosional top, and bottom contacts. The absence of the fluvial flood layer (Unit III) in core VN2 and Pit VN2 resulted from the erosion of the storm event in Unit II. Note that the distance interval of each core is 50 m, and the elevation of cores is based on the topographic elevation. A yellow circle in Pit 1, Pit

2, and Pit 3 indicates the OSL ages, whereas the modern age in Pit 1 and Pit 2 means less than 100 years (Kongsen et al., 2021b).....48

Figure 13 Stratigraphy of core VN1 with vertically plotted grain size parameters (mean, sorting, skewness, and kurtosis) and LOI (organic and carbonate contents) showing the unit of the storm and fluvial flood layers. Storm layers in Units II, IV, and VI mostly exhibited the set of normal and reverse grading with relatively low organic and carbonate contents, whereas the fluvial flood layer of Units III and V showed high organic and carbonate contents at 33-41-cm and 67-84-cm depths, respectively (Kongsen et al., 2021b).....51

Figure 14 Stratigraphy of core VN2 with vertically plotted grain size parameters (mean, sorting, skewness, and kurtosis) and LOI (organic and carbonate contents) showing the unit of the storm and fluvial flood layers. Storm layers in Units II, IV, VI, and VII mostly exhibited the set of normal and reverse grading with relatively low organic and carbonate contents, whereas Unit V was interpreted as the fluvial flood layer and showed high organic and carbonate contents at a 110-127-cm depth (Kongsen et al., 2021b).....53

Figure 15 Stratigraphy of core VN3 with vertically plotted grain size parameters (mean, sorting, skewness, and kurtosis) and LOI (organic and carbonate content) showing the unit of the storm and fluvial flood layers. Storm layers in Units II, IV, VI, and VII mostly exhibited the sets of normal and reverse grading with relatively low organic and carbonate contents, whereas the fluvial flood layer of Units III and V showed high organic and carbonate contents at 32-34-cm and 123-130-cm depths, respectively (Kongsen et al., 2021b).58

Figure 16 Close-up of the internal sedimentary structures of storm deposits and fluvial flood deposits from cores VN1, VN2, and VN3. In core VN1, a dark-brown mud layer with basal sharp contact was observed at 41-cm depth and parallel lamination of medium-fine sand with fragmented shells at 42-57-cm depth. In core VN2, a light-gray mud layer with basal sharp contact at 127-cm depth was deposited on a very fine sand layer. Then, medium sand with a sharp erosional top contact with a very

fine sand layer was observed at a 133-cm depth. In core VN3, very-fine-to-medium sand with basal sharp contact and parallel lamination was observed at 115-118-cm depth plus an mud rip-up clast at 121-cm depth, and then a light-gray mud with basal sharp contact deposited on a dark-gray color with medium-grained sand (Kongsen et al., 2021b).....60

Figure 17 Plots of the grain size distribution curves of Units I–VII in comparison with the shore-normal beach deposits (b) (location in Figure 2C). The number of grain size distribution curves in each unit is as follows: recent beach (n = 4), Unit I (n = 27), Unit II (n = 97), Unit III (n = 4), Unit IV (n = 177), Unit V (n = 2), Unit VI (n = 69), and Unit VII (n = 94). The characteristic of the grain size distribution of the storm sediments shows curves that are consistent with the curves of the shore-normal recent beach sediments in the range of coarse-to-medium sand, whereas the grain size curves of the fluvial flood sediments are different, being distributed in the range of very-fine sand to silt (Kongsen et al., 2021b).....64

Figure 18 Examples of OSL decay curves for representative aliquots of (A) a modern (ST1) and (B) an older (ST3) sample. This graph shows that the natural signal in the modern sample is too low for proper age determination. The inset displays the dose-response curve of the respective aliquot. Also shown are the dose distribution plots of (C) the modern and (D) the older example. For the latter, the positively skewed spread and high overdispersion of the D_e values call for the application of the Minimum Age Model (Kongsen et al., 2021b).....66

Figure 19 Plotting statistical values of mean grain size vs. (A) sorting, (B) sorting vs. skewness and (C) sorting vs. kurtosis. The number of the sediment samples plotted is as follows: recent beach (n=4), MMS (n=58), Unit I: topsoil (n=29), Unit II: 2004 IOT (n=86), Unit III: OBS 2004 IOT (n=20), Unit IV: UBS (n=458), Unit V: UFS (n=172) and Unit VI: storm (n=169). MMS, monsoon-driven storm surges; 2004 IOT, 2004 Indian Ocean Tsunami; OSB, old surface before Indian Ocean Tsunami; UBS, upper backshore sediment; UFS, upper foreshore sediment.79

Figure 20 Plotting statistical values of the mean grain size versus sorting. The number of sediments plotted is as follows: recent beach (n = 4), Unit I (n = 27), Unit II (n = 97), Unit III (n = 4), Unit IV (n = 177), Unit V (n = 2), Unit VI (n = 69), and Unit VII (n = 94). The dashed line divides the zone of a statistical distribution pattern of beach sediment, storm sediment, and fluvial flood sediment (Kongsen et al., 2021b).94

Figure 21 Plotting statistical values of the mean grain size vs skewness (A), mean grain size vs kurtosis (B), sorting vs skewness (C), sorting vs kurtosis (D), and skewness vs kurtosis (E). The dashed line in (A) and (B) divides the zone of a statistical distribution trend of beach and storm sediment from fluvial flood sediment. Next, the dashed line in (C) divides the zone of a statistical distribution trend of beach sediment, storm sediment, and fluvial flood sediment. Finally, the dashed line in (E) divides the zone of a statistical distribution trend of beach and storm sediment from fluvial sediment (Kongsen et al., 2021b).95

Figure 22 The episodic satellite imageries accessed through the Google Earth Timelapse showing the morphological change of the study area (Hoa Duan barrier) and the adjacent area (Thuan An inlet). (A) the morphology of the study area and Thuan An inlet in 1952 (modified from Lam et al., 2007), (B) The morphology of barrier formation before the flood in November 1999, (C) breaching of the Hoa Duan barrier after the Flood in November 1999 created the large accommodation space of trapping sediment materials from northwestward longshore current, (D), (E) and (F) recovering of Hoa Duan barrier that sand sediments were progressively filled up in 2001, 2002 and 2003, respectively. Red rectangular represents the study area in Hoa Duan barrier (Kongsen et al., 2021b). 101

CHAPTER 1

INTRODUCTION

1.1 Rationale

Coastal storm is one of natural hazards which can be regarded as the catastrophic event and can pose many serious threats to the coastal communities worldwide such as infrastructure, loss of life and properties, economic condition of nation, etc. (McGregor, 1995). At present, globally populated communities along the coastal areas seem to be at risk with respect to global climate variation. Also, the global warming resulting from anthropogenic activity gives rise to not only sea level rise, but also more intensified natural disasters, especially the event of the extreme coastal storm (commonly known as high energy event) such as Cyclone Nargis in 2008, Typhoon Haiyan 2013 in Philippine, Typhoon Lan 2017 in Japan, Hurricane Harvey, Hurricane Irma 2017 in USA and Tropical Storm Pabuk 2019 in Thailand. Over decades, coastal communities along the Andaman Sea and South China Sea have been suffered severely from the cyclone/typhoon events. Such catastrophic events underscore the fact that the coastal storm data are still lacking to assess trends of the future coastal storm occurrence although there has been the advancement in terms of meteorologically instrumental measurement.

Therefore, the necessity of preparation and countermeasures to keep pace with the advent of the future coastal storm should be taken into consideration seriously in places where historical and prehistorical storm sediments were discovered. In order to investigate the sedimentary traces of extreme coastal storm event, paleotempestological science (the study of ancient storm) is applied to this research by using the paleotempestological concept which is associated with several sciences including remote sensing, geomorphology, sedimentology, paleontology, geophysics, geochemistry and reliable dating technique. This concept holds to the principle that while the past typhoon occurred, it generated the unusual high waves (storm surge) directed toward the coastal area on account of its strong wind speed (Kongsen et al., 2021a). Coupled with high tide, the height of storm surges can be greatly increased (also called storm tide). These strong waves can transport and carry the sediments which belong to the specific part of coastal environments onshore such as sea floor, beach, beam and beach ridge. If these sediments deposit landward (also called washover sediments) in such appropriate areas as swale, lowlands and lagoon (Liu, 2007), and then are preserved by normal muddy sedimentation in the low energy condition (silt and clay). These preserved sediments will serve as the important record of historical and prehistorical typhoon event in the area which is beyond the instrumental records in the centennial to millennial scale.

1.2 Objectives

To analyze sedimentological characteristics of ancient storm deposits found along the coastal area of Andaman Sea, Thailand and the coastal area of South China Sea, Vietnam.

To define age determination of ancient storm deposits found along the coastal areas of Andaman Sea, Thailand and the coastal areas of South China Sea, Vietnam.

1.3 Scope and limitation

This research focused on the sedimentological analysis in the ancient washover deposits which were discovered from the coastal areas of the Andaman Sea, Thailand and the coastal areas of the South China Sea, Vietnam. Thus, the representative study site was divided into two main locations. The first location is located at Laem Son National Park, Kapoe, Ranong, southern Thailand and the second is located at Hoa Duan, Thua Thien Hue, central Vietnam.

1.4 Outputs

Based on the assumption above, this research will provide the important evidence of storm occurrence in the past discovered from the coastal area of Andaman Sea, Thailand and the coastal area of South China Sea, Vietnam. Therefore, the output of this research is to better understand various characteristics of the ancient storm deposits such as physical composition, sedimentology, sedimentary structure, stratigraphy, the depositional age of the ancient storm using OSL dating.

CHAPTER 2

LITERATURE REVIEWS

2.1 Paleotempestology

Paleotempestology is an emerging field of science that studies past tropical cyclone activity beyond the period of instrumental observations, typically spanning the last several centuries to five millennia. Tropical cyclones are known by different names in different regions of the world – hurricanes in North America, typhoons in the Northwest Pacific, and cyclones in South Asia and Australia. Here the term hurricane is sometimes used interchangeably with all other types of tropical cyclones (Liu, 2007). The records of tropical cyclone activity both in the United States and other parts of the world are confined to the last 150 years similar to our country (Thailand) last 76 years (Kongsen et al., 2021a). This record is too short to fully capture the occurrence of the rare but most destructive hurricanes – the catastrophic hurricanes of category 4 and 5 intensity based on Saffir-Simpson scale. Therefore, by providing a long-term, empirical record of hurricane activity back to 5,000 years, paleotempestology is useful for revealing the spatial and temporal variability of hurricane activity and deciphering its relationship with global climatic changes. Two main sources of data are available for reconstructing past hurricane activity to beyond the instrumental period – geological proxy records, and historical documentary records. Therefore, the underscore two major approaches to the study

of paleotempestology – geological and archival (Liu, 2007). In terms of geological proxy records, when a hurricane or a typhoon makes landfall, it can severely impact coastal landforms, ecosystems, sedimentary and hydrological processes on the coast. These impacts which left on the coast can be decoded by means of proxy techniques. Many geological and biological proxies are potentially benefit in reconstructing past hurricane or typhoon strike. However, the proxy that has proven the most useful is overwash sand layer deposited in the sediments of coastal lake or marsh (e.g., Liu and Fearn, 1993; Liu, 2007). Overwash sand layer in the coastal lake

During a hurricane or typhoon event, the strong onshore winds, particularly in the forward-right quadrant of the intense low-pressure system, generate storm surges directed towards the coast as foregoing description above. The intense hurricane can cause sand to be eroded from the beach or dunes and then deposited in the lake or marsh behind it. Stratigraphically, the overwash fan will be preserved and formed as sand layer which thickest near the shore and gradually thinner landward (Liu and Fearn, 1993, 2000; Liu, 2004). In a coastal lake that had been subjected to repeated overwash events in the past, the sediment stratigraphy should contain multiple sand layers that contain a stratigraphic record of intense hurricane strikes. These sand layers are composed of very fine to very coarse sand that is usually well-sorted and have abrupt contacts both above and below. Thickness's sand layer may range from a few mm to more than 10 cm. They can be identified either visually or by means of sedimentological techniques such as loss-on-ignition analysis of core samples (Liu

and Fearn, 2000). A chronology of past overwash event or hurricane strikes can be established by means of radiometric dating techniques such as radiocarbon (^{14}C) and thermoluminescence dating. Additionally, lead-210 (^{210}Pb), or cesium-137 (^{137}Cs) dating may be supplemented by using stratigraphic markers such as pollen and lead pollutants. For any particular location, the return period of hurricanes of a specific intensity category can be calculated by tallying up the number of events occurring over a given period of time.

2.2 Background of the study areas

2.2.1 Thailand

Tsunamis and storms are catastrophic events that occur along many coastlines worldwide and pose a serious threat to coastal communities. It was the destructive nature of the M 9.1-9.3 Sumatra-Andaman earthquake which triggered the Indian Ocean Tsunami (IOT) 2004, striking the coastal area in of parts of the Andaman Sea of Thailand, that called for the urgent necessity of countermeasures against such catastrophic events, including the installation of warning signs and warning houses as well as the establishment of evacuation plans. However, since such actions are costly, it is crucial to identify the nature and frequency of past high energy events to allow policymakers of coastal territories to set priorities in the planning and installation of suitable protection measures. One approach to assess the long-term vulnerability of different coastal stretch is identifying and dating sedimentary evidence such as washover sediments left inland by the high energy events.

However, a particular issue is the secure identification and differentiation of the deposition processes behind different types of sediments.

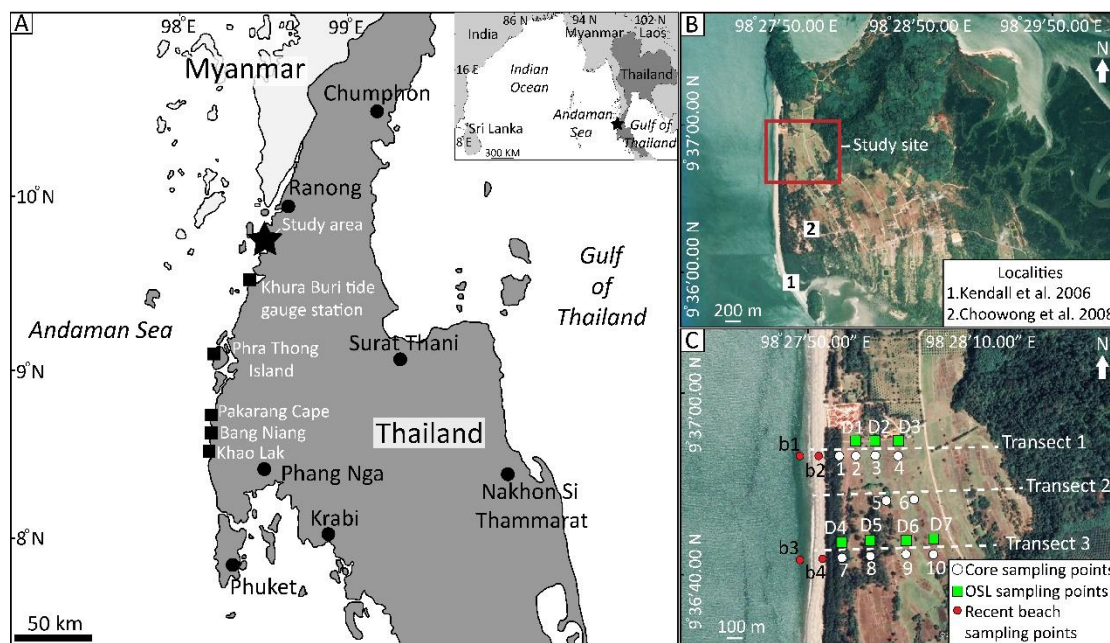


Figure 1 The study area at Laem Son National Park, Ranong Province, southern Thailand. (A) Map showing the overview of the southern peninsula, Thailand flanked by the Andaman Sea and the Gulf of Thailand. The study area is indicated by the black star. (B) and (C) Orthophotograph of the ridges and swales in the study site showing the locations of the previous work, the transect lines, the positions of the cores as well as sampling points for recent beach samples and location of OSL samples.

Globally, numerous studies have focused on describing and distinguishing sedimentological features in storm and tsunami deposits. The similarities of sedimentary characteristics and structures found for both kind of deposits make them often difficult to clearly differentiate between these two hazardous events (tsunami and storm). Both types of deposits usually show normal and reverse grading, mud rip-up clast, sharp and/or erosional contacts, laminated sand layering

and fragmented shell debris (e.g., Nanayama et al., 2000; Tuttle et al., 2004; Goff et al., 2004; Kortekaas and Dawson, 2007; Morton et al., 2007; Phantuwongraj and Choowong, 2012).

In Thailand, tsunamis are a coastal natural hazard that represents a serious threat to the coastal communities along the Andaman Sea coastline, while the coasts along the Gulf of Thailand are regularly affected by extreme storms including typhoons. Up to now, reconstructing the record of past tsunami events mainly focused in investigating deposits found in swale between beach ridges, such as at Phra Thong Island (Jankaew et al., 2008). While there have been many studies on tsunami deposits along the coastline of the Andaman Sea (e.g., Satake et al., 2006; Fagherazzi and Du, 2007; Hawkes et al., 2007; Choowong et al., 2007; 2008; 2009; Jankaew et al., 2008; Karlsson et al., 2009, Feldens et al., 2009; 2012; Sakuna et al., 2012), little work has focused on analyzing the sedimentological nature and occurrence of storm surges in this region (Sakuna-Schwartz et al., 2015). An example is Phra Thong Island where three sand sheets occurring interbedded with muddy swale deposits were attributed to tsunami events (Figure 1A; Jankaew et al., 2008; Monecke et al., 2008, Fujino et al., 2009; Prendergast et al., 2012). These were assigned to the 2004 IOT event, and two older tsunamis (sand sheets B and C). According to optically stimulated luminescence (OSL) dating, the two latter occurred ca. 700-550 years and 2800-2500 years ago, respectively (Jankaew et al., 2008; Brill et al., 2012).

In terms of storm, most of the cyclones within the Andaman Sea occur either in spring (April-May) or fall (October-November) (Kumar et al., 2008). These usually move in west or west-north-west directions, with some exceptions such as the Cyclone Nargis of 2008 which turned eastward. In comparison to the Bay of Bengal, the Andaman Sea coast has a relatively low cyclogenesis activity (Pentakota et al., 2018). Extreme coastal storms occur hence quite rarely in the region because of the overall climatic setting and the fact that the storm tracks usually follow an east to west direction (Kumar et al., 2008; Fritz et al., 2010; Pentakota et al., 2018). However, Cyclone Nargis in 2008 (Category 4 on the Saffir-Simpson Hurricane scale) is a good example of a anomalously moving catastrophic storm which hit the coastal area of Andaman Sea side of Myanmar with sustained wind speeds > 210 km/h and gusts of up to 260 km/h. Cyclone Nargis developed in the central area of the Bay of Bengal, with high storm surges (> 5 m) which flooded the densely populated low-lying area of the Irrawaddy Delta (also called Ayeyarwady Delta) more than 50 km inland (Fritz et al., 2010). This catastrophic event led to a high death toll of at least 146,000 (Webster 2008, Mcphaden 2009). Cyclone Nargis is the seventh deadliest storm ever recorded worldwide (Fritz et al., 2010), and one of the most damaging natural disasters recorded in the history of Myanmar. Importantly, the high number of fatalities and enormous damage inflicted on property emphasize the necessity of installing preventive measures, improving the awareness of the local population, and enhancing the readiness of emergency evacuation measures. The aim of this study is

to contribute towards a better understanding of the nature and frequency of high energy events affecting the Andaman Sea coast.

The study area encompassed here lies at Bang Bane Beach (0.33 km²) in the Laem Son National Park (Ranong Province), located about 628 km south of Bangkok (Figures 1 and 3). The characteristic landforms found in the area are shore-parallel progradational beach ridges and the low topographic relief of the seasonal wet swale covered with grassy plants (Figures 1C and 3C). The study area faces the Andaman Sea coast to the west and is bound by hilly landscape to the east. The altitude of the beach ridges and swales ranges from 0.8 to 2.4 m above mean tide level and the tidal range is 1.1 m, which is regarded as micro tidal (Figures 3D and E). Most of the sediments along the beach as well as in the beach ridges and swales are fine- to very fine-grained sands, while muddy sand and sandy mud are the main component of estuary environment at the back of the study area, about 2 km east. Site reconnaissance and field work were conducted during May 17th to 24th 2019. It is worth mentioning that the climatic condition of Thailand is mainly associated with two major monsoon winds including the southwest (SW) monsoon and the northeast (NE) monsoon. From this condition, during May–October the Andaman Sea coast is under the influence of strong wind and wave from the SW monsoon wind moving upward from the Indian Ocean toward Thai Peninsula in the southwest direction. Similarly, the Gulf of Thailand coast experience strong wind and wave from the NE monsoon wind during October-February moving downward from Mainland China to

the Gulf of Thailand in the north-east direction. During site reconnaissance, the deposition of washover sediments generated by small-scale, seasonal monsoon-driven storm surges were found along the beach front (Figures 2A and B). While some parts of the beach front are used for tourism, the center of the study area is not affected by anthropogenic activity (Figures. 1C and 3C).

Due to the geographical position, the coast of the Andaman Sea is not only facing the Sumatra-Andaman Subduction Zone, where shallow-, intermediate-, and deep-seated earthquakes are common (Somsa-Ard and Pailoplee, 2013), but is also regularly affected by cyclones and seasonal monsoon (Sudharam et al., 2006). The 2004 IOT resulted from a 9.1-9.3 magnitude submarine earthquake off the northwest coast of the Indonesian island Sumatra, on December 26th (Lay et al., 2005; Stein and Okal, 2005; Jankaew et al., 2008). This event is regarded as one of the worst tsunamis in history (Suppasri et al., 2012) as it severely impacted coastal areas of 15 countries and killed approximately 230,000 people (Bell et al., 2005; Satake et al., 2006; Suppasri et al., 2012). In the area of Laem Son National Park in Ranong, the 2004 IOT destroyed the coastal area and community, inflicting damage of approximately 383 million baht (ca. 118 million USD) (Chaimanee and Tathong, 2005). According to Choowong et al. (2008) (At locality 1 in Figure 1B), the wave run-up during the tsunami was ca. 3 m, which caused the inundation of a large area with supercritical flow conditions and limited only by the hilly landscape east of the study area. Sedimentary traces preserved in the area include capping bedforms with leesides

facing landwards, by this indicating the direction of tsunami inflow. The identified sedimentary structures include parallel laminae, cross-lamination, anti-dunes as well as normal and reverse grading. The grain size of 2004 IOT sediments range from medium- to very fine-grained sand. Moreover, Kendall et al. (2006) (at locality 2 in Figure 1B) observed shell fragment and invertebrate marine species of *Dotilla wichmanni* and *Ocypode ceratophthalmus* in the estuary and beaches of the Laem Son area after the 2004 IOT event.

2.2.2 Vietnam

For the past two decades, the global mean sea level (msl) has been rising at an average rate of 2.9 mm per year (Nerem et al., 2018). Such an increase will result in the permanent and periodic inundation of low-lying areas, increased erosion, saltwater intrusion, and damage to physical infrastructures (Gornitz, 1991; McGranahan et al., 2007). Currently, the low-lying coastal communities are vulnerable to sea-level rise and stronger storms brought on by climate change due to global warming (McGranahan et al., 2007; Cui et al., 2015; Bevacqua et al., 2018; Maanan et al., 2018). Storm wave characteristics and storm surges are also affected by climate change since sea-level rises contribute to increased storm surge events (Hemer et al., 2013; IPCC, 2014; Maanan et al., 2018; Vousdoukas et al., 2020). Coastal areas are one of the most densely populated and developed geographical zones of the world (Luijendijk et al., 2018; Vousdoukas et al., 2020). Therefore, coastal

hazards, such as coastal storms and erosion, constitute a severe danger to the physical, economic, and social systems of coastal communities (Bevacqua et al., 2018).

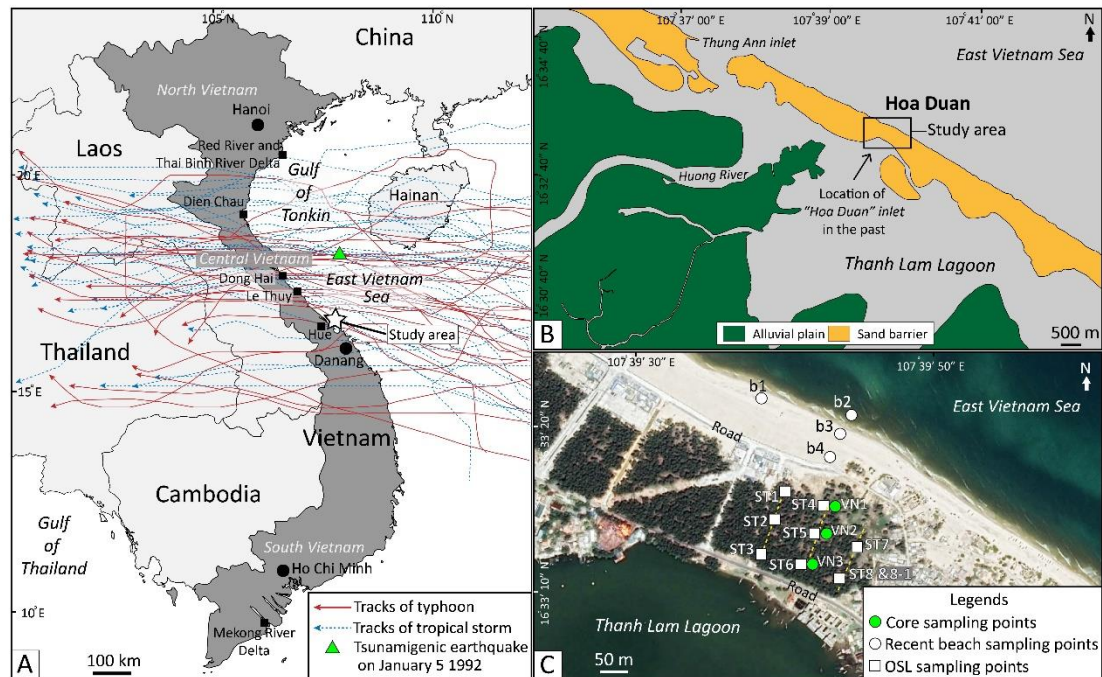


Figure 2 The study site at Hoa Duan, Thua Thien Hua, Central Vietnam. (A) Vietnam with tracks of major tropical storms and typhoons from 1952 to 2019, which mostly moved from east to west. Note that the tracks of tropical storms and typhoons are listed only for those in central Vietnam and are presented in Supplementary Table 2. (B) A geomorphological map of the study site showing the sand barriers, lagoons, alluvial plains, Thuan An inlet, and old Hoa Duan inlet (which was permanently closed), and (C) a close-up satellite image from Google Earth of the Hoa Duan barrier showing the sampling points of core samples, OSL dating, and recent shore-normal beach samples (Kongsen et al., 2021b).

Identifying and dating past extreme events (e.g., floods and storm surge) is an important tool to evaluate the vulnerability of a region and ultimately aid in preparing to limit the effects of natural hazards in the future. This is done by

investigating and dating the deposits of previous events with regard to their spatial context and nature. Sediment layers formed by storms and fluvial floods have been analyzed in a variety of settings around the globe (e.g., Nanayama et al., 2000; Yao et al., 2019) as they should have characteristic sedimentary structures due to differences in the transport process.

For instance, Nanayama et al. (2000) discovered layers of anomalous sediments in the coastal area of Hokkaido, Japan, and classified them as storm, tsunami, and fluvial flood using sedimentary structures and grain size characteristics. A 50-cm-thick layer of flood deposits was characterized by light gray sand mixed with gravel, while storm deposits contained marine sand with a foreset bedding structure. The tsunami deposit, which overlaid the storm layer, had a similar thickness (35-cm thick) and contained the same landward thinning geometry. However, the tsunami deposit was comprised of four layers associated with the landward and seaward flows of the two main tsunami waves, while the storm deposit contained a single layer (Nanayama et al., 2000).

Yao et al. (2019) classified the storm deposits and fluvial flood deposits induced by a hurricane in the wetland environment of Texas, United States, using sedimentary structure, loss-on-ignition (LOI), and X-ray fluorescence analyses. The flood deposit had a 9-cm-thick layer and was characterized as a light-gray rootless mud underlaid by a 5- to 10-cm-thick layer of the storm deposits (Yao et al., 2019). Khan et al. (2013) investigated the sediments of the 2011 Mississippi River Flood using

biological features as indicative of the fluvial origin to distinguish the flood deposit from the pre-surface sediment. Yamashita et al. (2011) discovered the fluvial flood deposits on the river mouth from Ise Bay, Central Japan. The layer of the fluvial flood deposits contained muddy particles that covered the sand material of the tidal flat, which was distinguished from the overbank deposit by a sharp basal contact. Yamada et al. (2016) identified the flooding layer of the Abu River in Yamaguchi City, Japan, from an overbank deposit. Their finding indicated the variety of flood sediments, ranging from muddy particles to cobbles.

The often reported characteristics of storm deposits preserved in coastal areas include sharp and erosional contacts, normal and reverse grading, mud rip-up clasts (MRCs), mud laminae, laminated sand, marine shells, marine fossils, and marine microfossils (e.g., Liu and Fearn, 1993, 2000a, b; Donnelly et al., 2001; Liu, 2004, 2007; Donnelly, 2005; Elsner, 2007; Morton et al., 2007; Williams, 2010, 2013; Phantuwongraj and Choowong, 2012; Phantuwongraj et al., 2013; Williams et al., 2016; Kongsen et al., 2021). In contrast, fluvial flood deposits can usually be identified by sharp and erosional contacts, lamination, cross-bedding, massive mud contents, well-sorted suspended sediment with a rounded shape due to long-distance transport, and a high organic matter (OM) and plant detritus content (e.g., Rubin et al., 1998; Zhu et al., 2005; Yamashita et al., 2011; Khan et al., 2013; Day et al., 2016; Matsumoto et al., 2016; Yamada et al., 2016). However, the individual

regional setting (e.g., substrate and coastal geomorphology) might produce specific features that are not generally common.

Vietnam has been severely affected by natural hazards, such as fluvial flood and tropical cyclones, for decades. More than 70% of the severe natural hazards affecting Vietnam are attributed to typhoons, whereas fluvial flooding is the second most frequent event (Imamura and To, 1997). The main cause for the vulnerability of Vietnam to these hazards is its geographical position, with approximately 3,260 km of coastline stretching longitudinally next to the Western Pacific Ocean (Imamura and To, 1997; Larson et al., 2014). This makes the population of Vietnam particularly vulnerable to a sea-level rise, floods, coastal erosion, and tropical cyclones (Imamura and To, 1997; Kleinen, 2002).

On average, Vietnam experiences five to six typhoons every year due to its proximity to significant tropical cyclone genesis zones (Wang et al., 2007) and the influence of the Mei-Yu front (Lee et al., 2006). During the 20th century, about 786 typhoons and tropical storms struck the Vietnamese coast, of which 348 had strong wind speeds (>120 km/h) (Kleinen, 2002). For example, there were two successive typhoons in 1985, starting with typhoon Andy (Category 2 on Saffir-Simpson Hurricane Scale) from October 1 to 3 in central Vietnam (Dong Hai and Le Thuy) (Figure 2A), followed by typhoon Cecil (Category 3 on Saffir-Simpson Hurricane Scale) on October 15 and 16. These were considered the most catastrophic disasters at that time,

causing over 1,000 casualties, 276,790 destroyed and damaged houses, and 3,300 wrecked fishing boats (Imamura and To, 1997).

Twelve years later (1997), tropical storm Linda was described as the most significant storm of the century, causing nearly 800 deaths, 2,132 missing people, and ruining over 300,000 houses (Kleinen, 2002). A severe fluvial flood occurred in November 1999 in central Vietnam, affecting numerous areas (IFRC, 2001; Beckman et al., 2002; Vu and Ranzi, 2017; Nga et al., 2018). The number of death was 793, and 52,500 houses were destroyed. Most damages occurred in the Hue region, where precipitation reached record levels of 2,288 mm, exceeding emergency thresholds. With the immense volume of water draining from the Huong River, the cities of Hue were submerged by 1–2 m of flood water, depending on the topography (Beckman et al., 2002). Moreover, apart from natural hazards, Hirai et al. (2008) stated that, if the global warming-induced sea level rise continues unabated, floods like the one in November 1999 will become more common. Sedimentary records of the past storm and fluvial flood events are essential for raising the awareness of people living in low-lying coastal areas. It has to be noted that, until today, very little has been known about the particular characteristics of the storm and fluvial deposits in Vietnam (Mathers and Zalasiewicz, 1999; Williams et al., 2019), and that the history of extreme events in this region is poorly investigated. Therefore, to enhance the understanding of the natural events that deposited material in Vietnam, this study

analyzed and provided the distinction between storm surge and fluvial flood deposits in the past centuries.

The study site, with an area of approximately 0.30 km², is located at Hoa Duan, Thua Thien Hue, central Vietnam (Hoa Duan, Hue City) (Figure 2), and is part of a 38-km-long barrier island that lies in a northwest-southeast direction. This barrier is narrow at the north, at about 300 m in width, and wider at the south, at about 4-km width. Elevation of the ground surface is low in the north at about 1–2 m above (a) msl and then rapidly increasing due to the change of topography from a coastal plain to sand dunes with an average height of about 15 m. The coast of the study area lies in a northeast direction, flanked by the East Vietnam Sea at the front with a large lagoon (Đ`âm Thanh Lam) at the back. The lagoon water, with an average depth of only 1 to 2 m is usually connected to the East Vietnam Sea by the Thuan An inlet, which is located near the mouth of the Huong River (Hirai et al., 2008). The tidal range in the region is about 0.4 m and is, thus, categorized as a microtidal system. The study area is influenced by the monsoon climatic regime that is responsible for the rainy and dry seasons in this area. From mid-October to February, the northeast monsoon that passes the South China Sea brings abundant precipitation to the coastal area. The flood season usually occurs from September through December due to the northeast winds and typhoons. Subsequently, the southwest monsoon, from May to September, usually generates hot weather due to the southwest winds

drying out after passing the high mountain range of the country (Nghiem et al., 2007). Therefore, the rainfall also decreased during the dry season.

Field investigations were carried out from January 8 to 15, 2019, after the end of the typhoon season (Larson et al., 2014). During the investigations, destroyed buildings and erosional marks on beach scarps were observed, indicating the highest wave impact during the preceding monsoon period (Figures 4A–C). The sediment investigated here was mainly sand (Figure 4D), which has differences in grain size. Finer-grained sediment was found on the surface in some areas, particularly at low-relief topography. Most of the surface was vegetated with grass. The highest point of the area is 2.5 m above the mean tide level (amtl) (Figure 4E). There was almost no anthropogenic modification in the study area, except for conifers planted along the barrier. However, outside the study area, a built-up area of coastal communities, restaurants, hotels, and resorts was found throughout the barrier island. In the northwest, there was a breach from the flood in November 1999 (Lam et al., 2007), which left an ephemeral inlet connecting Thanh Lam Lagoon and the East Vietnam Sea until it closed in 2001. This breach at Hoa Duan was the consequence of a washout process caused by a flood event that included more than 2,000 mm of rain in a week and an unusually high-water level in the lagoon of about 4-m amsl (Hirai et al., 2008). According to the study of Nguyen Huu and Duong (2015), flooding in 1999 completely devastated this area, destroying 13.2 hectares and consequently forming a new inlet at Hoa Duan.

According to the historical records, the barrier here is associated with the closing and opening of the Hoa Duan and Thuan An inlets (Figure 2B; Lam et al., 2007; Schweyer, 2018). Lam et al. (2007) stated that the Hoa Duan inlet first opened in AD 1404 and closed in AD 1467, and then reopened in AD 1498 and closed again in AD 1909, and opened once again from the flood in November 1999 and most recently closed in 2001. Based on the historical record representing the existence of the barrier (Lam et al., 2007; Schweyer, 2018), the sea-level history of the area can be inferred from the location of the barrier, which has changed slightly in the centennial scale.



CHAPTER 3

METHODOLOGY

3.1 Pre-fieldwork

3.2 Fieldwork

3.2.1 Topographic survey and stratigraphy

3.2.1.1 Laem Son area

Across the sandy beach ridges of Laem Son National Park, three transects perpendicular to the coastline were measured from east to west (Figs. 1C and 2C-E). The topographical measurement was conducted by using a total station survey camera SOKKIA (SET630R) together with providing reference points of all stations by a hand-held GPS (Kongsen et al., 2021a; b). The obtained topographic values were then referenced with the tide table of Khura Buri tide gauge station for the time of measurement (Figure 1A; Thai Royal Navy, 2019). The ranges of tide (mean tide, high tide and low tide) were calculated by the following method of William et al. (2016) which computes the elevation, and then changed into meters a.m.s.l (above mean sea level). Along the three transects, three-inch-diameter plastic tubes were prepared for collecting core samples. Before coring, 40- to 50-cm-deep pits were excavated at each location to analyze the sedimentary profile and for OSL sample collection. Ten cores were collected inland at 50-m intervals and designated as core 1 to core 10 (Figures 1C and 3C-E). All of the sample cores obtained from the swales were

cleaned and sealed with adhesive cloth tape. Furthermore, recent beach sediments were collected and were labeled as b1, b2, b3 and b4 (Figure 1C).

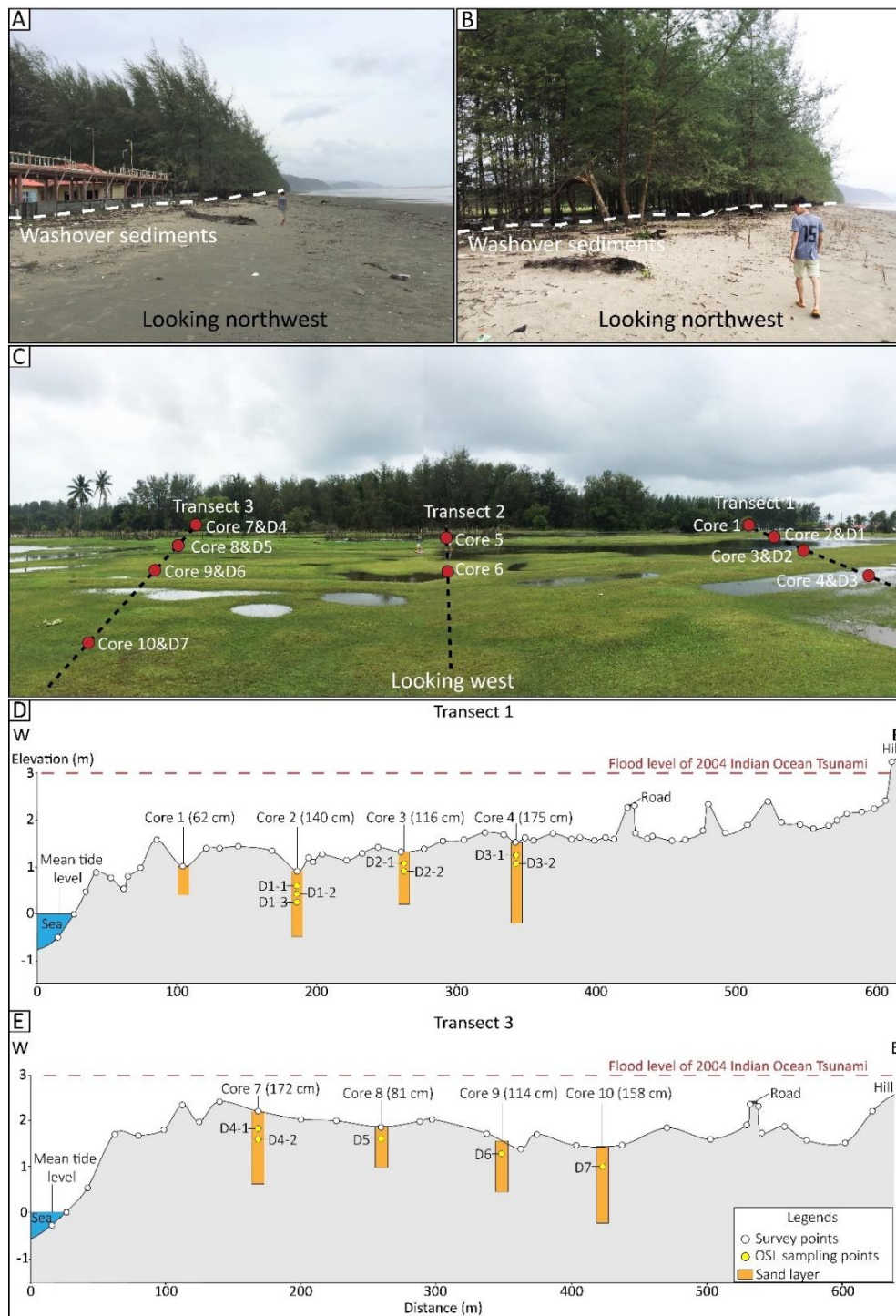


Figure 3 Laem Son area, (A) the traces of the washover sedimentation and a derelict building on the beach zone by the monsoon. (B) The traces of the washover

sediments and saltwater penetrated inland by the monsoon. (C) Three transects perpendicular to the shoreline where the 2004 IOT propagated and the positions of core and OSL samples. All photographs were taken on May 18, 2019. (D) and (E) Cross-sections of Laem Son area showing the detailed topography from west to east. Transect 1 with positions of core 1, 2, 3 and 4 and OSL samples (a yellow circle) of D1-1, D1-2, D1-3, D2-1, D2-2, D3-1 and D3-2, and transect 3 with the positions of core 7, 8, 9 and 10 and OSL samples of D4-1, D4-2, D5 and D6.

3.2.1.2 Hoa Duan, Thua Thien Hue, central Vietnam

At the barrier beach ridge, a transect was mapped perpendicular to the East Vietnam Sea (northeast), drawn from the sea level to the Đầm Thanh Lam lagoon (southwest) (Figures 2B and C). Topographic measurement of this transect was conducted using a total station survey camera SOKKIA (SET630R) to obtain its true elevation with reference to the water table of the Dong Ha meteorological station at the time of surveying. A handheld GPS was used to provide reference points of all stations. The accuracy of distance measurement using the fine average measurement mode with a prism was $\pm (2 + 2 \text{ ppm} \times D) \text{ mm}$ (Kongsen et al., 2021). Tidal ranges of the area were established, including the mean tide, high tide, and low tide, by converting elevation into meters amsl, following the method of Williams et al. (2016). Additionally, three cores were collected inland at 50-m intervals along the transect and designated as VN1, VN2, and VN3 (Figures 2C and 4E). Before coring, 40- to 50-cm-deep pits (Pit1, Pit2, and Pit3; Figure 12) were dug at each station to examine the deposition profile and prepare for the OSL sample collection. Pits could not be more profound because of the water table. Subsequently, three-inch-diameter plastic

tubes were percussed from the ground surface to collect core samples, which were cleaned, sealed with duct tape, and, once secured, the cores were cut into two halves, photographed, logged, and sampled. In addition to collecting core samples, sediment samples from the shore-normal processes at the beach were also collected at the ground surface for comparing the sedimentary properties with the storm and fluvial flood deposits and were designated as b1, b2, b3, and b4 (Figure 2C).

3.2.2 Sedimentology and loss on ignition

Sediments in the cores were collected at 0.5- to 1-cm intervals for a layer from the top to the bottom, especially in places where the distinctive sedimentary structures of the sediments were observed, such as planar lamination or parallel lamination. Samples were separated into pairs of subsamples for physical property analysis. Physical properties of the sediments, such as composition (Fritz and Moore, 1988; Rothwell, 1989; Rosenthal et al., 2018), roundness, and sphericity (Powers, 1953) were observed under a microscope and photographed. For grain size analysis, the sediment samples were analyzed using Mastersizer 3000 (Malvern Instruments Limited, Malvern, United Kingdom). Each 1 cm interval of the sand sample was put in water. Laser obscuration was set between 5 and 15%. Before measuring, ultrasound was used for 10 s to disperse the finer grains surrounding each sand grain. Each sample was run three times and then averaged. The average data of each sample were calculated in GRADISTAT Version 8 (Blott and Pye, 2001) using the logarithmic

method of moment (Folk and Ward, 1957), especially for Vietnam area, while grain size distribution parameters of Laem Son area were calculated with the logarithmic method of moments (Krumbein and Pettijohn, 1938; Folk and Ward, 1957; McBride, 1971; Blott and Pye, 2001). All sedimentological data are plotted against depth to visualize changes within the sedimentary column.

Various statistical parameters, including the mean grain size, sorting, skewness, and kurtosis, were calculated. Mean grain size can be used to identify the type of sediment according to the Wentworth scale (Wentworth, 1922). Sorting was used to measure the distribution of grain sizes from the mean. Skewness refers to the asymmetry of a given frequency distribution, in which a positive value specifies a coarse-dominated sample, whereas a negative value indicates a fine-dominated sample (Folk and Ward, 1957). Kurtosis indicates the concentration of grains relative to the average (Blott and Pye, 2001). It is similar to standard deviation in that high values indicate well-sorted distributions, while low values indicate a poor distribution (Cadigan, 1961). Also, a high kurtosis tends to match normal (mesokurtic) to very highly peaked distribution curves, while a low kurtosis indicates flattened distribution curves (platykurtic).

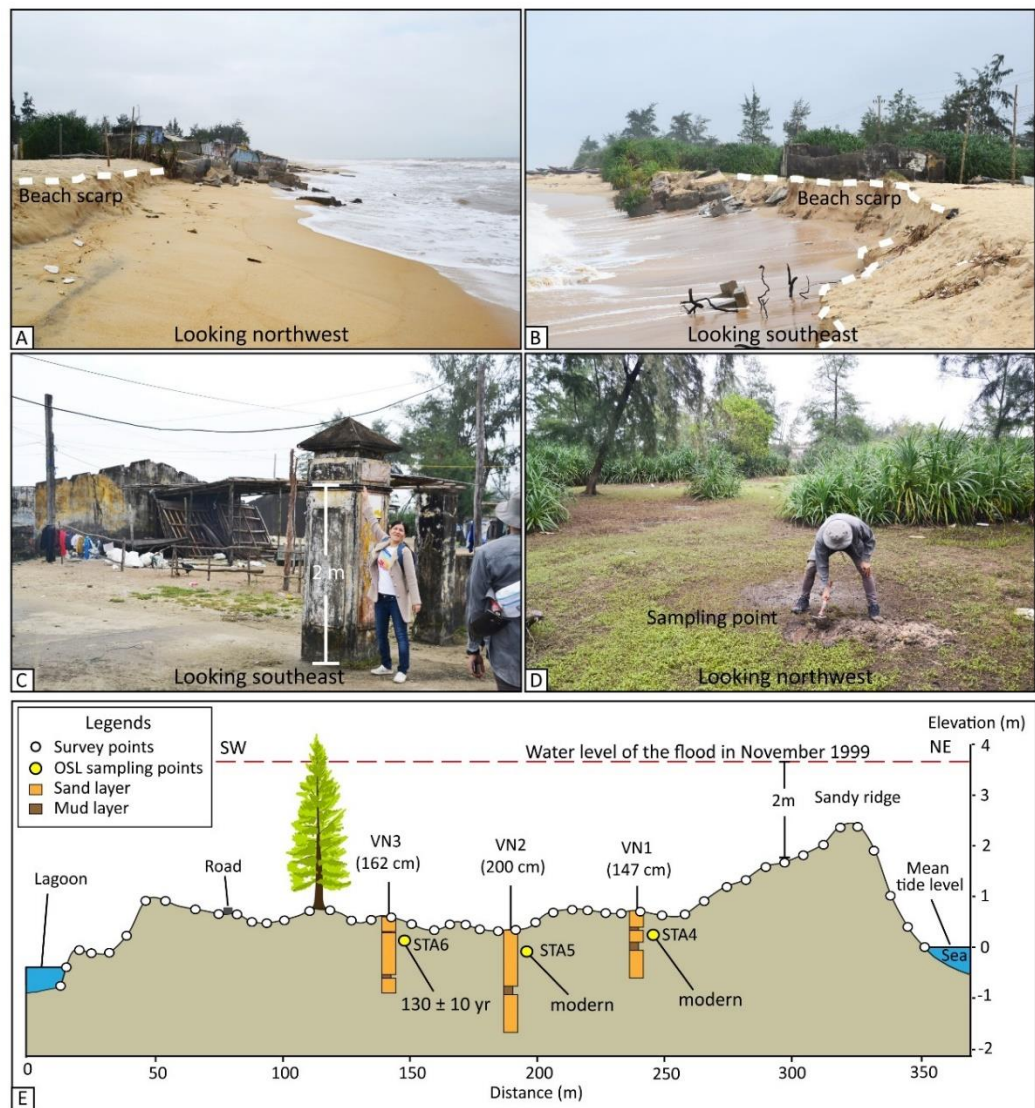


Figure 4 Hoa Duan barrier. (A, B) Beach scarps and derelict buildings resulting from wave erosion during the typhoon season that indicated the maximum wave height during the typhoon season. (C) A local villager showing a water mark level of the flood in November 1999 (2 m). (D) The VN1 and ST4 sampling points in the low topography of the Hoa Duan barrier. (E) Cross-section of Hoa Duan, measured using a total station survey camera, coupled with core locations with depth and the OSL ages (a yellow circle). A dashed red line indicates the water level of the flood in November 1999 that inundated this area (2-m depth). The OSL dating of STA4, STA5, and STA6 indicated the depositional ages as modern, modern, and 130 ± 10 years, respectively. The modern age means less than 100 years. The correlations are

presented in detail in Figure 12. All photos were taken on January 12, 2019 (Kongsen et al., 2021b).

The LOI was used to determine the organic and carbonate contents. For the LOI analysis, samples were dried and then grounded by hand to a homogenous texture. Then, 1 g of each sample was weighed and prepared in crucibles. A high-temperature furnace (Nabertherm® muffle furnace LE 6/11) heated the samples according to the protocol for LOI (Heiri et al., 2001). The OM content was measured first by heating at 550°C for 4 h, and then reweighing. After that, the same samples were heated at 950°C for 1 h and then reweighed to determine their carbonate content. Results are presented vertically from top to bottom.

3.2.3 Optically stimulated luminescence dating

3.2.3.1 *Laem Son area*

Along the transects 1 and 3, small pits were excavated for collecting OSL samples from the ground surface (see detailed information in Figures 1C and 3C-E). Pit depth was limited to between 40-60 cm depth due to high ground water level. A plastic tube (0.5 cm thick wall and 4 cm diameter) was used to collect samples for equivalent dose (D_e) determination. Opaque tubes were used to prevent erasing of the OSL signal by sunlight exposure. For annual dose (AD) determination, samples were taken from the sand surrounding the D_e sample. All of the OSL sampling points were referenced by a hand-held GPS.

3.2.3.2 Hoa Duan, Thua Thien Hue, central Vietnam

Three lines of OSL sampling points were aligned on the barrier perpendicular to the shoreline (Figure 2C). All OSL samples were collected at 50 cm depth using protected-light plastic tubes for equivalent dose samples (De), except for ST8-1, which was collected at 30 cm depth. About 290 g of annual rate dose samples surrounding the equivalent dose samples were collected in plastic bags. The first line consisted of three OSL samples (ST1, ST2, and ST3), as did the second (ST4, ST5, and ST6) and third (ST7, ST8, and ST8-1) lines. The OSL samples of ST8 and ST8-1 were collected in the same profile but at different depths. Note that the positions of three OSL samples (ST4, ST5, and ST6) are consistent with the positions of cores VN1, VN2, and VN3, respectively. The remaining OSL samples from nearby locations were collected in order to cross-check.

A small amount of each dose rate sample was separated to measure its water content by weighing before and after drying at 105°C. Another part was dried in the oven and sieved through an 841- μ m sieve (mesh 20) pan. The amount of the dose rate sample in the pan was weighed (290 g) and packed in a suitable container for at least 1 month. Later, the natural radioisotope concentration was measured using high-resolution gamma spectrometry (Canberra).

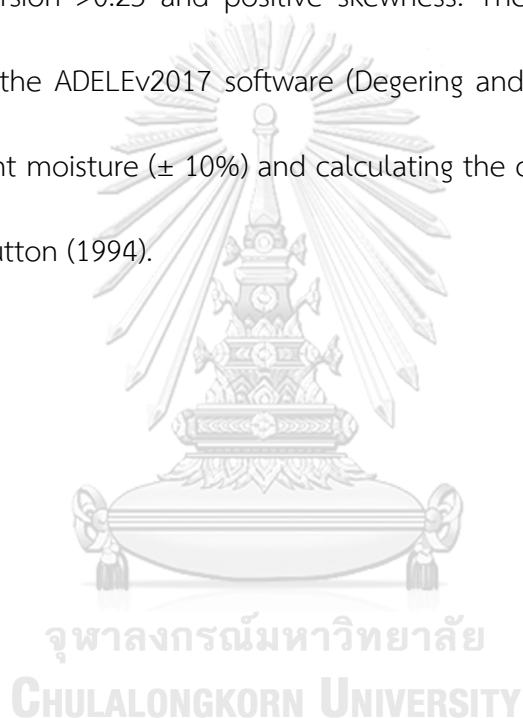
For De determination, sample preparation was done in a room with subdued red light (to avoid light exposure) at the Sedimentological Lab, Chulalongkorn University. The sediments were wet-sieved and cleaned through a 125- μ m sieve

(mesh 120) and a 180- μm sieve (mesh 80) to obtain a sand fraction in the range of 125–180 μm . To remove carbonates, the samples were then treated in 10% (v/v) HCL until the chemical reaction (bubbles) ended and subsequently rinsed three times with clean water. To eliminate organic matter, the samples were treated with 30% (v/v) H₂O₂ overnight, rinsed three times with clean water, etched by 40% (v/v) HF for 60 min to dissolve feldspar minerals, and then cleaned and rinsed three times with clean water. The De samples were dried in the oven at 40°C for 48 h and packed in sunlight-proof containers. Subsequently, an iso-dynamic magnetic separator was applied to the dried-aliquot samples to remove ferro-minerals.

The derived quartz grains were placed on stainless steel discs of 10 mm diameter coated with silicon oil (2 mm stamps). The luminescence of the samples was measured using a Risø TL/OSL-DA-15C/D reader equipped with an internal 90Sr/90Y beta source (ca.0.102 Gys⁻¹) and a bialkali EMI photomultiplier. Blue diodes emitting at 470 nm and 7.5-mm-thick Hoya U-340 filters were used for the measurement. A single-aliquot regenerative dose protocol with three dose points was applied to all samples (Murray and Wintle, 2000). Before measuring, a preheat plateau test was run to identify the most suitable preheat setting (220°C for 10 s prior to all OSL measurements).

For De determination, between 40 and 54 aliquots were measured per sample and analyzed using the Analyst.V4.31.7 software. An individual De value was accepted under the criteria of recuperation < 5%, recycling ratio within 10%, test

dose error <10%, IR depletion ratio within 10% of unity, the adequate fit of the growth curve, and enclosure of D_e by regenerative doses. Between 1 and 10 aliquots had to be rejected per sample for not meeting one or more of these criteria. The mean D_e was calculated either using the Central Age Model or the Minimum Age Model (MAM) (Galbraith et al., 1999). The MAM was applied when the D_e distribution showed overdispersion >0.25 and positive skewness. The dose rate and age were determined using the ADELEv2017 software (Degering and Degering, 2020) using the measured sediment moisture ($\pm 10\%$) and calculating the cosmic dose rate according to Prescott and Hutton (1994).



CHAPTER 4

RESULTS

4.1 Laem Son area, Ranong, Thailand

Based on their sedimentological properties and the sedimentological sequence, six distinct sedimentary units, named Unit I to Unit VI, were identified in transects 1 and 3 (Figures 5 and 6; Tables 1 and 2). Each unit and its sedimentological properties are described below and are presented in online Supplementary Material. Additionally, deposits recognized in the most seawards core of section 1 have been classified as monsoon-driven storm surges sediments (MSS) which are described together with the samples taken from the recent beach below.

4.1.1 Sediment characteristics of modern beach deposits and monsoon-driven storm surges sediments

Recent beach sediment samples are characterized by greyish sand and have similar physical properties, including sphericity (high), roundness (sub-angular to rounded), and composition (Tables 1 and 2). They mainly consist of 96-97% quartz, 1-2% bioclasts, and 1-2% of heavy minerals, respectively. The organic matter content ranges from 0.96 % to 1.3% while the carbonate content ranges from 0.8% to 2.3%. Only a minority of foraminifera is detected. The sediments are fine (b1) to very fine (b2-b4), moderately well sorted sands. The grain size distribution of all four samples is fine-skewed and very leptokurtic.

Table 1 Range of sediment composition grain properties of the six identified units as well as the recent beach and monsoon sediments. MMS, monsoon-driven storm surges; 2004 IOT, 2004 Indian Ocean Tsunami; OSB, old surface before Indian Ocean Tsunami; UBS, upper surface sediment; UFS, upper foreshore sediment.

Sediment types	Quartz (%)	Bioclast (%)	Heavy mineral (%)	Organic (%)	Carbonate (%)	Sphericity	Roundness
Recent beach sediment	96-97	1-2	1-2	0.96-1.54	0.83-2.18	High	Sub-angular to rounded
MMS sediment	96-98	0-2	1-3	0.74-1.84	0.11-2.29	Low to high	Sub-angular to rounded
Topsoil sediment (Unit I)	98-99	0-1	1-2	0.78-13.93	0.00-1.12	Low to high	Angular to rounded
2004 IOT sediment (Unit II)	99	0	1	0.72-3.68	0.01-0.60	Low to high	Sub-angular to rounded
OSB 2004 IOT sediment (Unit III)	99	0	1	0.99-3.51	0.03-0.37	Low to high	Angular to sub-angular
UBS (Unit IV)	98-99	0-2	1-2	0.19-2.21	0.00-0.80	Low to high	Angular to rounded
UFS (Unit V)	96-99	1-3	1-2	0.60-1.68	0.20-3.69	Low to high	Sub-angular to rounded
Storm sediment (Unit VI)	82-98	1-17	1-2	0.67-5.75	0.71-17.57	Low to high	Sub-angular to rounded

The sediments observed in core 1 (4-62 cm depth) are characterized by greyish sand with fragmented shells, exhibit slight laminated sand layers, and are interpreted as resulting from monsoonal-driven storm surges (Figures 5, 7 and 9; Tables 4.1 and 4.2). They show varying sphericity and roundness, with their composition being predominantly quartz (96-99%), 1-2% bioclasts and 1-2% heavy minerals. Their organic matter content ranges from 0.7% to 1.8%, whereas the carbonate contents are in between 0.1% and 2.3%. Carbonate content correlates with depth, with low contents (0.1-0.9%) in the upper 25 cm, increased content

around the center of the core at depth of 26 cm to 38 cm (0.9% to 2.3%), and medium carbonate content in the range of 0.5% to 1.1% in the lower portion of the core (Figure 9). Only a minority of foraminifera is detected. The fine to very fine sands are moderately well to well sorted and their grain size distribution is finely skewed and very leptokurtic. The sands show normal and reverse grading (Figure 9).

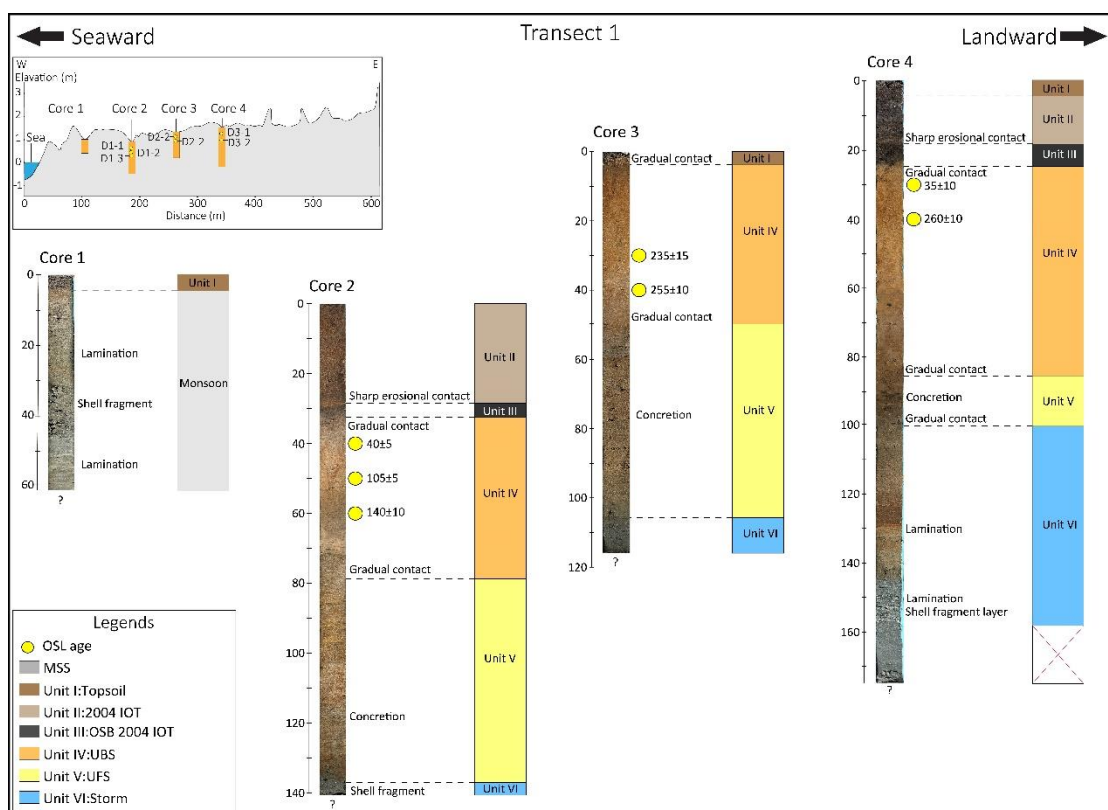


Figure 5 Detailed topography of Laem Son area in transect 1 showing the interpreted stratigraphy of cores 1, 2, 3 and 4. The OSL dating (a yellow circle) of D1-1, D1-2, D1-3, D2-1, D2-2, D3-1 and D3-2 indicated the depositional ages as 40 ± 5 yr, 105 ± 5 yr and 140 ± 10 yr, 235 ± 15 yr and 255 ± 10 yr, 35 ± 10 yr and 260 ± 10 yr, respectively. MSS, monsoon-driven storm surges; 2004 IOT, 2004 Indian Ocean Tsunami; OSB, old surface before Indian Ocean Tsunami; UBS, upper backshore sediment; UFS, upper foreshore sediment.

4.1.2 Sedimentological characteristics of each unit

In the stratigraphy of the cores retrieved in transect 1 and 3, six stratigraphic units can be identified which can be correlated between cores based on color, composition, sedimentary structures and grain size distributions (Figures 5-10; Tables 1 and 2). From top to bottom these units are as follows: Unit I: organic-rich sandy topsoil (present surface), Unit II: 2004 IOT, Unit III: original surface before 2004 IOT, Unit IV: upper backshore, Unit V: upper foreshore and Unit VI: storm sediment.

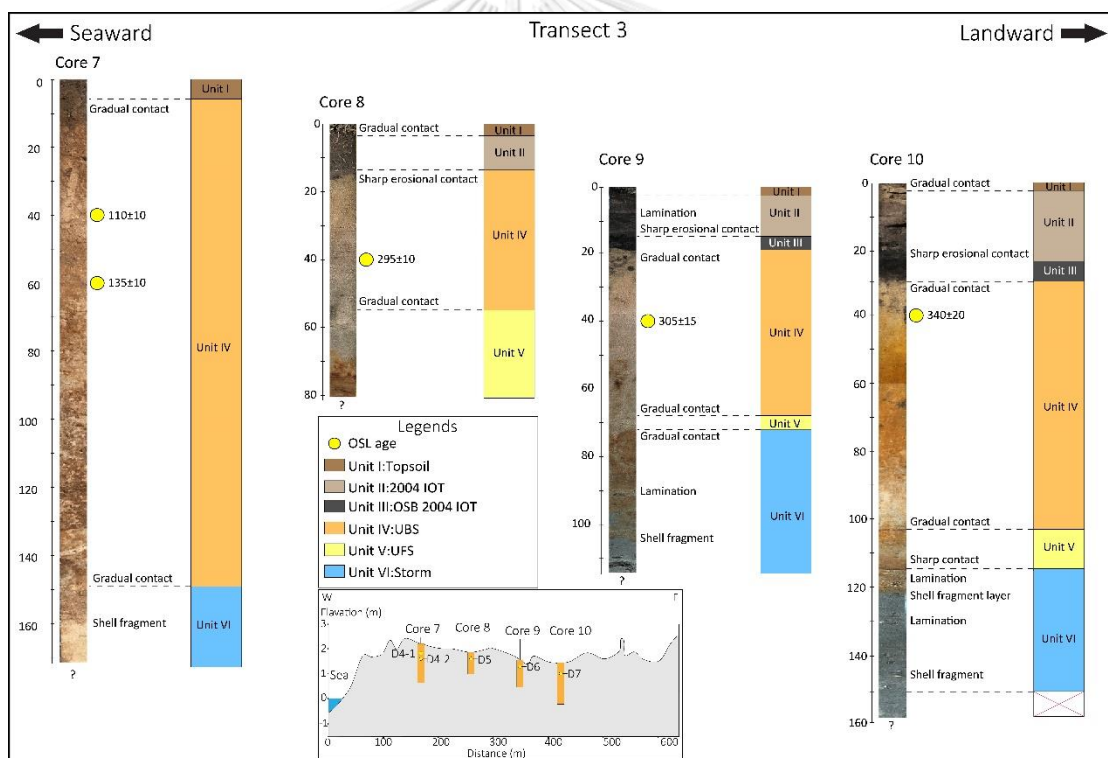


Figure 6 Detailed topography of Laem Son area in transect 3 showing the interpreted stratigraphy of cores 7, 8, 9 and 10. The OSL dating (a yellow circle) of D4-1, D4-2, D5, D6 and D7 indicated the depositional ages as 110±10 yr, 135±10 yr, 295±15 yr, 305±15 yr and 340±20 yr, respectively. 2004 IOT, 2004 Indian Ocean Tsunami; OSB, old surface before Indian Ocean Tsunami; UBS, upper backshore sediment; UFS, upper foreshore sediment.

Unit I (Figures 5-10; Tables 1 and 2)

This unit is characterized by dark brown sand with a high organic matter content. This layer is present in all but core 2 and has a thickness of 3–6 cm. Grass and rootlets can be observed at the top of the layer. The transition to the underlying layer is gradational. Normal grading can be observed through all cores, while reverse grading is recognized in core 7.

The layers contain predominantly quartz (98–99%), with minor heavy mineral content (1%) and bioclasts (1%), which is due to the presence of freshwater gastropods. The organic matter content of the layers is relatively high (0.8%–14%), while the carbonate contents are in between 0.1% and 1.1%. The fine and very fine sands are moderately to moderately well sorted and their grain size distribution shows a range of skewness (coarse skewed to very fine skewed) and are positive to very positive with regards to their kurtosis.

Table 2 Range of grain size distribution parameters, sedimentary structures and marine fossil and microfossil for each stratigraphic unit. MMS, monsoon-driven storm surges; 2004 IOT, 2004 Indian Ocean Tsunami; OSB, old surface before Indian Ocean Tsunami; UBS, upper surface sediment; UFS, upper foreshore sediment.

Sediment types	Mean (phi)	Sorting (phi)	Skewness (phi)	Kurtosis (phi)	Sorting	Sedimentary structure	Marine and microfossil
Recent beach	2.91 - 3.1	0.50 - 0.52	0.08 - 0.17	2.30 - 2.54	Well sorted to moderately well sorted	-	Foraminifera
MMS	2.66 - 3.1	0.45 - 0.53	0.08 - 0.25	2.30 - 3.05	Well sorted to moderately well sorted	Lamination, shell fragment	Foraminifera
Topsoil (Unit I)	2.37 - 3.21	0.47 - 0.96	-0.68 - 0.61	1.85 - 4.63	Well sorted to moderately sorted	Gradational lower contact, normal and reverse grading	-
2004 IOT (Unit II)	2.29 - 3.13	0.56 - 0.90	-0.57 - 0.57	2.04 - 4.44	Moderately well sorted to moderately sorted	Erosional lower contact and gradational top contact, slight lamination, normal and reverse grading, fining landward trend	-
OSB 2004 IOT (Unit III)	2.83 - 3.03	0.56 - 0.75	-0.01 - 0.58	2.17 - 3.12	Moderately well sorted to moderately sorted	Erosional top contact, gradational bottom, sharp bottom contact, normal and reverse grading	-
UBS (Unit IV)	2.06 - 3.16	0.42 - 0.74	-0.24 - 0.69	2.21 - 3.87	Well sorted to moderately well sorted	Gradational top and bottom contact	-
UFS (Unit V)	2.69 - 3.18	0.43 - 0.62	-0.02 - 0.43	2.22 - 2.96	Well sorted to moderately well sorted	Gradational top contact and erosional bottom contact, shell fragment	Crustacean, crinoid, foraminifera, ostracod
Storm (Unit VI)	2.4 - 3.08	0.44 - 1.24	-1.49 - 0.28	2.27 - 5.98	Well sorted to poorly sorted	Sharp erosional top contact, gradational top contact, normal and reverse grading, lamination, shell fragment	Bivalve, spicule, foraminifera, ostracod

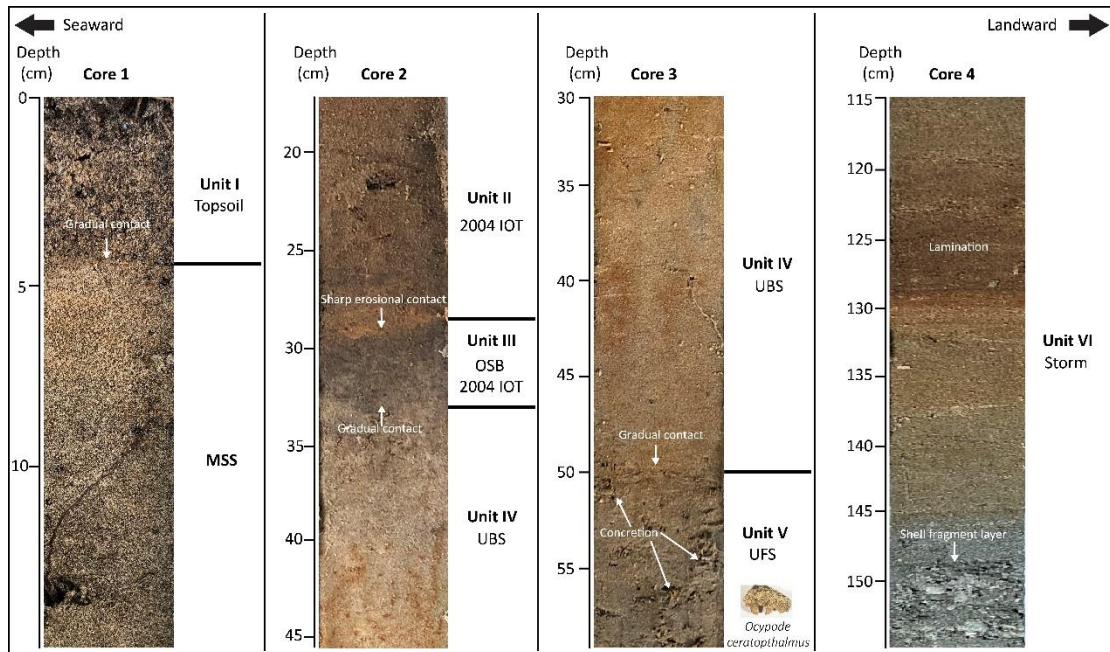


Figure 7 Close-up of the six sedimentary units from cores 1, 2, 3 and 4. In core 1, monsoon sediments are identified at 4 to 62 cm depth and are characterized by grey to orange sand with slight lamination. In core 2, Unit II is identified at 0 to 29 cm depth which is characterized as dark brown to orange sand. The erosional lower contact of Unit II with Unit III in core 2 is recognized at 29 cm depth. In core 3, Unit IV is identified at 4 to 50 cm depth and contain gradational lower contact with Unit V. In Unit V of core 3, the concretion and crab remain (*Ocypode ceratophthalmus*) are observed. In core 4, Unit VI is observed at 101 to 157 cm depth which is characterized as brown to grey sand with lamination at 123 to 133 cm depth and shell fragment layer at 149 to 157 cm depth. MMS, monsoon-driven storm surges; 2004 IOT, 2004 Indian Ocean Tsunami; OSB, old surface before Indian Ocean Tsunami; UBS, upper backshore sediment; UFS, upper foreshore sediment.

Unit III (Figures 5-10; Tables 1 and 2)

This unit is characterized by blackish sand. The thicknesses of this layer ranges from 4 to 6 cm. The top boundary to Unit II is of erosional nature while it has a gradual basal boundary to the underlying Unit IV. Normal and reverse grading are observed within the unit.

This Unit is comprised of 99% quartz and 1% heavy minerals. It has an organic matter content between 0.99% and 3.51%, while its carbonate content is ranging from 0.03% to 0.37%. The fine to very fine sands are moderately to moderately well sorted and their grain size distribution show a wide range of skewness and positive kurtosis.

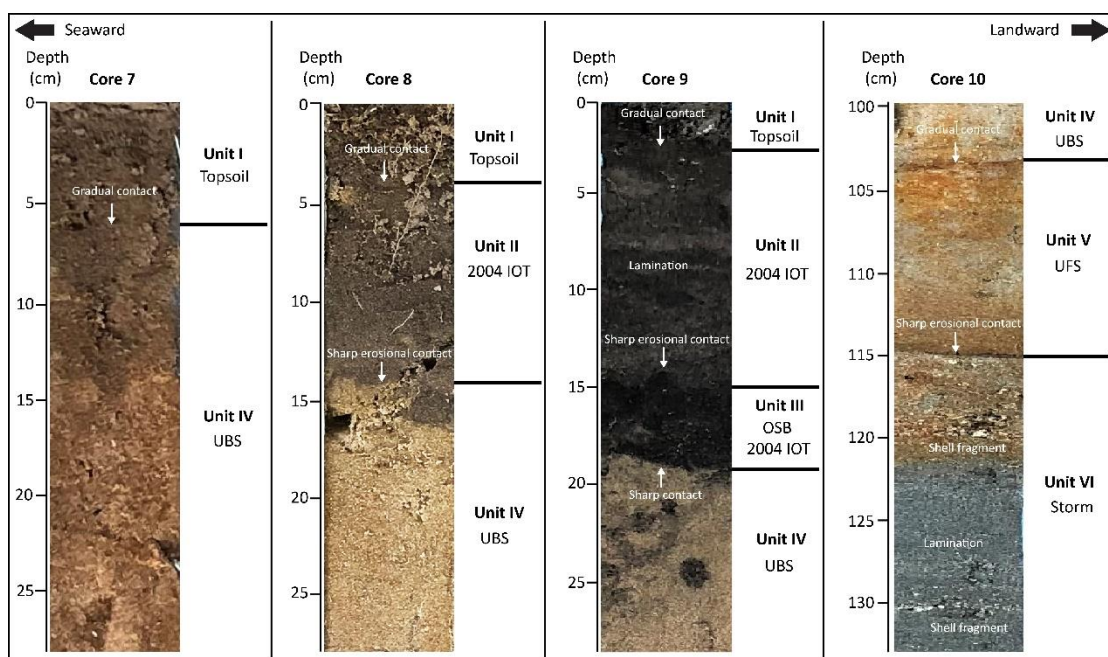


Figure 8 Close-up of the detailed sedimentary characteristics from cores 7, 8, 9 and 10. In core 7, Unit I is classified at 0 to 6 cm depth and are characterized as brown sand overlying Unit IV. In core 8, Unit II is identified at 4 to 14 cm depth which is characterized as dark brown sand with the erosional lower contact overlying the Unit IV. In core 9, Unit II is identified is observed at 3 to 15 cm depth and is characterized as black sand overlying the darker sand layer of Unit III in range of 15 to 19 cm depth. The lamination of Unit II in core 9 is recognized at 4 to 10 cm depth and the erosional lower contact with Unit III is recognized at 15 cm depth. In core 10, Unit V is identified at 103 to 115 cm depth which contain the erosional top contact with Unit IV at 103 cm depth and the sharp erosional lower contact with Unit VI at 115 cm depth. Unit VI in core 10 is observed at 115 to 150 cm depth which contain shell

fragmented and lamination at 115 to 121 cm depth. 2004 IOT, 2004 Indian Ocean Tsunami; OSB, old surface before Indian Ocean Tsunami; UBS, upper backshore sediment; UFS, upper foreshore sediment.

Unit IV (Figures 5-10; Tables 1 and 2)

This layer is characterized by orange to brown sand. The massive sand has a gradational contact with the overlying Unit as well as with the underlying Unit V. The thickness of the unit varies from 41 to 143 cm, sedimentary structures include normal and reverse grading.

The sands consist of 98–99% quartz, 0–2% bioclasts and 1–2% heavy minerals. The organic matter and carbonate contents of this unit range from 0.19% to 2.21% and from 0% to 2.21%, respectively. The fine to very fine sands are well to moderately well sorted. Their grain size distributions show a wide range of skewness and are positive to very positive with regards to their kurtosis.

Unit V (Figures 5-10; Tables 1 and 2)

The thicknesses of the unit ranging from 5 to 58 cm. It should be noted that the thickness of the unit in core 8 and core 9 cannot be the minimal thickness. This unit is characterized by brown to rusty sand, with some parts showing a rusty mottled characteristic. It also contains remains of marine organisms (*Ocypode ceratophthalmus*: a kind of marine crab), which occur as concretions distributed throughout the layer (Figure 7). The boundary to the overlying Unit IV is of

gradational nature while the boundary to the underlying unit VI is erosional. Normal and reverse grading are observed.

The sediments are comprised of 96–99% quartz, 1–3% bioclasts and 1–2% heavy minerals. The organic matter and carbonate contents of the sediments in this unit range from 0.6% to 1.7% and from 0.2% to 3.7%, respectively. The fine to very fine sands which are well to moderately well sorted have a grain size distribution which is near symmetrical to very fine skewed. The kurtosis is of very leptokurtic nature.



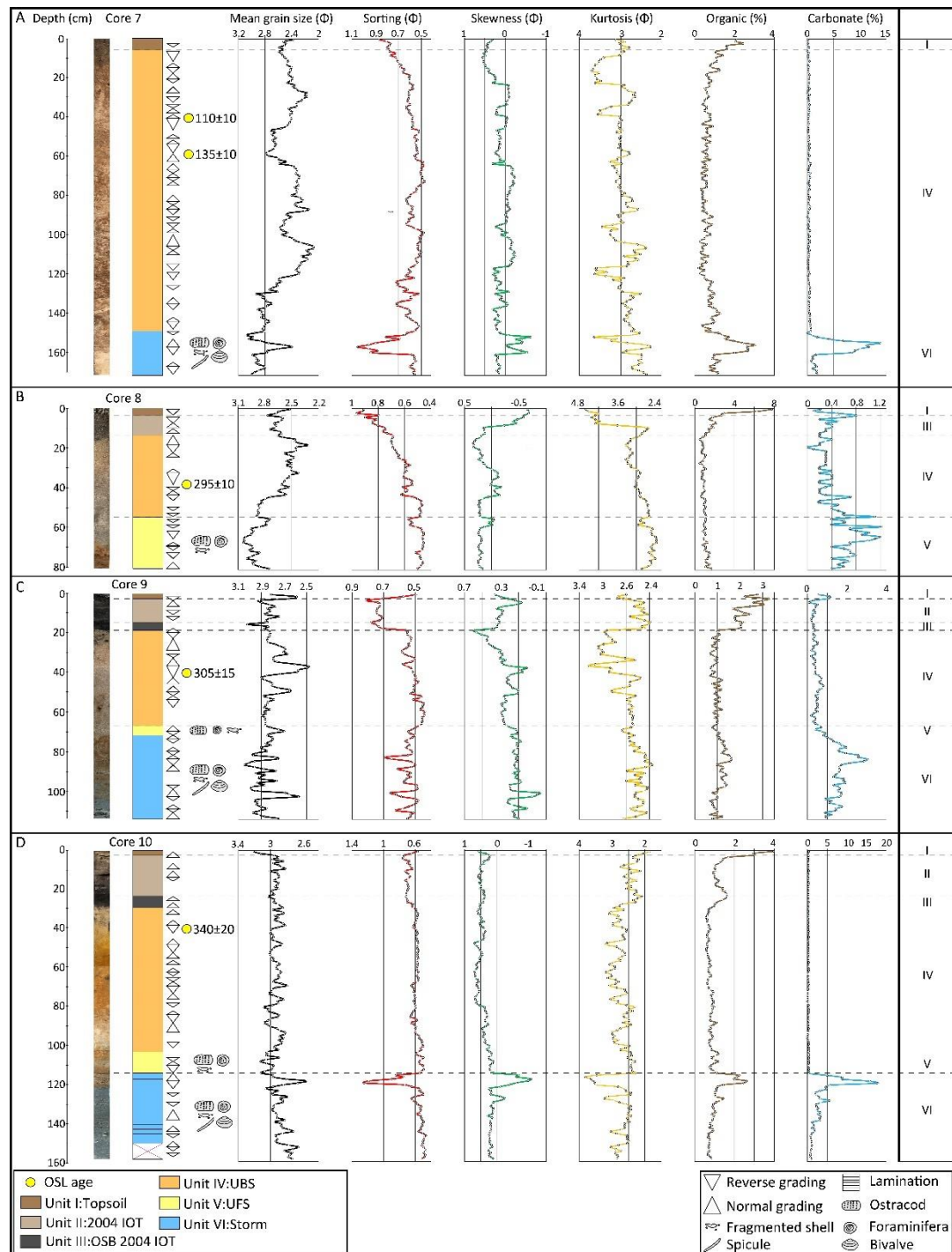


Figure 9 Stratigraphic sequence, grain size distribution and composition data of cores of transect 1. The MMS sediments are identified in core 1. The topsoil layer (Unit I) is recognized in cores 1, 3 and 4. The IOT 2004 layer (Unit II) is identified in cores 2 and 4. The OSB 2004 IOT layer (Unit III) is observed in cores 2 and 4. The UBS layer (Unit III) is recognized in cores 2, 3 and 4. The UFS layer (Unit V) is recognized in cores 2, 3 and 4. The storm layer is identified in cores 2, 3 and 4. MMS, monsoon-driven storm

surges; 2004 IOT, 2004 Indian Ocean Tsunami; OSB, old surface before Indian Ocean Tsunami; UBS, upper backshore sediment; UFS, upper foreshore sediment.

Unit VI (Figures 5-10; Tables 1 and 2)

The thickness of the unit ranging from 3 to 58 cm. It should be noted that the thickness of the unit in cores 2 and 3 represents a minimum thickness. This unit is characterized by brown to grey sand transitions between oxidizing and reducing environments are visible in several cores. Generally, the upper boundary of the unit is gradual to the overlying Unit V while a sharp erosional upper contact is observed in core 10. The sedimentary structures include laminated sands and fragmented shell layers. Normal and reverse grading were observed. Numerous remains of marine organisms were also identified such as bivalves, gastropod, scaphopod, spicule, foraminifera, ostracods and radiolarian.

The main composition of the sediments is 82–98% quartz, 1–17% bioclasts and 1–2% heavy minerals. The organic matter and carbonate contents range from 0.7% to 5.7% and from 0.7% to 17.6%, respectively. The sediments of this unit are fine to very fine sands which are poorly to well sorted. The grain size distributions exhibit a wide range of skewness and are very leptokurtic to extremely leptokurtic.

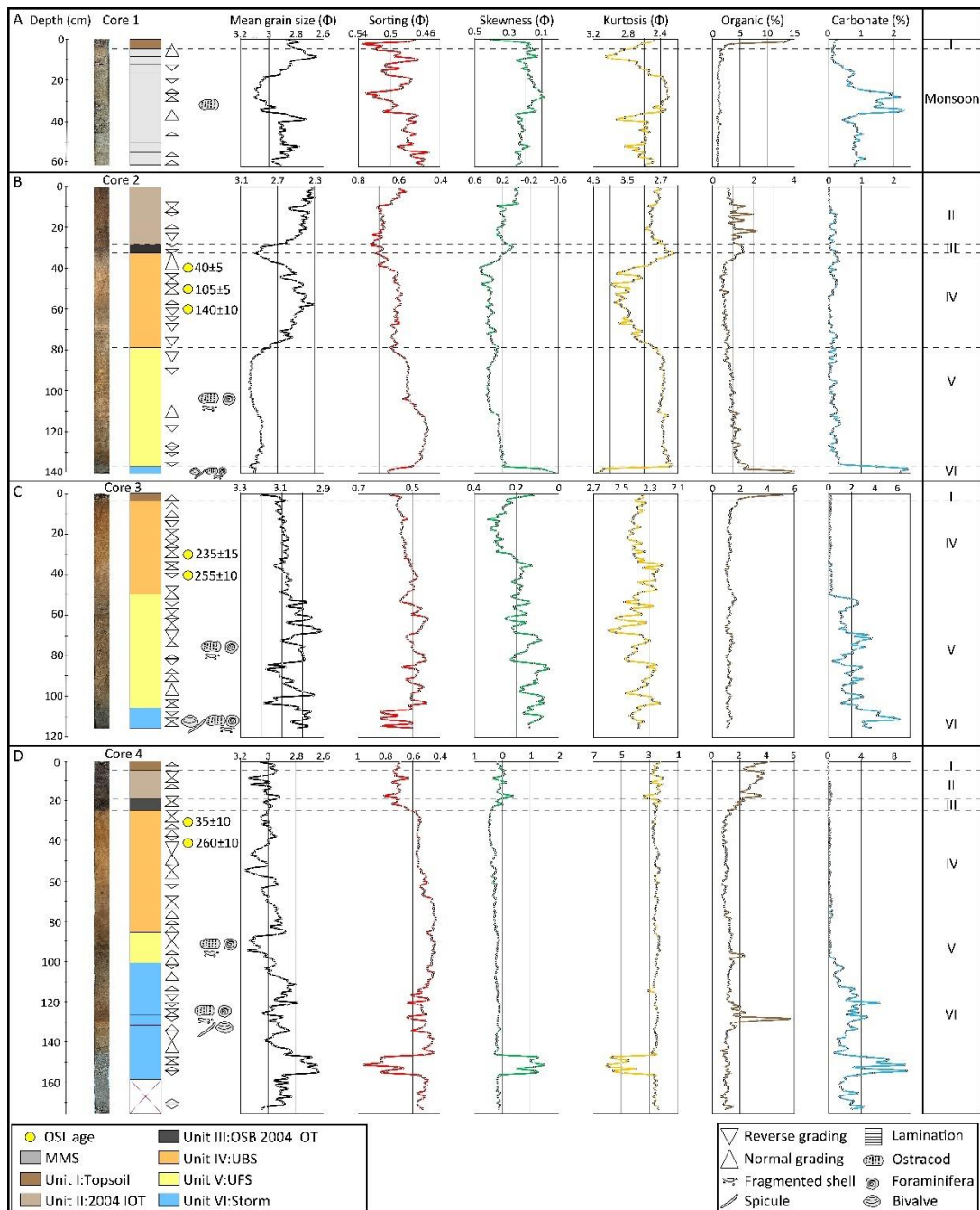


Figure 10 Stratigraphic sequence, grain size distribution and composition data of cores of transect 3. (A) core 7, (B) core 8, (C) core 9 and (D) core 10. The topsoil layer (Unit I) is recognized in cores 7, 8, 9 and 10. The IOT 2004 layer (Unit II) is identified in cores 8, 9 and 10. The OSB 2004 IOT (Unit III) is observed in cores 9 and 10. The UBS layer (Unit III) is recognized in cores 7, 8, 9 and 10. The UFS layer (Unit V) is recognized in cores 8, 9 and 10. The storm layer is identified in cores 7, 9 and 10.

2004 IOT, 2004 Indian Ocean Tsunami; OSB, old surface before Indian Ocean Tsunami; UBS, upper backshore sediment; UFS, upper foreshore sediment

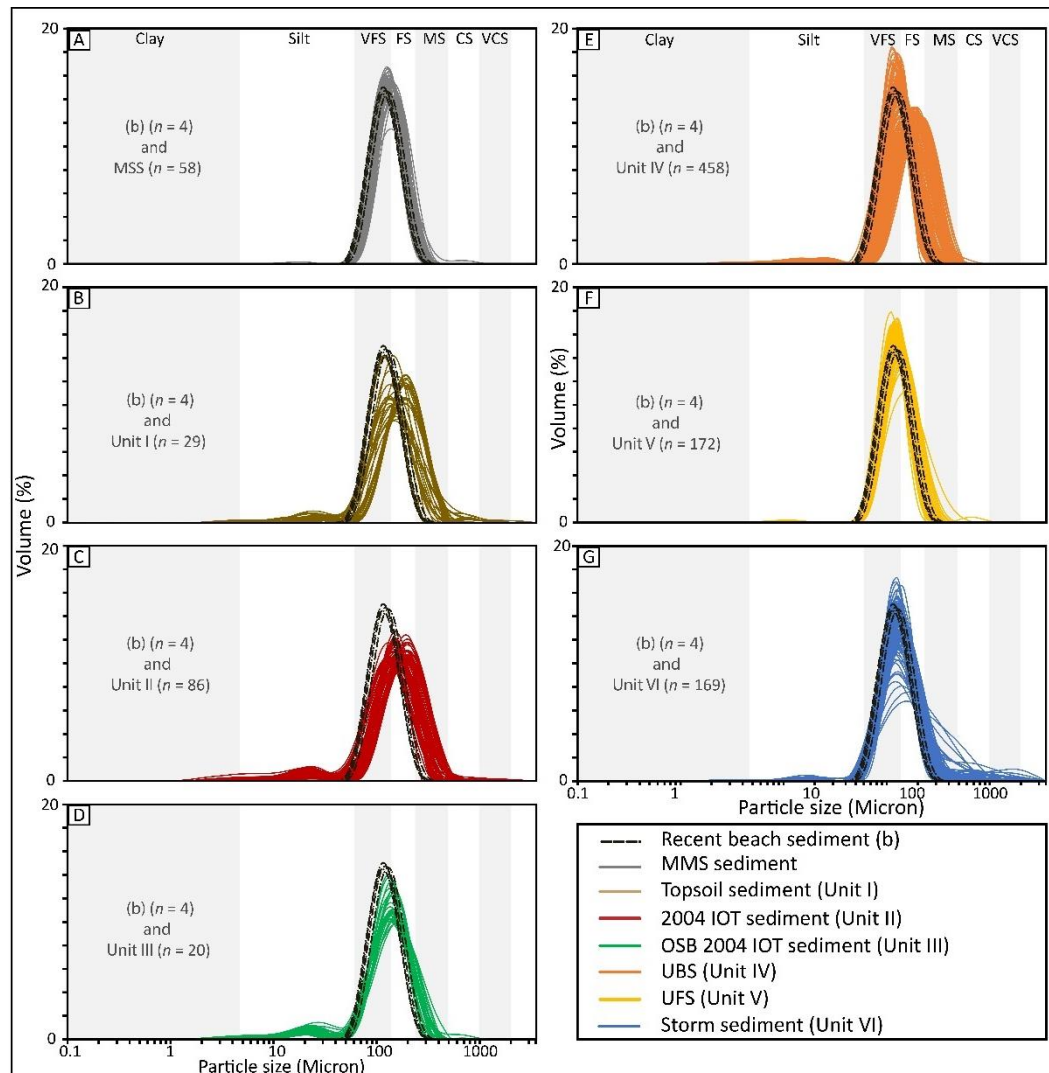


Figure 11 Comparison on grain size distribution curves of the recent beach sediments and various sediments from the study area. (A) Recent beach sediment ($n=4$) and MMS sediments ($n=58$), (B) Recent beach sediment ($n=4$) and Unit I: topsoil sediments ($n=29$), (C) Recent beach sediment ($n=4$) and Unit II: 2004 IOT sediments ($n=86$), (D) Recent beach sediment ($n=4$) and Unit III: OSB 2004 IOT sediments ($n=20$), (E) Recent beach sediment ($n=4$) and Unit IV: UBS ($n=458$), (F) UFS ($n=4$) and Unit V: paleo-beach sediments ($n=172$), (G) Recent beach sediment ($n=4$) and Unit VI: storm sediments ($n=169$). Grain size distributions of the monsoon sediments, Unit IV, V, and VI are similar to the distribution of grain sizes at the present day beach. In contrast,

the grain size distribution of Unit I and II show a shift towards coarser grain sizes. MMS, monsoon-driven storm surges; 2004 IOT, 2004 Indian Ocean Tsunami; OSB, old surface before Indian Ocean Tsunami; UBS, upper backshore sediment; UFS, upper foreshore sediment.

4.1.3 Comparison on grain size distribution curves

In this section, we compare the grain size distribution curves of all sediments in each unit with the curves of the recent shore-normal beach samples (Figure 11). All of four recent beach sediment samples show a unimodal distribution of fine and very fine sand. The monsoon-driven storm surges sediments show very similar grain size distribution to the recent beach sediments, exhibiting the same unimodal distribution (Figure 11A). Units I to II exhibit a bimodal grain size distribution, with the majority of grains ranging from fine to very fine sand while a small proportion of the grains are of silt size (Figures 11B-D). The peak of silt sized grains is much less pronounced in Unit IV (Figure 11E), where the majority of grains are very fine to fine sand size and the bimodality of the distribution becomes less pronounced. Unit V exhibits a unimodal distribution very similar to the recent beach sediments (Figure 11F) while Unit VI displays a trimodal distribution with a major mode in the range of fine to very fine sand and two minor modes in the range of silt and medium to coarse sand.

Table 3 Summary of the results of OSL dating in Laem Son area with the concentration of a dose-relevant element (K, Th, and U), measured sediment moisture, the total dose rate (D), observed overdispersion (od), the applied age model (CAM = central age model; MAM = minimum age model), mean D_e , and resulting OSL age.

Sample	Depth (cm)	K (%)	Th (ppm)	U (ppm)	Th (ppm)	Water (%)	D (Gy ka ⁻¹)	n	od	Model	D_e OSL (Gy)	Age (yr)
D1-1	40	0.29 ± 0.01	13.46 ± 0.11	3.55 ± 0.01	13.46 ± 0.11	19.5	0.614 ± 0.01	20/18	0.21	CAM	0.07 ± 0.01	40 ± 5
D1-2	50	0.23 ± 0.01	21.90 ± 0.16	5.76 ± 0.02	21.90 ± 0.16	19.9	0.517 ± 0.01	20/19	0.07	CAM	0.29 ± 0.01	105 ± 5
D1-3	60	0.27 ± 0.01	16.30 ± 0.12	4.66 ± 0.02	16.30 ± 0.12	19.6	0.605 ± 0.01	20/18	0.20	CAM	0.31 ± 0.02	140 ± 10
D2-1	30	0.57 ± 0.01	6.50 ± 0.06	1.47 ± 0.01	6.50 ± 0.06	23.3	0.497 ± 0.01	20/18	0.21	CAM	0.30 ± 0.02	235 ± 15
D2-2	40	0.62 ± 0.01	5.59 ± 0.05	1.11 ± 0.01	5.59 ± 0.05	27.4	0.481 ± 0.01	20/19	0.14	CAM	0.30 ± 0.01	255 ± 10
D3-1	30	0.60 ± 0.01	4.76 ± 0.05	1.05 ± 0.01	4.76 ± 0.05	25.2	0.743 ± 0.01	20/16	0.44	MAM	0.04 ± 0.01	35 ± 10
D3-2	40	0.38 ± 0.01	8.73 ± 0.07	2.01 ± 0.01	8.73 ± 0.07	24.8	0.970 ± 0.01	20/19	0.20	CAM	0.35 ± 0.02	260 ± 10
D4-1	40	0.35 ± 0.01	6.62 ± 0.06	1.49 ± 0.01	6.62 ± 0.06	7.1	0.738 ± 0.01	20/20	0.33	MAM	0.14 ± 0.01	110 ± 10
D4-2	60	0.26 ± 0.01	7.89 ± 0.07	2.04 ± 0.01	7.89 ± 0.07	17.1	0.738 ± 0.01	20/20	0.08	CAM	0.17 ± 0.01	135 ± 10
D5	40	0.28 ± 0.01	11.19 ± 0.09	2.41 ± 0.01	11.19 ± 0.09	24.1	0.738 ± 0.01	20/18	0.14	CAM	0.44 ± 0.02	295 ± 15
D6	40	0.41 ± 0.01	4.13 ± 0.05	0.68 ± 0.01	4.13 ± 0.05	32.0	0.738 ± 0.01	20/18	0.21	MAM	0.25 ± 0.01	305 ± 15
D7	40	0.28 ± 0.01	5.88 ± 0.06	1.50 ± 0.01	5.88 ± 0.06	24.2	0.738 ± 0.01	20/19	0.20	CAM	0.38 ± 0.02	340 ± 20

D, dose rate; n, used number of aliquots per accepted number of aliquots; od, over dispersion; and D_e , equivalent dose of OSL. Ages rounded to 5 years and water content = ±10%.

4.1.4 Optically stimulated luminescence dating

The location of all 12 OSL samples in the Laem Son area is presented in Figures 1C and 3C-E and the dating results are summarized in Table 3. It is noted that all OSL samples were determined for the upper backshore sediment (UBS) layer (Unit IV) below the 2004 IOT layer. In transect 1 (Figures 3D and 5), three locations with OSL samples were designated as D1, D2 and D3. Location D1 consists of three OSL samples (D1-1, D1-2 and D1-3) stacked at different depth (40 cm, 50 cm and 60 cm). These yield OSL ages of 40±5 yr, 105±5 yr and 140±10 yr, respectively. Location D2 comprises two OSL samples (D2-1 at 30 cm and D2-2 at 40 cm) with depositional ages of 235±15 yr and 255±10 yr, respectively. The sample at location D3 (D3-1 = 30 cm and D3-2 = 40 cm) has ages of around 35±10 yr and 260±10 yr, respectively.

In transect 3 (Figures 3E and 6), four locations of with OSL samples were designated as D4, D5, D6 and D7. Location D4 comprises two OSL samples (D4-1 = 40 cm and D4-2 = 60 cm) with ages 110 ± 10 yr and 135 ± 10 yr, respectively. OSL samples D5, D6 and D7 (all taken 40 cm below the surface) shown depositional ages of 295 ± 15 yr, 305 ± 15 yr and 340 ± 20 yr, respectively.

4.2 Hoa Duan area, Thua Thien Hue, central Vietnam

Based on stratigraphical correlation, the three percussion cores (VN1, VN2, and VN3) collected from the Hoa Duan barrier were used to establish lithological correlations with reference to the stratigraphy, lithology, color, sedimentary structures, type of sediment, grain size, grading, and percentage of organic, carbonate, and microfossil contents (Figures 12-15). Core VN1, taken from the seaward side behind a sandy ridge about 100 m from the sea, was 147-cm long, whereas VN2, the longest core (200 cm), was taken from the center of the barrier, around 50 m from VN1 and provided the clearest picture of several events in the Hoa Duan area. Core VN3 (162-cm long) was taken from the landward side of the barrier, adjacent to the lagoon. Following stratigraphic correlation, deposition in Hoa Duan can be divided into seven units as follows (Figure 12): Unit I: sandy topsoil; Unit II: storm layer; Unit III: fluvial flood; Unit IV: storm layer; Unit V: fluvial flood; Unit VI: storm layer, and Unit VII: storm layer. A more detailed description is given below. The

composition, LOI, roundness, sphericity data, and the values of the statistical parameters (mean, sorting, skewness, and kurtosis) are presented in Tables 4 and 5.

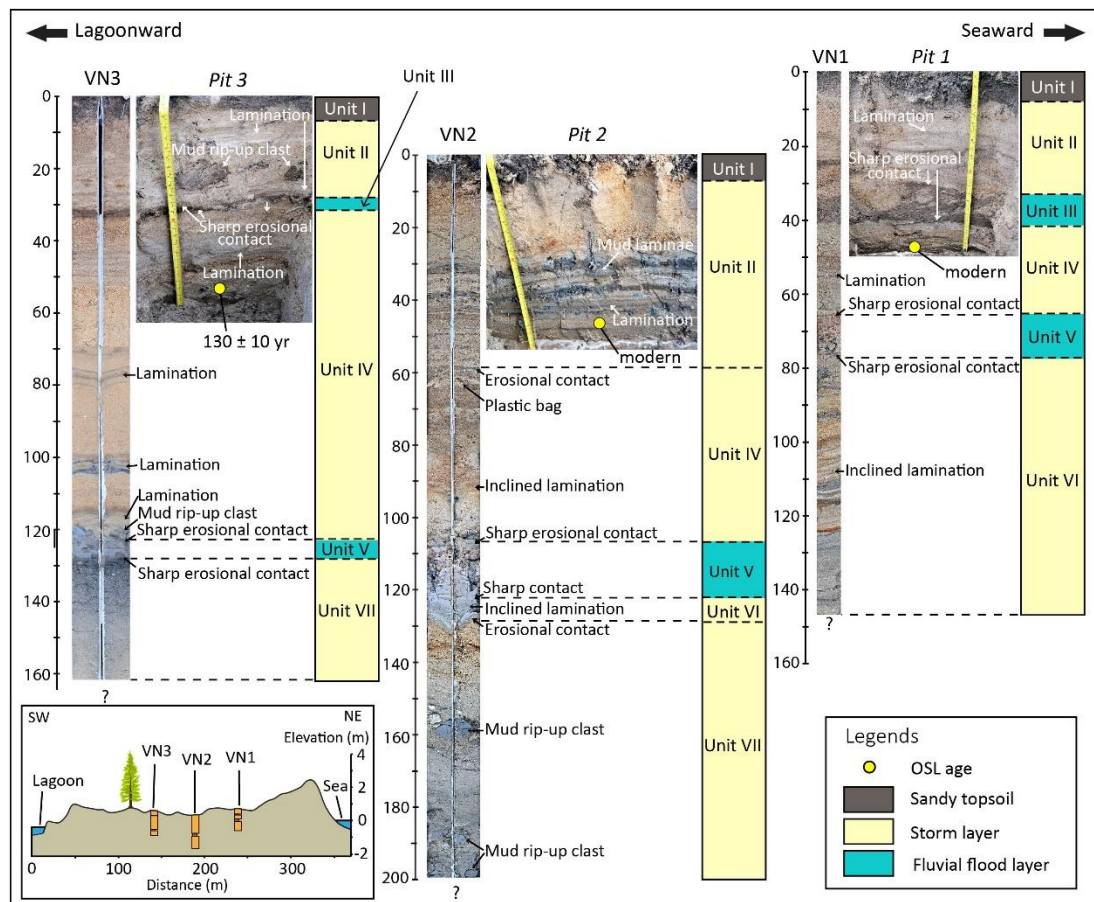


Figure 12 Cores VN1, VN2, and VN3 and pits of VN1, VN2, and VN3 represent the units of deposition between the storm and fluvial flood layers with the dominant sedimentary structures. Units II, IV, VI, and VII, which were considered to be the storm layers, mostly contained sharp basal contact and inclined and parallel lamination, whereas Units III and V, classified as the fluvial flood layers, were characterized as a mud grain layer with sharp, erosional top, and bottom contacts. The absence of the fluvial flood layer (Unit III) in core VN2 and Pit VN2 resulted from the erosion of the storm event in Unit II. Note that the distance interval of each core is 50 m, and the elevation of cores is based on the topographic elevation. A yellow circle in Pit 1, Pit 2, and Pit 3 indicates the OSL ages, whereas the modern age in Pit 1 and Pit 2 means less than 100 years (Kongsen et al., 2021b).

4.2.1 Sediment characteristics of modern beach deposits

The recent beach samples b1 and b4 (see Figure 2 for location) were collected to examine the shore-normal processes. These were classified as coarse-grained sand (0.73 and 0.92 phi, respectively), while the mean grain sizes of b2 and b3 indicate a medium-grained sand composition (1.50 and 1.16 phi, respectively). Sorting values of all shore-normal process samples (b1, b2, b3, and b4) were slightly different (Tables 4 and 5), where b1 was a moderately sorted sand (0.74 phi), b2 was a well-sorted sand (0.46 phi), and b3 and b4 were moderately well-sorted sand (0.52 and 0.64 phi, respectively). The skewness of b1 was -0.23 phi, which is very coarse skewed. Samples b2 and b3 were 0.27 and 0.22 phi, respectively, which identifies them as fine skewed. Sample b4 had a phi value of -0.05, which is nearly symmetrical. Kurtosis values of the shore-normal process samples b1, b2, b3, and b4 were 2.99, 2.38, 2.80, and 2.98 phi, respectively, which are all very leptokurtic. Organic (0.23–0.86%) and carbonate (0.44–0.69%) contents were relatively low and varied little across the four samples (Tables 4 and 5). Shore-normal process sediment samples b1, b2, b3, and b4 were composed of quartz, rock fragments, heavy minerals, fragmented shells, and microfossils (such as foraminifera). No ostracods were found in the recent beach samples. Quartz is the major component, forming up to 96% of the samples (Tables 4 and 5). Rock fragments, shell fragments, and marine microfossil contents were all relatively low, at around 1% (w/w) each. The number of foraminifera was low too. At least three species of foraminifera were present in each

sample, mainly *Quinqueloculina auberiana* and *Cellanthus craticulatus*. The sphericity of these samples was relatively similar, with b1 and b3 being characterized as high sphericity, while b2 and b4 were characterized as low sphericity. Roundness was also similar across all the samples, with subangular, subrounded, and rounded grains.

Table 4 The values of sediment composition, grain properties, LOI, sphericity and roundness of various sediments (Kongsen et al., 2021b).

Sediment types	Quartz (%)	Bio clast (%)	Rock fragment (%)	Heavy mineral (%)	Organic (%)	Carbonate (%)	Sphericity	Roundness
b1	97	1	1	1	0.23	0.69	Low	Sub-angular to rounded
b2	96	1	2	1	0.36	0.44	Low	Sub-angular to rounded
b3	98	0	1	1	0.54	0.54	Low	Sub-angular to rounded
b4	97	1	1	1	0.86	0.61	Low	Sub-angular to well-rounded
Topsoil (Unit I)	97-98	0	1-2	1-3	0.67-6.68	0.01-0.24	Low to high	Angular to well-rounded
Storm (Unit II)	90-98	0-5	2-5	1	0.32-1.92	0.01-1.33	Low to high	Very angular to well-rounded
Fluvial flood (Unit III)	94-97	0	2-5	1	0.35-5.49	0.05-1.41	Low to high	Angular to rounded
Storm (Unit IV)	94-97	0-2	1-3	0-2	0.20-1.54	0.01-1.15	Low to high	Very angular to well-rounded
Fluvial flood (Unit V)	96-97	0	2-3	2	2.27-22.51	0.45-2.14	Low	Very angular to sub-rounded
Storm (Unit VI)	92-98	0-5	1-2	1-2	0.09-3.89	0.02-1.12	Low to high	Very angular to well-rounded
Storm (Unit VII)	94-98	0-3	1-2	1-2	0.21-2.58	0.01-0.63	Low to high	Angular to well-rounded

Note that the detailed composition of fluvial flood sediments (Units III and V) come from sand materials.

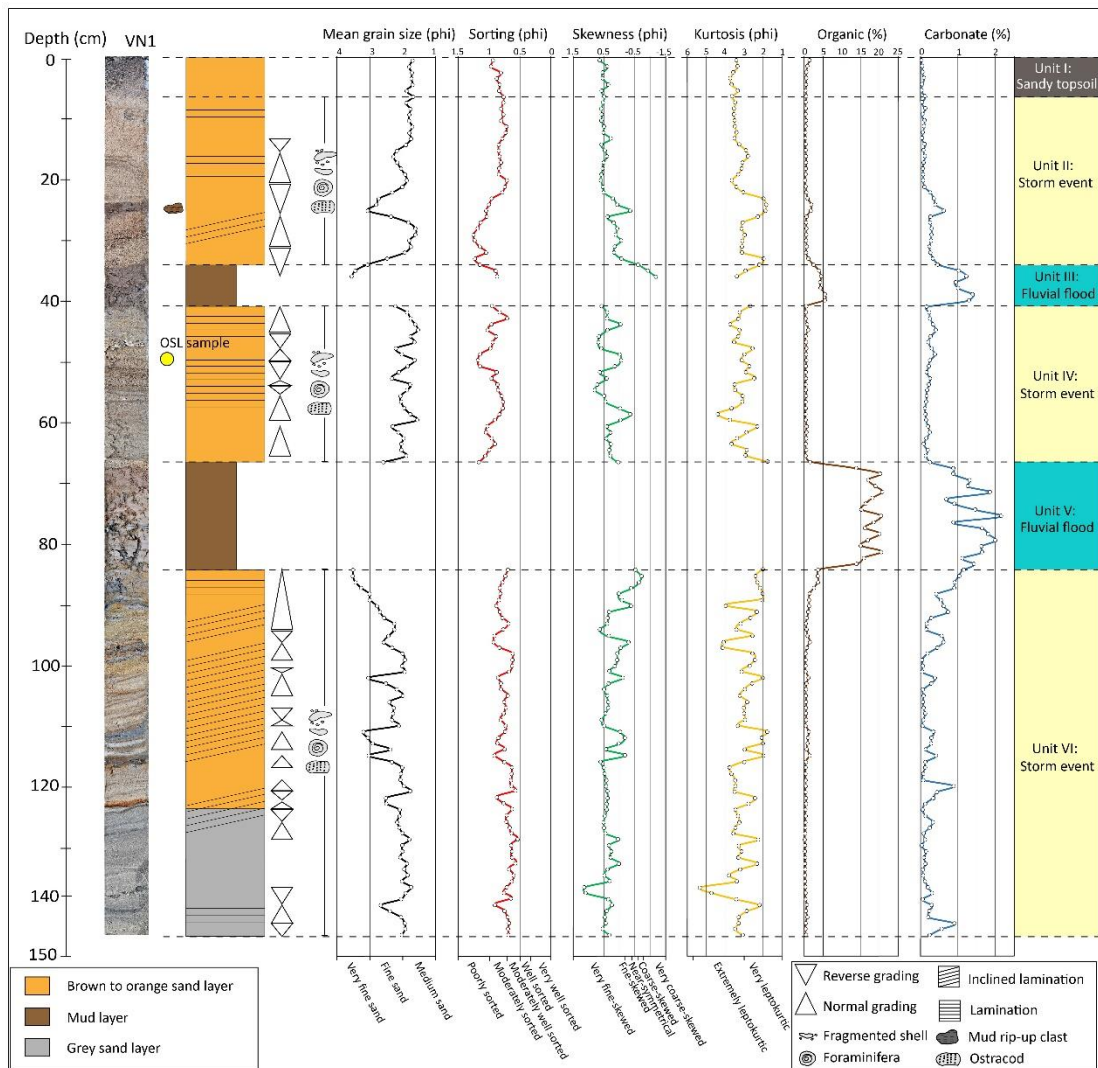


Figure 13 Stratigraphy of core VN1 with vertically plotted grain size parameters (mean, sorting, skewness, and kurtosis) and LOI (organic and carbonate contents) showing the unit of the storm and fluvial flood layers. Storm layers in Units II, IV, and VI mostly exhibited the set of normal and reverse grading with relatively low organic and carbonate contents, whereas the fluvial flood layer of Units III and V showed high organic and carbonate contents at 33-41-cm and 67-84-cm depths, respectively (Kongsen et al., 2021b).

4.2.2 Sedimentological characteristics of each unit

Unit I: Sandy

Topsoil The sandy topsoil of each core was limited by a black organic sand layer of 0-9 cm (Figures 12–15), with a gradational contact at 9 cm in VN2 and at 8 cm in VN3, respectively. Internal structures, such as normal and reverse grading, were present in VN2. The thickness of the sandy topsoil in VN1, VN2, and VN3 was 7, 8, and 7 cm, respectively. The mean grain size of the sandy topsoil was between 1.47 and 2.89 phi, classified as medium- to fine-grained sand. This layer was moderate to poorly sorted, from 0.92 to 1.60 phi, and the skewness varied between -0.74 and 1.60 phi. All samples were very finely skewed, except for two samples in VN1, one of which was very coarse skewed (-0.74 phi), and the other was finely skewed (0.24 phi). Kurtosis of Unit I ranged from 2.09 to 5.10 phi, and so was very to extremely leptokurtic. The organic and carbonated content of this unit ranged from 0.67 to 6.68% and 0.01 to 0.24%, respectively.

Unit I (Sandy topsoil) is the uppermost layer, and so was regarded as the most recent. This topsoil layer was comprised of quartz, rock fragments, and heavy minerals covered with the remains of leaf litter. There were no bioclasts, such as fragmented shells, marine fossils, or microfossils (foraminifera and ostracods) in this unit. Quartz was the main component, accounting for up to 97%, with rock fragments and heavy minerals, making up the remaining 1 to 3%. Most samples had a low to high sphericity, except for one from VN3, which showed low sphericity. Roundness

ranged from angular to well-rounded grains, except for VN1, which did not have rounded or well-rounded grains.

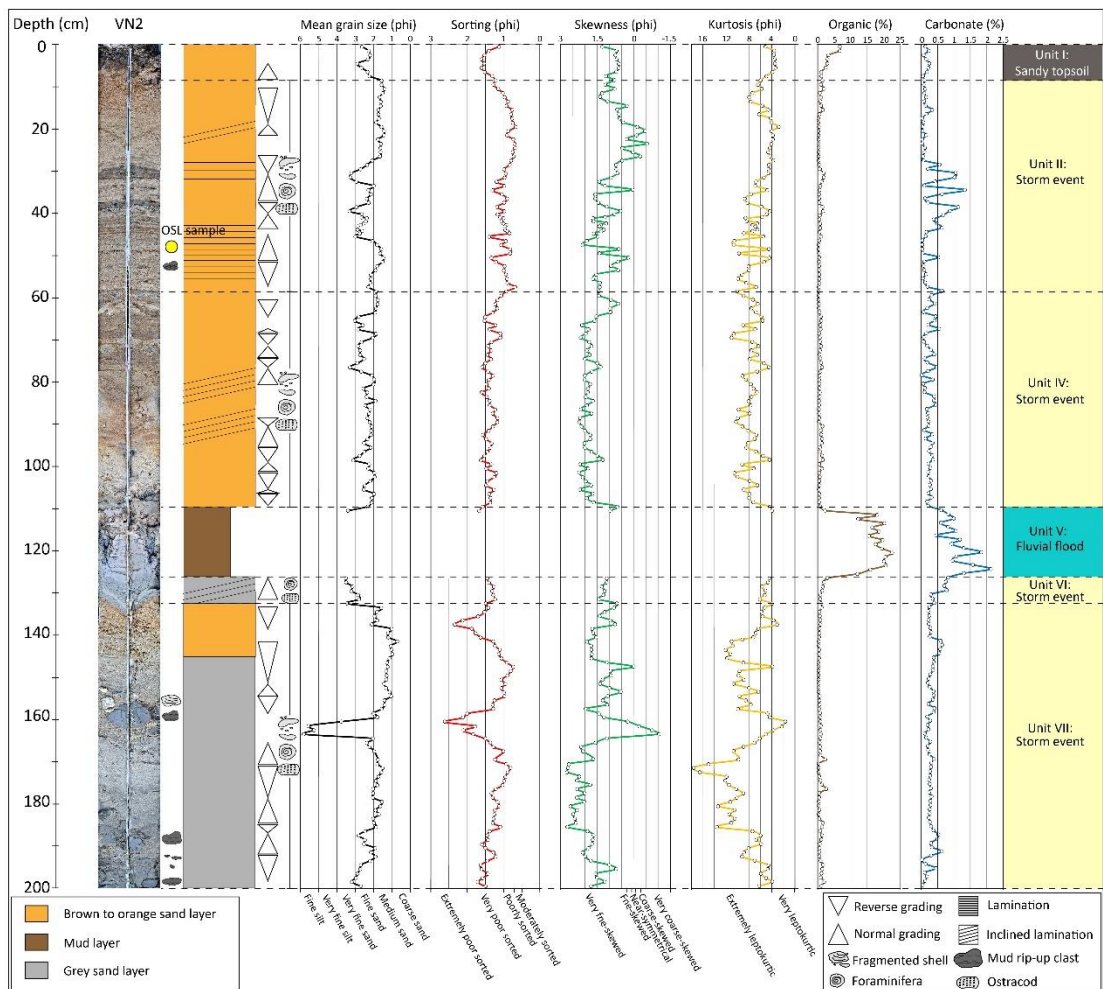


Figure 14 Stratigraphy of core VN2 with vertically plotted grain size parameters (mean, sorting, skewness, and kurtosis) and LOI (organic and carbonate contents) showing the unit of the storm and fluvial flood layers. Storm layers in Units II, IV, VI, and VII mostly exhibited the set of normal and reverse grading with relatively low organic and carbonate contents, whereas Unit V was interpreted as the fluvial flood layer and showed high organic and carbonate contents at a 110-127-cm depth (Kongsen et al., 2021b).

Unit II: Storm Layer

This layer mainly consisted of quartz, bioclasts (fragmented shells, foraminifera, and ostracods), rock fragments, and heavy minerals. Quartz was still the main component of this unit, similar to Unit I, with up to 90% quartz, while 1 to 5% of bioclast was present and was classified as several species of foraminifera in high concentrations (2,335 counts) with a low number of ostracods (41 counts). Bivalves and gastropods were also observed in this unit. Rock fragments and heavy minerals accounted for 1 to 2%. The sphericity ranged from low to high, with low sphericity in VN2 and VN3 and no high sphericity in VN1. Roundness ranged from very angular to well-rounded grains, the majority of which were angular to subrounded. Very angular grains were present in VN2 and VN3, while well-rounded grains were only found in VN2.

A layer of light brown to orange sand was observed at 8 to 33 cm depth in VN1, 9-59 cm in VN2, and 8-32 cm in VN3 (Figures 12-15). The thicknesses of these layers in VN1, VN2, and VN3 were 25, 50, and 26 cm, respectively. In VN1 and VN3, this layer contained a cobble-sized MRC at 26 to 27 cm depth and 23 to 25 cm depth, respectively. Mud laminae were present in VN2 at 30 to 46 cm depth. Cross and parallel lamination with fragmented shells was found in VN1, VN2, and VN3 at 16-30, 19-23, and 18-29 cm, respectively. Note that VN1 seemed to have two mud layers at 22 to 23 cm and 33 to 42 cm depth, but, actually, the top mud layer was part of the eroded mud layer of Unit III (Figure 12). The contacts of this layer with the

topsoil layer above were gradational. Sharp erosional contacts with the mud layer below were found at the base of Unit II. The mean grain sizes in this unit ranged from 0.96 to 3.32 phi, indicating medium to fine to very fine sand. This unit was poorly sorted, moderately sorted, and moderately well sorted, ranging from 0.66 to 1.40 phi. Grain size distributions were very fine skewed, fine skewed, near symmetrical, coarse skewed, and very coarse skewed, ranging between -0.53 and 2.07 phi. Kurtosis was between 1.83 and 10.63 phi, and so very to extremely leptokurtic. Organic and carbonate contents were 0.32-1.92 and 0.01-1.33%, respectively.

Unit III: Fluvial flood layer

A dark brown mud layer was observed at a depth of 33-41 cm in VN1 and 32-34 cm in VN3 (Figures 12, 13, 15, 16), but was not present in VN2. The layer was 8- and 2-cm thick in VN1 and VN3, respectively. Its sedimentary structures were limited to sharp erosional contacts between the coarser-grained sediments of Units II and IV. Although this layer mainly contained mud throughout its entire thickness and could be visually classified, some small parts of this layer, especially at the top of the layer, were composed of sand. The sandy sediment was comprised of quartz, rock fragments, and heavy minerals, at 94-97, 2-5, and 1%, respectively. The sphericity was low to high, and the roundness ranged from angular to rounded. Mean grain sizes of this sand were between 3.1 and 3.71 phi, indicating very fine sand. Sorting values varied between 0.73 and 1.15 phi, indicating poorly sorted and moderately sorted sand. Skewness ranged from -1.26 to -0.6 phi, showing very coarse-skewed

distributions, while the Kurtosis ranged from 2.10 to 3.59 phi, reflecting very to extremely leptokurtic distributions. The organic and carbonate content of this unit varied from 0.35-5.5 to 0.05-1.41%, respectively.

Table 5 The values of grain size distribution parameters and sedimentary structures for each stratigraphic unit (Kongsen et al., 2021b).

Sediment types	Mean (phi)	Sorting (phi)	Skewness (phi)	Kurtosis (phi)	Sedimentary structure
b1	0.73	0.73	-0.23	2.99	-
b2	1.5	0.46	0.27	2.38	-
b3	1.16	0.51	0.22	2.8	-
b4	0.92	0.64	-0.05	2.98	-
Topsoil (Unit I)	1.47 - 2.89	0.92 - 1.60	0.36 - 1.29	2.09 - 5.10	Gradational bottom contact, normal and reverse grading
Storm (Unit II)	0.96 - 3.32	0.66 - 1.40	-0.53 - 2.07	1.83 - 10.63	Gradational top contact, sharp erosional bottom contact, mud rip-up clast, mud laminae, lamination, cross lamination, normal and reverse grading
Fluvial flood (Unit III)	3.10 - 3.71	0.73 - 1.15	-1.26 - -0.60	2.10 - 3.59	Sharp erosional top and bottom contact
Storm (Unit IV)	0.64 - 3.30	0.60 - 1.62	-0.38 - 2.24	1.81 - 10.97	Sharp erosional top and bottom contact, lamination, normal and reverse grading
Fluvial flood (Unit V)	3.32 - 3.39	0.85 - 1.67	-0.51 - 0.96	2.16 - 3.98	Sharp erosional top and bottom contact
Storm (Unit VI)	1.76 - 3.55	0.54 - 1.47	-0.71 - 1.44	1.78 - 6.13	Sharp erosional top contact, erosional bottom contact, lamination, normal and reverse grading, wedge sharp profile
Storm (Unit VII)	0.69 - 3.20	0.55 - 2.34	-0.53 - 2.70	2.17 - 17.58	mud rip-up clast, normal and reverse grading

Note that the detailed composition of fluvial flood sediments (Units III and V) come from sand materials.

Unit IV: Storm Layer

The unit was comprised of quartz, bioclasts, rock fragments, and heavy minerals, which accounted for 94-98, 0-2, 1-2, and 1-2%, respectively. Marine fossils (bivalves and gastropod) and microfossils (foraminifera and ostracods) were also found in this unit. The sphericity of this unit covered the whole range (low and high sphericity), as did its roundness (very angular to well-rounded grains).

A dark to light brown sand layer was present at a depth of 41-67 cm in VN1, 59-110 cm in VN2, and 34-123 cm in VN3 (Figures 12–15), and was characterized as fine- to coarse-grained sand. The thicknesses of this layer in VN1, VN2, and VN3 were 26, 51, and 89 cm, respectively. The sedimentary structures inside consisted of parallel and incline lamination with fragmented shells at 42-57 cm depth in VN1 (Figure 16), 92-97 cm in VN2, and 43-52, 70-80, and 100-122 cm depth in VN3. Moreover, a plastic bag fragment was recognized in VN2 at 63 cm depth. A pebble-sized MRC was visually identifiable at the base of this sand layer in VN3 at 122 cm depth with sharp erosional contacts.

Internal structures, such as coarsening and upward fining, were also observed. Mean grain sizes ranged from 0.64 to 3.30 phi, indicating coarse, medium, fine, and very fine sand. Sorting values were between 0.60 and 1.62 phi, in the range of poorly, moderately, and moderately well-sorted sand. Distributions were very coarse skewed, fine skewed, very fine skewed, and near symmetrical, ranging between -0.38 and 2.24 phi. Kurtosis varied between 1.81 and 10.97 phi. Organic and

carbonate contents were relatively low, varying from 0.20 to 1.54% and 0.01 to 1.15%, respectively.

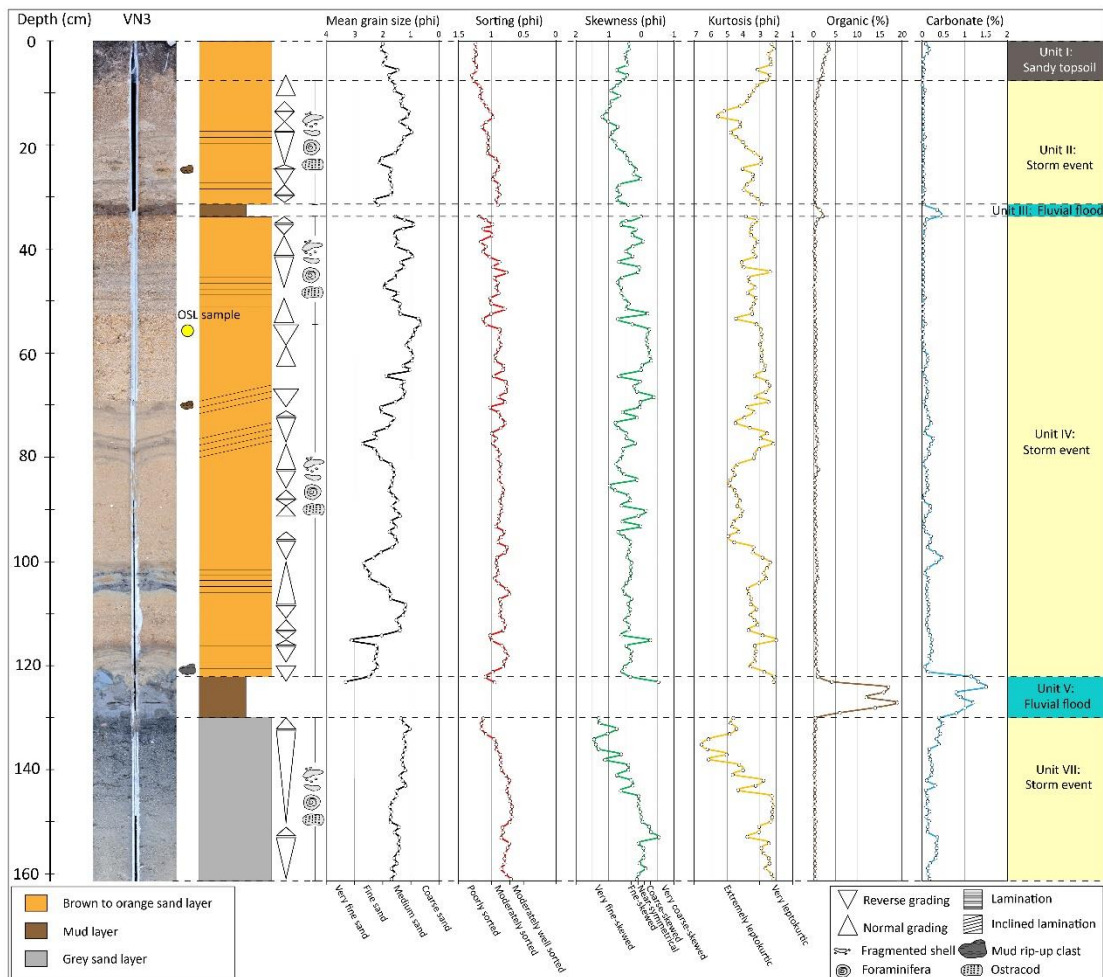


Figure 15 Stratigraphy of core VN3 with vertically plotted grain size parameters (mean, sorting, skewness, and kurtosis) and LOI (organic and carbonate content) showing the unit of the storm and fluvial flood layers. Storm layers in Units II, IV, VI, and VII mostly exhibited the sets of normal and reverse grading with relatively low organic and carbonate contents, whereas the fluvial flood layer of Units III and V showed high organic and carbonate contents at 32-34-cm and 123-130-cm depths, respectively (Kongsen et al., 2021b).

Unit V: Fluvial flood layer

A dark-brown to dark-gray mud layer was found at 67-85-cm depth in VN1, 110-127 cm in VN2, and 122-130 cm in VN3 (Figures 12–16). The thicknesses of this layer in VN1, VN2, and VN3 were 18, 17, and 8 cm, respectively. It had sharp erosional contacts with the sand layers, both above and below.

This layer was similar to the layer of Unit III, which was mainly contained mud throughout, but some small part of this layer, especially at the top, was composed of sand. The sand contained quartz, rock fragments, and heavy minerals, at 96–97, 2–3, and 2%, respectively. The sphericity was low, and the roundness varied from very angular to subrounded grains. Mean grain sizes were between 3.32 and 3.39 phi, indicating very fine sand. Sorting values ranged from 0.85 to 1.67 phi, indicating poorly and moderately sorted sand. Skewness ranged from -0.51 to 0.96 phi, indicating very fine-skewed and very coarse skewed distributions. Kurtosis ranged from 2.16 to 3.98 phi, indicating very to extremely leptokurtic distributions. Organic and carbonate concentrations were relatively high, ranging from 2.27 to 22.51% and 0.45 to 2.14%, respectively.

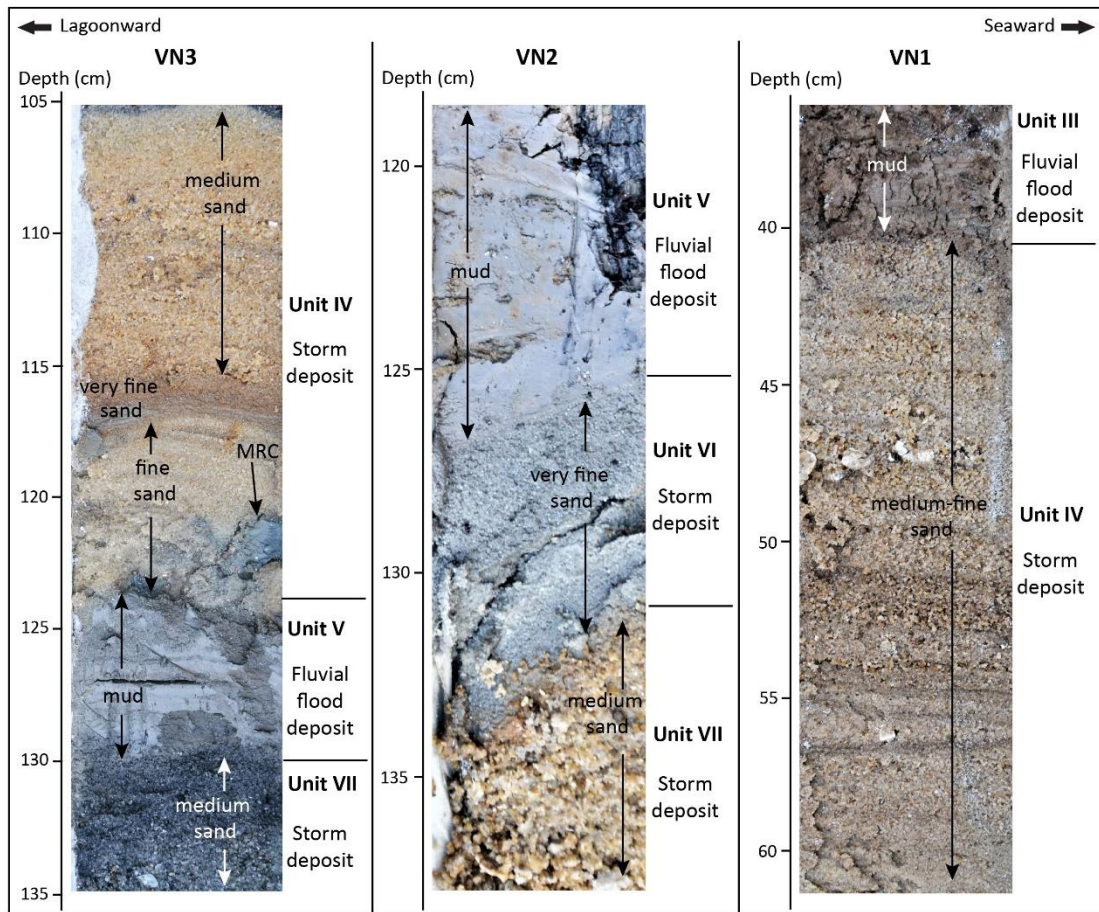


Figure 16 Close-up of the internal sedimentary structures of storm deposits and fluvial flood deposits from cores VN1, VN2, and VN3. In core VN1, a dark-brown mud layer with basal sharp contact was observed at 41-cm depth and parallel lamination of medium-fine sand with fragmented shells at 42-57-cm depth. In core VN2, a light-gray mud layer with basal sharp contact at 127-cm depth was deposited on a very fine sand layer. Then, medium sand with a sharp erosional top contact with a very fine sand layer was observed at a 133-cm depth. In core VN3, very-fine-to-medium sand with basal sharp contact and parallel lamination was observed at 115-118-cm depth plus an mud rip-up clast at 121-cm depth, and then a light-gray mud with basal sharp contact deposited on a dark-gray color with medium-grained sand (Kongsen et al., 2021b).

Unit VI: Storm Layer

The unit was composed of quartz, bioclasts, rock fragments, and heavy minerals. The sphericity of this layer was low to high. There were only three samples in VN2 with low sphericity. All classes of roundness were present, but the majority of samples were in the subangular to the subrounded range.

This unit was colorful, especially in VN1, with orange, brown, white, and gray shades. It was recognized only in VN1 (85-147 cm) and VN2 (127-133 cm), respectively (Figures 12–14 and 16), and did not appear in VN3. The thickness of the layer was 61 cm in VN1 and 6 cm in VN2, and so likely got thinner and finer landwards. Sedimentary structures were striking inclined laminations and could be observed throughout the unit, especially in VN1. The sharp erosional top contact with the muddy layer of Unit V was observed in VN1 and VN2, while a sharp bottom contact (in grain size) with a coarser sand layer was found in VN2. Mean grain size ranged from 1.76 to 3.55 phi, indicating medium, fine, and very fine sand. Sorting values were between 0.54 and 1.47 phi, indicating moderately sorted, moderately well-sorted, and poorly sorted sand. Skewness varied between -0.71 and 1.44 phi, indicating very coarse-skewed, coarse-skewed, near-symmetrical, fine-skewed, and very fine-skewed distributions. Kurtosis was between 1.78 and 6.13 phi, in the range of very and highly leptokurtic distributions. Organic and carbonate contents varied from 0.09-3.89 to 0.02-1.12%, respectively.

Unit VII: Storm Layer

The layer was composed of quartz, bioclasts, rock fragments, and heavy minerals. Its sphericity covered the whole range, from low to high. However, most samples had low sphericity. Roundness ranged from angular to well-rounded, but most samples had angular to subrounded grains.

Predominantly dark- to light-gray sand was observed in VN2 and VN3 at a depth of 136-200 cm and 130-162 cm, respectively. A small part of this unit was orange to light-gray sand, as observed at the top in VN2 (Figure 16). The thicknesses of the unit were 55 cm in VN2 and 33 cm in VN3, respectively. A pebble-sized MRC was present in VN2 at 158- to 161-cm depth, together with an oyster valve. The contacts of this layer were a sharp erosional top with very fine sand in VN2 and a muddy layer in VN3. Mean grain sizes were between 0.69 and 3.20 phi, indicating coarse to very fine sand. Sorting values ranged from 0.55 to 2.34 phi, indicating poorly sorted, moderately sorted, and moderately well-sorted sand. Skewness was -0.53 to 2.70 phi, ranging through very coarse-skewed, coarse-skewed, near-symmetrical, fine-skewed, and very fine-skewed distributions. Kurtosis varied from 2.17 to 17.58 phi, including very and extremely leptokurtic distributions. Organic and carbonate contents ranged from 0.21 to 2.58 and 0.01 to 0.63%, respectively. Moreover, four samples of the mud ball found in VN2 were sedimentologically analyzed. Their mean grain size ranged between 3.75 and 5.8 phi, indicating very fine sand and medium silt. Sorting values ranged from 1.77 to 2.62 phi, reflecting poorly

sorted and very poorly sorted sand. Skewness ranged from -0.26 to -0.97 phi, indicating fine-skewed, coarse-skewed, and very coarse-skewed distributions. Kurtosis ranged from 1.65 to 4.96 phi, including very and extremely leptokurtic distributions.

4.2.3 Comparison on grain size distribution curves

Comparisons of the grain size distribution curves of the shore-normal beach sediment and each unit found in Hoa Duan stratigraphy are presented in Figure 17. The comparative graphs of the grain size distribution curves indicated different sources from which the sediment was transported to each environmental zone. Grain size curves of the recent beach sediment clearly showed a unimodal distribution in the range of coarse to medium sand. Grain size distributions of topsoil sediments were unimodal and bimodal. The distribution of grain size curves in all samples of storm sediment (Units II, VI, and VII) and fluvial sediments (Units III and V) displayed unimodal distributions. A comparison of the grain size distribution of the shore-normal beach and other units is discussed in see section “Age of Depositional Events.”

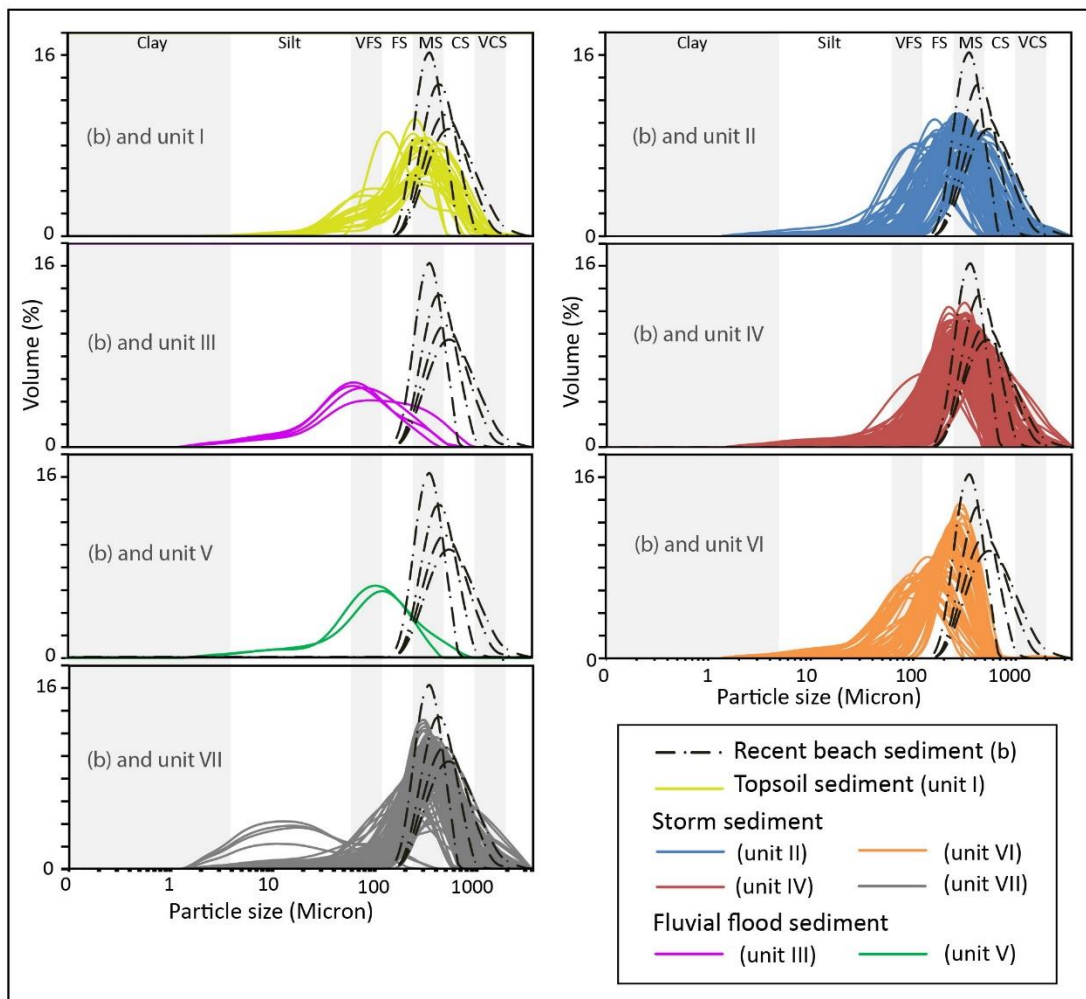


Figure 17 Plots of the grain size distribution curves of Units I–VII in comparison with the shore-normal beach deposits (b) (location in Figure 2C). The number of grain size distribution curves in each unit is as follows: recent beach ($n = 4$), Unit I ($n = 27$), Unit II ($n = 97$), Unit III ($n = 4$), Unit IV ($n = 177$), Unit V ($n = 2$), Unit VI ($n = 69$), and Unit VII ($n = 94$). The characteristic of the grain size distribution of the storm sediments shows curves that are consistent with the curves of the shore-normal recent beach sediments in the range of coarse-to-medium sand, whereas the grain size curves of the fluvial flood sediments are different, being distributed in the range of very-fine sand to silt (Kongsen et al., 2021b).

Table 6 Summary data of OSL dating in the Hoa Duan area with the concentration of dose-relevant elements (K, Th, and U), measured sediment moisture, total dose rate (D), observed overdispersion, the applied age model (CAM = central age model; MAM = minimum age model), mean D_e , and resulting age (Kongsen et al., 2021b).

Sample	Depth (cm)	U (ppm)	Th (ppm)	K (%)	Water (%)	D (Gy/ka ⁻¹)	n	od (%)	Model	D_e OSL (Gy)	Age (yr)
ST1	40	0.43 ± 0.01	1.01 ± 0.02	0.15 ± 0.001	4.1	0.50 ± 0.02	55/44	0.68	CAM	0.02 ± 0.01	modern
ST2	40	0.31 ± 0.01	1.19 ± 0.02	0.33 ± 0.001	7.2	0.63 ± 0.04	40/36	0.22	CAM	0.33 ± 0.01	520 ± 25
ST3	40	0.65 ± 0.01	2.38 ± 0.04	0.49 ± 0.001	9.3	0.91 ± 0.13	40/36	0.42	MAM	0.32 ± 0.02	350 ± 25
ST4*	40	0.44 ± 0.01	1.11 ± 0.02	0.15 ± 0.001	3.1	0.51 ± 0.17	40/34	0.69	MAM	0.03 ± 0.02	modern
ST5*	40	0.40 ± 0.01	1.08 ± 0.02	0.13 ± 0.002	3.0	0.47 ± 0.20	40/34	0.70	MAM	0.04 ± 0.02	modern
ST6*	40	0.44 ± 0.01	1.46 ± 0.03	0.42 ± 0.002	5.9	0.77 ± 0.07	42/41	0.15	CAM	0.10 ± 0.01	130 ± 10
ST7	40	0.79 ± 0.01	2.44 ± 0.04	0.35 ± 0.002	17.2	0.78 ± 0.14	42/40	0.47	MAM	0.27 ± 0.04	350 ± 50
ST8	20	0.49 ± 0.01	1.34 ± 0.03	0.36 ± 0.002	14.1	0.67 ± 0.11	44/41	0.58	MAM	0.20 ± 0.03	300 ± 50
ST8-1	40	0.47 ± 0.01	1.40 ± 0.03	0.34 ± 0.002	5.9	0.66 ± 0.06	44/40	0.37	MAM	0.22 ± 0.02	340 ± 60

***OSL samples associated with coring and pitting (ST4 = VN1, ST5 = VN2, and ST6 = VN3). D, dose rate; n, used number of aliquots per accepted number of aliquots; od, over dispersion; and D_e , equivalent dose of OSL. Age rounded to 5 years and water content = ±10%. Modern indicates ages of not more than few decades.

4.2.4 Optically stimulated luminescence dating

The studied samples showed relatively bright OSL signals and excellent performance during the SAR protocol (Figures 18A and B). However, for three samples, the level of the natural OSL signal was too low to allow for a precise determination of the age. For these samples, we received mean D_e values of 0.02±0.01 Gy (ST1), 0.03±0.02 Gy (ST4), and 0.04±0.02 Gy (ST5), with associated uncertainties of 50% or more. Hence, we regard these samples to be of “modern” (close to zero) age. Considering the dose rates observed, the age can securely be attributed to being younger than 100 years. For core VN1 and VN3, the OSL samples (ST4 and ST6) were collected at the storm layer of Unit IV, which provided an age of modern and 130 10 yr, respectively. In core VN2, the OSL sample (ST5) was collected

from the storm layer of Unit II, and has a modern age (Figures 4E and 12). For all the other samples, ages range between 130 ± 10 and 520 ± 25 years (Table 6). The implications of this are discussed in see section “Dynamic and Evolution of the Hoa Duan Sand Barrier.”

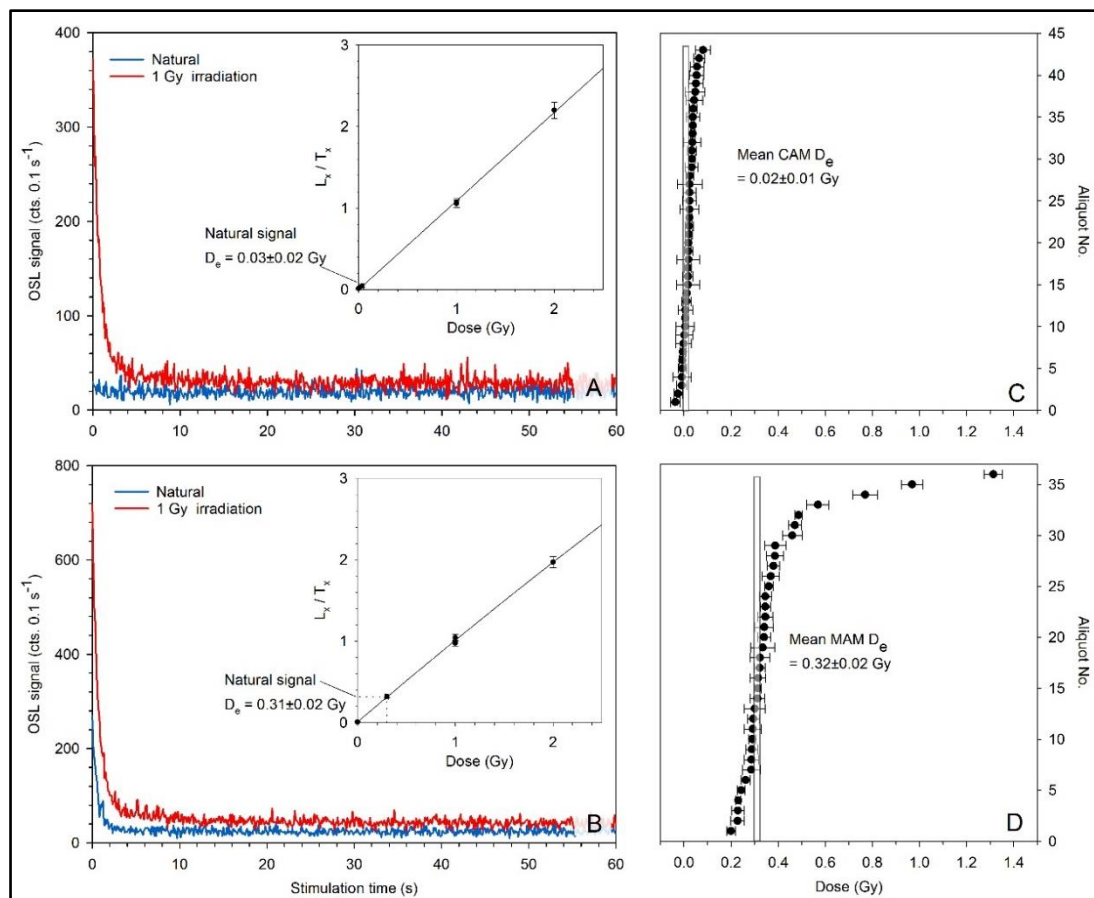


Figure 18 Examples of OSL decay curves for representative aliquots of (A) a modern (ST1) and (B) an older (ST3) sample. This graph shows that the natural signal in the modern sample is too low for proper age determination. The inset displays the dose-response curve of the respective aliquot. Also shown are the dose distribution plots of (C) the modern and (D) the older example. For the latter, the positively skewed spread and high overdispersion of the D_e values call for the application of the Minimum Age Model (Kongsen et al., 2021b).

CHAPTER 5

DISCUSSION

5.1 Laem Son National Park, Ranong Thailand

5.1.1 Diagnostic key to identify monsoon sediments

The sediments identified in core 1 (Figures 5 and 7) are interpreted to have been deposited by wave action during the strong monsoonal conditions with the high stress uni-directional wind patterns which create waves higher and stronger than normal conditions in the fair-weather. In fact, the sediment transport process between strong monsoonal condition and high energy storm surge is the same, but different in wind and wave intensity which can limit inland. Three types of the terms can be classified based on the maximum sustained wind speed such as <61 km/h = Tropical depression, between 62 and 119 km/h = Tropical storm and >119 km/h = Tropical hurricane, cyclone and typhoon (calling is based on the location of the ocean) (Kongsen et al., 2021a). Hence, the monsoonal wind can be regarded as a tropical depression which may vary in the maximum sustained wind speed.

These monsoonal sediments are solely observed in core 1 and cannot be linked or correlated with units found in the other cores and sections of our study. The deposition of monsoon-driven storm surges sediments is controlled by the irregular topography of the coastal area, and they may be found inland of the beach ridges (Phantuwonraj et al., 2013). The fact that core 1 is much closer to the

present-day shoreline than all other cores indicates that monsoon-driven storm surges sediments in the study area is limited to the area close to the beach and does not occur further inland. The monsoon-driven storm surges sediments have very similar sedimentary characteristics as the present-day beach sands which highlights that they are the result of processes which transport them from the beach inland to topographic lows where they are deposited. Moreover, the sedimentary structures observed in the monsoon-driven storm surges sediments, including slight lamination, normal and reverse grading, can be interpreted as the result of the wave pulse processes (Williams et al., 2016; Kongsen et al., 2021a; b). During field work traces of washover sediments were observed several tens of meters inland from the beach (Figures 3A and B), which supports the interpretation that wave action occurs at times much further inland.

5.1.2 Diagnostic key to identify a normal condition sediment deposit

Based on their sedimentological properties (Figures 9 and 10), four layers of normal condition sediment deposit (Units I, III, IV and V) were identified in the studied transects, of which Unit I and III are classified as topsoil layers (Figures 5-8). Unit I is characterized as dark black, fine- to very fine-grained sand, developed on top of the underlying Unit II, covered by vegetation and is thought to have formed after the deposition of Unit II during the 2004 IOT event. Unit III is also characterized by black fine- to very fine-grained sand and developed on top of Unit IV. It has been eroded during the event leading to the deposition of Unit II and is thus interpreted as

the surface or the topsoil layer prior to the erosion by the 2004 IOT (OSB 2004 IOT: old surface before 2004 IOT). The main reason for interpreting Units I and III as topsoil layers is the high amount of organic matter and the low amount of carbonate. This implies a gradual in-situ soil formation over times without direct marine influence (Figures 9 and 10; Tables 1 and 2). While the organic matter and carbonate content in Unit III is similar to Unit II, we distinguish these by evidence for high energy processes at the base of Unit II, which resulted in the sharp erosional contact between the units. Furthermore, Unit III is darker in color (Figures 7 and 8).

Unit IV is interpreted as the old beach ridge sediments at the upper backshore zone (UBS layer) as it is characterized by yellow to orange, fine- to very fine-grained, massive sand with a low organic matter and a low carbonate content (0.2% to 2.2% and 0% to 0.8%, respectively) (Figures 7-10; Tables 1 and 2). It should be noted that no remains marine organisms (shells) were found in this unit. Visually, the striking feature of this unit is the color (yellow to orange) which can discriminate this unit from the other units. Additionally, the mean grain size of this unit seems to be coarser than other surrounding units, although this size is in the same range (fine- to very fine-grained sand). That is, the mean grain size of the beach ridge sediments ranges from 2.06 phi to 3.16 phi, while the mean grain size of unit III and V is in the range of 2.71 phi to 3.03 phi and 2.73 phi to 3.18 phi, respectively (Table 2). The existence of the gradational both top and bottom contacts of this unit also support the interpretation of this unit.

Unit V can be distinguished from the other layers due to the lithology, sedimentary structures, the percentage of organic matter and carbonate content and the existence of remains of marine organisms contain different compared to the storm deposit layer (Unit VI) (Figures 5-10). Crab remains (*Ocypode ceratophthalmus*) are identified only in this layer (Figure 7). The sediments of this unit are characterized by orange to dark brown, fine- to very fine-grained sand and contain organic matter in the range of 0.6% to 1.7% and carbonate content in the range of 0.2% to 3.7%. The main characteristic of this layer is the massive sand which has a gradual contact with the overlying upper backshore sediments (Unit IV) and an erosional contact with the underlying storm deposits (Unit VI). Unit V is interpreted as an old beach in the upper foreshore zone (UFS layer) because it contains remains of marine organisms such as crustaceans (*Ocypode ceratophthalmus*) covered by carbonate concretions throughout the layer. Carbonate concretions are often found in the marine sediments where organic matter has been decomposed and they can preserve marine organisms in their center (Berner, 1968; Yoshida et al., 2018). The presence of very well preserved *Ocypode ceratophthalmus* remains, which are commonly found in between the upper foreshore slope and the backshore zone of present-day beaches (Lucrezi et al, 2009), indicates that this section can also be interpreted as a beach environment.

5.1.3 Diagnostic key to identify high energy event sediments

Shore-normal sedimentation in the littoral zone can be observed from Units I, III, IV and V as mentioned above, showing the difference of sediment characteristics in each unit such as dark black sand with a high amount of organic matter and the low amount of carbonate content in Unit I and III, yellow to orange sand with a low organic matter and a low carbonate content in Unit IV orange to dark brown sand, a moderate organic matter and high carbonate content with *Ocyropsis ceratophthalmus* in Unit V. However, the sediment characteristics observed from Unit II and VI are different which are identified as high energy event deposits.

Globally, high energy event sediments of both tsunami-induced and storm-induced deposits preserved inland have been extensively reported to include lamination, cross-bedding, mud rip-up clasts, normal and reverse grading, erosional and sharp contacts, thinning and fining landward, remains of marine organisms including corals (e.g., Atwater, 1987; Bryant et al., 1992; Liu and Fearn, 1993; Moore, 2000; Donnelly et al., 2001; Fujiwara et al., 2003; Gelfenbaum and Jaffe, 2003; Panegina et al., 2003; Liu, 2004, 2007; Donnelly, 2005; Higman et al., 2006; Moore et al., 2006, 2011; Satake et al., 2006, Choowong et al., 2007, 2008, 2009. Elsner, 2007; Fagherazzi and Du, 2007; Hawkes et al., 2007; Monecke et al., 2008; Morton et al., 2007; Jankaew et al., 2008; Monecke et al., 2008; Feldens et al., 2009, 2012; Williams, 2010, 2013; Rhodes et al., 2011; Goff et al., 2012; Phantuwongraj and Choowong, 2012; Phantuwongraj et al., 2013; Williams et al., 2016; Kongsen et al., 2021a; b).

In our study area, the 2004 Indian Ocean Tsunami sand sheet is interpreted to be represented by Unit II. The deposits are characterized by black to dark brown, fine-to very fine-grained sands (Figures 7-10). Most of the 2004 Indian Ocean Tsunami sediments are intercalated between the two topsoil units, i.e., the present land surface and the old surface before the 2004 Indian Ocean Tsunami event (Unit III) (Figures 7 and 8). It shows slight lamination and an erosional contact to the underlying Unit III as well as a gradational contact to the overlying Unit I. Unit II sediments are overlying sediments of Unit IV which have been dated by OSL to 35 ± 10 to 40 ± 5 years (OLS samples D1-1 and D3-1). Using these ages as a cut-off reference age there are no other historical records of flooding in the study area within the last 50 years other than the 2004 Indian Ocean Tsunami, which flooded the whole study area (Kendall et al. 2006; Choowong et al., 2008). Thus, these sediments have to be the result of the 2004 Indian Ocean Tsunami.

In case of storm deposit, Unit VI, which is interpreted as storm sediments, contains orange to dark grey, fine-to very fine-grained sands with a high organic matter content (0.7%–5.7%) and a high carbonate content (0.7%–17.6%). These laminated sands contain fragmented shells and shell fragment layer and have a sharp erosional contact with the overlying Unit V (upper foreshore sediments; UFS layer) and have a gradual contact with the sediments below (Figure 8). It should be noted that although the structure of laminated sand can be usually observed in the shore-normal sedimentation of the littoral zone, the percentages of the organic

matter and carbonate content are sharply different when compared to shore-normal sedimentation of recent beach sediments, Units IV and V. That is, the overall carbonate content in Unit VI (storm deposits) is much higher, while recent beach sediments, Units IV (upper backshore sediments) and V (upper foreshore sediments) has a lower carbonate content (Table 1) suggesting the different source of the transported material. In addition, the remains of marine organisms observed in this layer differ from those identified in recent beach sediment, Units IV and V, highlighting a shallow marine origin of the sediment. For example, Unit VI contains numerous bivalves, gastropod, scaphopod, spicule, foraminifera, ostracod and ostracod, while the recent beach sediment contains only a minority of foraminifera and the upper foreshore sediment (Unit V; UFS) contains a minority of foraminifera, and crustacean remains.

In terms of thicknesses of the storm layer found in unit VI, it is apparent that a thinning landward trend do not occur, although the base of this unit still cannot be discovered. Conversely, it shows thicknesses of more than 50 cm at the most inner position as appeared in Core 4 which is contrast to several literatures reported about the criteria of storm deposit. However, in rare case, especially in the extreme storm event, thinning landward trend do not also recognize in storm deposit (Brill et al., 2016; Kongsen et al., 2021b). Moreover, the topographical configuration of study area tends to be higher landward and is blocked by the mountain behind (Figures 1B and C). Thus, in the extreme case which the storm wave flooded the whole area, it is

possible that the transportation of the sediments would be blocked by the mountain and reflect in the pattern of backwash sedimentation, making it thicker landward other than thinner.

For the reasons of interpreting this unit as storm deposits other than tsunami deposits, this can be explained from the sediment structure which reflect the different wave process between storm and tsunami. Flooding of tsunami in this study area is triggered from Sumatra- Andaman Subduction Zone generating a long wave train of tsunami directed toward the coast. Flooding in the area is prone to form massive sand with sharp erosional contact as observed from Unit II (Figures 7 and 8). Moreover, apart from the 2004 Indian Ocean Tsunami layer, two more layers of tsunami event were identified from Phra Thong Island (Figure 1A) that occurred ca. 700-550 years and 2800-2500 years ago, respectively (Jankaew et al., 2008; Brill et al., 2012). No lamination has been reported in these two tsunami layers. On the other hand, storm waves are resulted from the cyclonic wind circulation generating the strong and high wave in the pulsing pattern. Therefore, the presence of the laminated structure observed in Unit VI is more possible be a storm origin associated with the flow regimes and bottom current of the storm surge wave (Phantu Wongraj et al., 2008).

5.1.4 Environmental reconstruction

The studied sediments (Figures 9 and 10) are mainly dominated by fine-to very fine-grained sand which show the depositional characteristics of sand-over-sand

features which have variable composition. Sea level reconstructions of the Andaman Sea coast of Thailand show that sea level was 2.5-3.0 m higher than today around 5000 years ago (Scheffers et al., 2012). Sea level gradually dropped and has been 0.4-1.0 m above present during the last 2500 to 500 years and has further declined to the present-day sea level since then. The lower most Units VI and V were interpreted to represent storm deposit and old beach deposits. The depositional age of these two units cannot be established because we cannot collect OSL sample at the lower most part. Moreover, two layers of tsunami event during ca. 700-550 years and 2800-2500 years ago dated by Jankaew et al. (2008) and Brill et al. (2012) did not recognize in this study area. However, based on our oldest OSL age that is 340 ± 20 years ago of Unit IV at 40 cm depth (Figure 6), the deposition of these two units is expected to be older by forming somewhere around 2500-500 years ago. Along shore currents likely played a major role and supplied sediments from north to east (Brown, 2007). The formation of the upper backshore sediment (Unit IV) was influenced by the dropping sea level since around 500 years ago, with oldest sediments of the beach ridge forming around 350 years ago at the location of core 10, then younger toward the sea and deposition occurring as recently as 35 ± 10 yr. Following sea level decrease Unit III filled the swales within the beach ridge and was later eroded by Unit II, the 2004 IOT deposits. These deposits were subject to soil formation during the last 18 years, leading to the development of Unit I.

5.1.5 The 2004 Indian Ocean Tsunami deposits

Compared to the composition of the old beach and present-day beach deposits, which reflect the environmental conditions during normal shore sedimentation, the deposits of Unit II which was formed during the 2004 Indian Ocean Tsunami have a much lower carbonate content and no remains of marine organisms. The likely explanation for the absence of remains of marine organisms in the 2004 IOT layer is related to the energy of the tsunami flow and/or the insufficient quantity of core samples and heterogeneous distribution of the remains of marine organism (Kitamura et al., 2018) . The comparison between 2004 Indian Ocean Tsunami sediments in this thesis and 2004 Indian Ocean Tsunami sediments by Choowong et al. (2008) (Figure 1B; about 500 m south from the study area) reveals that the grain size and sorting of the sediments is slightly different. In this study, 2004 Indian Ocean Tsunami sediments is in range of fine to very fine, moderately to moderately well sorted sand grain while Choowong et al. (2008) stated the grain size and sorting in range of medium to very fine, moderately sorted sand to silt. According to Choowong et al. (2008), the wave run-up of 2004 Indian Ocean Tsunami in this area was 3 m, while the wave run-up in the other affected places in Thailand was much higher such as Phra Thong Island (6 to 8 m), Pakarang Cape (15 m), Bang Niang and Khao Lak (9 to 10 m) and Phuket (4 to 7 m) (Figure 1A). This is due to the original direction of the 2004 Indian Ocean Tsunami wave train which affected various coastal places differently. In front of the study area many small islands occur which

can serve as the natural buffer to attenuate and disrupt the energy of the tsunami wave train. This can directly influence the direction of the tsunami wave, tsunami wave height and intensity. The attenuated energy of the 2004 Indian Ocean Tsunami wave train in the study area is reflected in the lower potential and capability of transporting and carrying suspended materials including marine species. Although the tsunami wave flooded the beach ridge of the study area, the intensity of the tsunami wave and its bottom current was still high as evidenced by the erosion of the former surface. Entrainment of remains of marine organisms was likely minor and deposition of these limited to the beach zone during flooding inland against the maximum height of the beach ridge (approx. 1.8 m above M.S.L in transect 1 and approx. 2.4 m above M.S.L in transect 3; Figures 3D-E). While the wave was gradually rising till it flooded across the beach ridge, eroding parts of it and the inland swale. This is backed by the presence of the sharp erosional top contact in Unit III, and the similarity in color between the layers of the original surface and 2004 Indian Ocean Tsunami (Figures 7 and 8). Apart from the similarity of the color, the organic matter content between the 2004 Indian Ocean Tsunami layer and the original surface layer is similar (Table 2). This illustrates that the sediment source of the 2004 Indian Ocean Tsunami layer came from the beach. This sediment was then transported to the topographic lows behind the beach ridge and deposited. Note that this is in line with where Unit II can be found spatially: in the low topographic relief (swale) in cores 2, 4, 8, 9 and 10 whereas not in the ridge areas in cores 3 and 7 (Figures 5 and 6). This

also matches local witness reports which indicate a slow moving tsunami wave train. This also explains why the tsunami deposits are relatively thin (maximum and minimum are 29 cm and 10 cm, respectively) compared to the wave run-up of approximately 3 m.



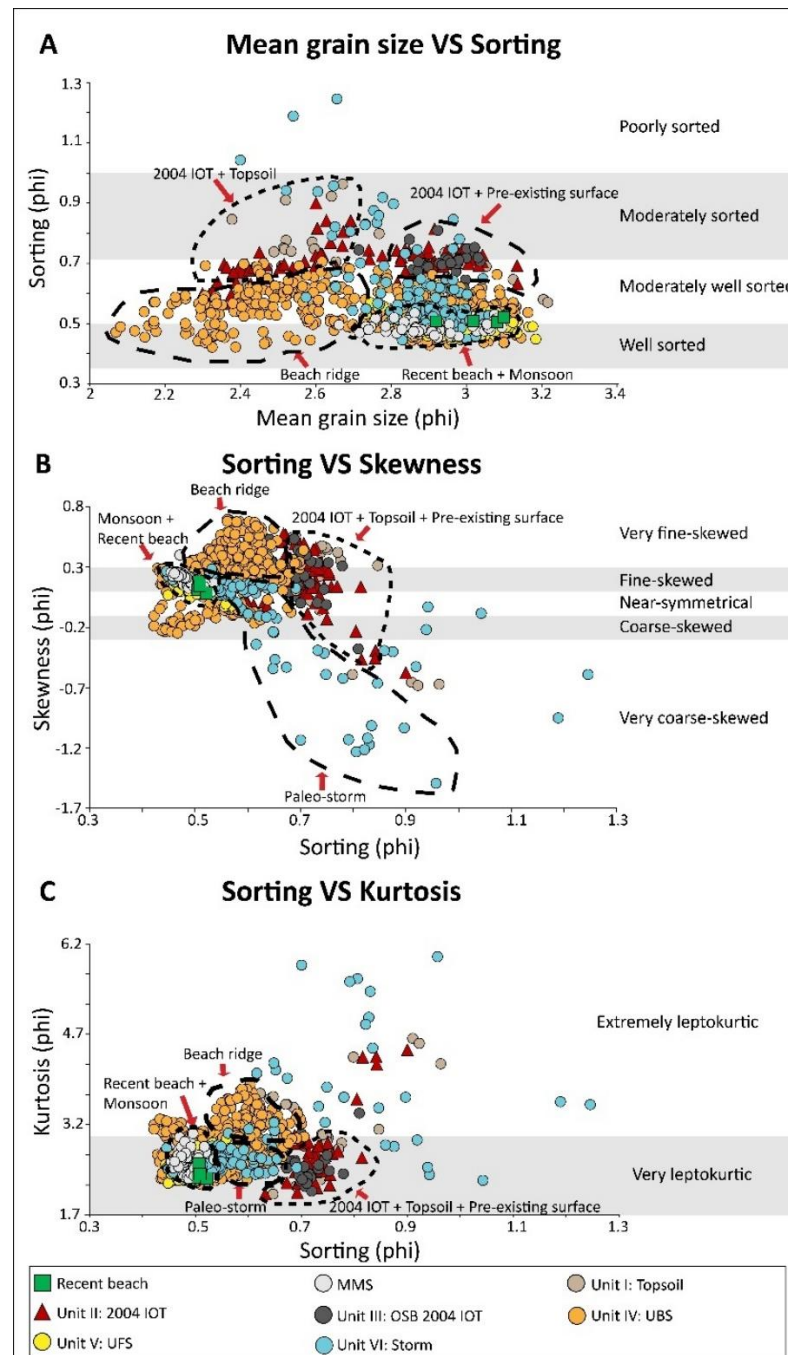


Figure 19 Plotting statistical values of mean grain size vs. (A) sorting, (B) sorting vs. skewness and (C) sorting vs. kurtosis. The number of the sediment samples plotted is as follows: recent beach (n=4), MMS (n=58), Unit I: topsoil (n=29), Unit II: 2004 IOT (n=86), Unit III: OBS 2004 IOT (n=20), Unit IV: UBS (n=458), Unit V: UFS (n=172) and Unit VI: storm (n=169). MMS, monsoon-driven storm surges; 2004 IOT, 2004 Indian Ocean Tsunami; OSB, old surface before Indian Ocean Tsunami; UBS, upper backshore sediment; UFS, upper foreshore sediment.

5.1.6 Grain size distribution parameters and flow energy

Analysis of the grain size distribution parameters and their correlations, reveals several trends which can be used to identify the different depositional processes of the studied units.

Monsoon-driven storm surges sediments and recent beach sediments are grouped in similar clusters in mean grain size versus sorting, sorting versus skewness, and sorting versus kurtosis plots (Figure 10). This is because during monsoon-driven storm surge conditions average wind speed and wave height are closer to fair weather conditions than to high energy events. This is highlighted by the fact that inundation of monsoonal waves is limited to the beach zone (Phantuwongraj et al., 2008; Kongsen et al., 2021b). In rare cases monsoonal flooding may overtop the beach ridge and inundate the low-lying coastal area, however compared to high energy events the inundation is limited to short distances from the beach ridge. The similar grain size parameters also reflect the fact that the provenance of the sediment transportation that indicated beach deposits are the source of monsoon-driven storm surges sediments.

The topsoil sediments mostly compounded with the 2004 Indian Ocean Tsunami and the original surface before the 2004 Indian Ocean Tsunami (OSB 2004 IOT) sediments (Figure 19). The topsoil sediments were mainly originated from the transportation of the rain, wind blown input, the chemical reactions and biodegradation. Hence, the dynamics of transportation is completely different from

the other sediments which belonged to the long-distance transportation. However, the values of the grain size parameter change slightly. Grain size parameters of the topsoil units (Unit I and III) fall in similar areas as the sediments of the 2004 Indian Ocean Tsunami in all three plots (Figure 19). This is not very surprising as the 2004 Indian Ocean Tsunami eroded the underlying topsoil unit and reworked it only slightly, mixing it with sediments from the beach ridge which was also eroded by the high energy event. As the present-day topsoil developed in the 2004 Indian Ocean Tsunami deposits, it has similar grain size parameters. However, the 2004 Indian Ocean Tsunami sediments clearly can be differentiated from the other normal condition deposits and high energy deposits (Figures 19B-C).

Similarly, overlapping between old surface before 2004 Indian Ocean Tsunami sediments and the 2004 Indian Ocean Tsunami sediments was observed in every plot. Unsurprisingly, this overlapping suggested the original source of 2004 Indian Ocean Tsunami sediments which was eroded by the inland tsunami wave train and transported the beach sediments. However, the 2004 Indian Ocean Tsunami sediments can be separated from the sediments of recent beach, upper backshore zone, upper foreshore zone and storm deposit (Figures 19B-C).

The upper backshore sediments seem to distribute strikingly and can be distinguished from other sediments, although some part compounded with the upper foreshore zone. The upper backshore sediments mainly mixed with the sediments of storm deposit and upper foreshore sediment. The storm sediments can

be distinguished from topsoil sediment, 2004 Indian Ocean Tsunami sediment, old surface before 2004 Indian Ocean Tsunami sediment and some part of upper backshore sediments (Figure 19).

5.2 Hoa Duan area, Thua Thien Hue, central Vietnam

5.2.1 Identification of storm deposits

Units II, IV, VI, and VII were classified as storm layers as they contained typical sedimentary structures: sharp top and bottom contacts, mud rip-up clasts, laminated and inclined laminated sand, and marine fossils, and microfossils. For example, the presence of mud rip-up clasts in Unit II of VN1 and VN3 (Figure 12) was very clear evidence of intense wave energy during storms. Building erosional traces on the preexisting surface (Unit III) by forming observable erosional contacts and pebble-sized mud rip-up clast at the base of Unit II cannot be formed by normal waves during fair weather. Although the distance between core VN1 and the present sea level (psl) is relatively short (approximately 120 m), the relatively high ridge crest (2.5-m aml) would serve as a buffer to protect the site from wave flooding during a high tide (0.4-m aml) and monsoon waves (Figure 3E). As the field work was conducted just after the typhoon season, erosional marks were observed, such as beach scarps along the coastline at 1-m aml (Figures 3A-B). Annual monsoon waves were certainly unable to top the crest of the barrier ridge (Dastgheib et al., 2016; Thuy et al., 2017). Therefore, wave processes topping the ridge crest from high tide and monsoon waves can be ruled out. Waves generated by typhoons are much

stronger than the usual fair-weather waves. These waves are strong and high enough to top the barrier ridge and deposit on its landward side.

The parallel-laminated, inclined-laminated sand, and normal and reverse grading found in Units II, IV, and VI (Figures 12 and 16) are additional important evidence of storms, similar to previous studies (Leatherman and Williams, 1983; Sedgwick and Davis, 2003; Phantuwongraj et al., 2013; Kongsen et al., 2021a). However, although foreset bedding, which is often recognized in storm deposits (Nanayama et al., 2000; Phantuwongraj et al., 2013; Kongsen et al., 2021) was not observed in the storm deposit of this area, the presence of laminated sand indicates wave pulses that carried sediments that were then deposited after the dissipation of each pulse.

Slope wash and mass wasting can be eliminated from the range of the sedimentation processes in this area because the elevation and the degree of the slopes of the Hoa Duan barrier are too low to slide or slump landwards during heavy rainfall. Based on cross-section topography (Figure 3E), the highest point of the barrier crest was approximately 2.5 m, while the topographic heights of core positions VN1, VN2, and VN3 were approximately 0.9, 0.5, and 0.2 m, respectively. When considering the height and slope degree between the barrier crest and core positions, slumping and sliding of the sand mass should occur around the seaward area (from ridge crest to beach), but not in the area behind the crest. If the sand mass had slumped and/or slid landwards in the location of the cores, the stratigraphy discovered in the Hoa

Duan area would contain a sharp contact without erosional contact between the preexisting layer surface and the overlaid sand mass with difference in sand color (black and orange), but this kind of stratigraphy was not found here.

Furthermore, the sand layers are unlikely to have been formed by a tsunami. Although there are reports of prehistorical tsunami deposits preserved in the Dien Chau district (Figure 2A), about 420 km northwest of Hoa Duan (Rogozhin, 2016; Trieu et al., 2017), the preservation potential for prehistorical tsunamis may not be possible at this study site because the topographic condition was different from that reported at Hoa Duan. Rogozhin (2016) observed a sand layer with mollusk shells, with their fragments deposited 200 m from the recent shoreline on a coastal sand dune at 10–15 m above the apsl, indicating the occurrence of a tsunami deposit in Dien Chau approximately 650 years ago. Trieu et al. (2017) deduced three paleotsunami events at Dien Chau dating to 4,500–4,300, 4,100–3,900, and 900–600 years ago by abundantly discovering mounds of marine fossils of *Arca granosa* mixed with *Placuna placenta* near the mountain side at an elevation of 5–10 m. The marine fossils were discovered on the coastal plain at a distance of 2 and 7 km from the present shoreline. However, the average height of topography behind the sandy ridge on the barrier island here is 0.8-m apsl. Such a height is too low to preserve the ancient tsunami sediments compared with the well-preserved one on the sand dune at 10 to 15 m apsl (Rogozhin, 2016) and on the coastal plain at 5 to 10 m apsl (Trieu et al., 2017). Therefore, the topography here may not be suitable for preserving

prehistoric tsunamis due to its exposure to floods and storm surges that can erode and sweep away prior to tsunami sediments. Furthermore, we did not find any evidence of those marine species reported in the Hoa Duan barrier (Trieu et al., 2017).

The tsunamigenic earthquake that occurred on January 5, 1992, near the center of Tonkin Bay (Figure 2A) is regarded as the closest event to Thua Thien Hue, Hoa Duan. The estimated magnitude of the earthquake that triggered this tsunami was approximately 3.7, generating a 0.8-m-high wave and causing no casualties (Nguyen 2012). There is no record of tsunami floods affecting inland central Vietnam. However, although there was a flooding of the tsunami on January 5, 1992, in the coastal areas of central Vietnam, Hoa Duan was probably not affected because the relatively low wave height (0.8 m) would not have been able to top the 2-m barrier crest. Moreover, investigations of satellite images using the Google Earth Timelapse can confirm that there was no geomorphological change in both the Thuan An and Hoa Duan areas during 1991–1993.

5.2.2 Identification of fluvial flood deposits

Units III and V were classified as layers deposited by fluvial floods. The unique sedimentary structures found in the Hoa Duan area only consisted of sharp and erosional contacts (Figures 12 and 16). Although these sedimentary structures were similar to the storm deposits (sharp erosional contacts), and some literature did not

mention the sharp erosional contact that was created by the fluvial flood deposits (e.g., Nanayama et al., 2000; Khan et al., 2013; Matsumoto et al., 2016; Yao et al., 2019), the different colors and sediment types are shown in the lithology are very clear, indicating transported sediments. Basically, the sediment color in each environmental zone is different. For example, in the Hoa Duan stratigraphy, orange indicates beach processes in the barrier sand, similar to the color of the beach that we observed. The water table makes the sand color different due to redox reactions. Therefore, dark-brown mud, which contains a minority amount of sand (Units III and V) in the Hoa Duan stratigraphy must have been deposited by transport processes that were not shore-normal.

In addition to the sand color variations in the barrier deposition, the sediment types in the stratigraphy were clearly different themselves. That is to say, based on sediment settlement, coarse-grained sediment (sand and gravel) reflects high-energy deposition conditions, indicating transportation media, such as waves, streams, and currents. Therefore, coarse-grained sediment is common and consistent with barrier formation here, where waves and the tide play a role. In contrast, fine-grained deposits (silt and clay) reflect low-energy sedimentation processes, which are often naturally occurring under still water environments, such as lakes, lagoons, and swamps (Liu, 2004).

In this research, although the Thanh Lam lagoon is located at the back of the Hoa Duan barrier (Figures 2B-C), the deposition of fine-grained sediments by the

fluctuation of the lagoon water is impossible and can be ruled out. Because the elevation between the barrier and lagoon is different, especially compared to the fine-grained sediment layer of Units III and V to the lagoon floor level (Figures 4E and 12), the flow velocity of the lagoon water is relatively low. Apart from fine-grained deposits that existed in the low-energy environment, they are the main suspended materials that were carried in the water column of the fluvial process (Owens et al., 2005).

However, the sediment influx of a river discharge would be mostly constrained in the lagoon area and drained to the open sea through the Thuan An inlet (Figure 2B). The flow velocity of the flood in November 1999 in the Thuan An inlet and the lagoon has been recently computed (Lam et al., 2007). The maximum flow velocity of Thuan An inlet and lagoon during the flood in November 1999 was 3.7 m/s and approximately 2.7 m/s, respectively, whereas the flow velocity in the normal situation fluctuated between 0 and 0.5 m/s. Moreover, flooding in November 1999 inundated the Hoa Duan barrier (Lam et al., 2007). The existence of a muddy layer in the Hoa Duan barrier and a high concentration of coarse-grained sediment indicate an anomalous process that could transport these fine-grained sediments seawards and deposited here under a calm water circumstance. Thus, considering the boundary between the present river, lagoon, and Hoa Duan barrier, the fluvial flood event are the only reasonable candidates for the origin of fine-grained deposits.

The LOI results helped to confirm fluvial flood event as the source of these two layers (Units III and V), which contained high percentages of organic and carbonate matter, markedly different from the topsoil and storm deposits (Figures 13–15; Tables 4 and 5). For instance, the ranges of organic and carbonate contents of Unit V of VN2 were 2.27-25.51 and 0.45-2.12%, respectively, while the ranges of organic and carbonate contents of the topsoil, storm deposits, and beach sediments were 1.0-6.68% and 0.07-0.24, 0.21-2.58, and 0.02-0.63, and 0.2-0.8% and 0.4-0.6%, respectively. In principle, the organic components of sediments can include plants, animal detritus, cells, tissue, and substances derived from microbial synthesis (Brady and Weil, 1999).

Despite the coastal ecology of Hoa Duan being a potential source of these kinds of organic matter, the LOI supports that the retained organic matter content here is low as considered from topsoil sediments. However, Units III and V were classified as fluvial flood deposits because there was no organic matter source that was higher than the fluvial origin in this case, which served as the potential source of the OM. Although they contained a relatively high carbonate content, there were no marine fossils (bivalves and gastropods) or microfossils (foraminifera and ostracods). Hence, the carbonate content of these fluvial flood deposits was more likely to have been transported from the lagoon, which has a high-carbonate content (Cooper, 1989; Kontopoulos and Bouzos, 2011; Avramidis et al., 2013) during flooding seaward compared with the carbonate content of the shore-normal beach sediments (0.44-

0.69%) and storm layers of the other units (Tables 4 and 5). However, the carbonate content of the storm layer in Unit II of VN2 (Figure 14) was relatively high at 0.08-1.33%. Clearly, the high organic matter content in Unit II of VN2 was associated with the mud laminae at a depth of 29-44 cm (Figure 14). According to the absence of the mud layer in Unit III of VN2, it can be assumed that the mud layer (Unit III) had existed before the advent of the storm and then was eroded by a storm in Unit II and redeposited as the mud laminae. This assumption is supported by the existence of cobble-sized mud rip-up clast in Unit II of Pit 3 (Figure 12), which indicated the very strong erosion energy of the storm that formed Unit II. Thus, the formation of a mud layer in Units III and V by a storm can be ruled out and refuted from the percentage carbonate content. If the mud layers (mud cap) in Units III and IV were formed by the still water of a storm, their carbonate contents between the mud and sand layers can be correspondent and/or slightly different, not sharply different, and the contact should be gradational, not sharp erosional (Figures 12–15).

5.2.3 Flow behavior of the storm and fluvial flood deposits

Based on stratigraphic correlations, the flow mechanisms of storms and fluvial flood deposit can be identified (Figures 4E and 12). To begin with storm deposits, the sedimentary structures involved in Units VII, VI, IV, and II are both similar and different. The storm layers of Units VI, IV, and II show parallel and landward-inclined lamination. Thinner and finer landward deposits (wedge-shaped profiles) are found

only in the storm layer of Unit VI (VN1 to VN2), while, in Units IV and II, the storm sediment layer seems to show a thicker landward deposit. The mud rip-up clasts are only present in Units VII, IV, and II. Sharp and erosional contact and normal and reverse grading are presented in every storm layer. Unit VII of VN2 shows erosional top contact with the storm layer of Unit VI, whereas Unit VII of VN3 exhibits sharp erosional contact with overlying fine-grained sediment of the fluvial flood layer (Unit V). Similarly, Unit IV of VN1 and VN3 displays sharp erosional contact with the overlying and underlying fine-grained sediment of the fluvial flood layers (Units V and III), while Unit VI of VN2 shows erosional top contact with the storm layer of Unit II. In principle, the deposition of storm sediments is associated with the wave action generated from strong winds. As mentioned earlier about the sedimentary structures of the storm deposit in each unit, the storm impact scale proposed by Sallenger (2000) has four main regimes (swash, collision, overwash, and inundation) that can be used to explain storm deposition. All units of storm deposit discovered in this thesis showed evidence of overwash and inundation regimes (Sallenger, 2000; Morton and Sallenger, 2003; Masselink and Heteren, 2014; Goslin and Clemmensen, 2017). The other two regimes (swash and collision) can be eliminated because they cannot deposit inland.

Parallel lamination and landward-inclined sand in the internal structures of multiple sets of normal and reverse grading were recognized in Units II, IV, and VI (Figures 13-15). This might indicate the flowing of storm waves and tackling of

sediments by surge pulses in the time of deposition associated with local topography, shear velocity, and size of sediment (Bridge, 1978, 1984) that developed from an upper flow regime and an upper plane bed (Allen, 1984; Cheel, 1990; Fielding, 2006). In addition, mud rip-up clasts in the storm layer (Units VII, IV, and II) reflect the flowing of storm waves under shear stress and frictional force, eroding preexisting layers and redepositing them with clasts of finer-grained sediment (Williams et al., 2016; Kongsen et al., 2021a).

Moreover, thinner and finer landward deposits (wedge-shaped patterns) are present in Unit VI of VN1 and VN2. This indicates storm flooding from the direction of the sea under overwash and inundation regimes (Sallenger, 2000), which forms the continuity of the storm layers. The landward thinning wedge is generally thicker in cores taken closer to the sea. Core VN1 (Unit VI), closest to the sea, contained the thickest layer of storm sediments with coarser-grain sand, while VN2 (Unit VI) contained a thinner layer with finer-grained sediment landward as a result of the diminished energy of storm waves (Liu and Fearn, 1993, 2000a, b; Liu, 2004). However, there is no wedge shape in the storm layer of Units IV and II, excluding Unit VII due to the lack of information on the layer thickness. This can be explained by the topography before the storm layer of Unit IV was deposited, and the intensity of the storm at that time. The storm sediment layers in VN3 are thicker than in VN1 and VN2 (Figure 12). The topography around VN3 probably caused stronger inundation by storm waves than at other locations, trapping water and suspended material in such

a way that more of it could settle evenly. Otherwise, the intensity of the storms depositing Units II and IV was very strong until they flooded across all areas of the barrier and deposited in the lagoon.

The features of Units V and III show they were deposited by fluvial flood that result from excessive and torrential rainfall at high altitudes, which drain downstream into coastal lowlands. Units V and III contained only sharp and erosional contacts with the storm-deposited sand layers both above and below (Figure 12). Due to the wide space between the Thanh Lam lagoon and the Hoa Duan barrier, it can be assumed that, when fluvial flood occurred, the water column was strong and high enough to propagate across the lagoon basin. Normally, the sediments of fluvial flood are suspended material (silt and clay) from terrestrial organic matter sources (Owens et al., 2005). These sediments were then combined with lagoon sediment and water (a source of organic and carbonate content) under turbulent (Cheel, 1990; Fielding, 2006) and hyperpycnal flows (Zavala and Pan, 2018), and then transported seawards and deposited on the sandy barrier. Under these flows, fluvial flood could have disturbed the bed sediment in the lagoon (silt and clay), dispersing and suspending them in the flood waters.

However, the continuity of fluvial flood layers in Unit III of core VN2 is absent because this layer was eroded and scoured by the storm flooding of Unit II, as indicated by the mud rip-up clasts in VN1 and VN3, and Pits 1 and 3 of Unit II. If this was the case, the fluvial flood layer should have a wedge-shaped profile getting

thicker and finer seaward. It is possible that fluvial flooding was wider than storm inundation, propagating to the open sea (not limited to the barrier area) until it weakened and was calm enough to deposit the fine-grained sediments as Units III and V. Thus, the thickness of the fluvial flood during the deposition layers is dependent on the local topography.

Moreover, some parts of the fluvial flood deposits include sand-sized materials, which indicate reworking of preexisting sediment in the barrier area, redeposited by the flood itself. Although some fluvial flood sedimentation contains sand-grained sediment similar to storm deposits, geochemical data from LOI indicate a substantial shift in the organic and carbonate contents toward the overlying and underlying layers (Figures 13-15). These shifts appear in peaks between the storm and fluvial flood deposits, suggesting different flow directions; that is, storm floods flowed landward, transporting sediments from the sea, while fluvial flood flowed seawards, carrying terrestrial and marine (lagoon) sediments.

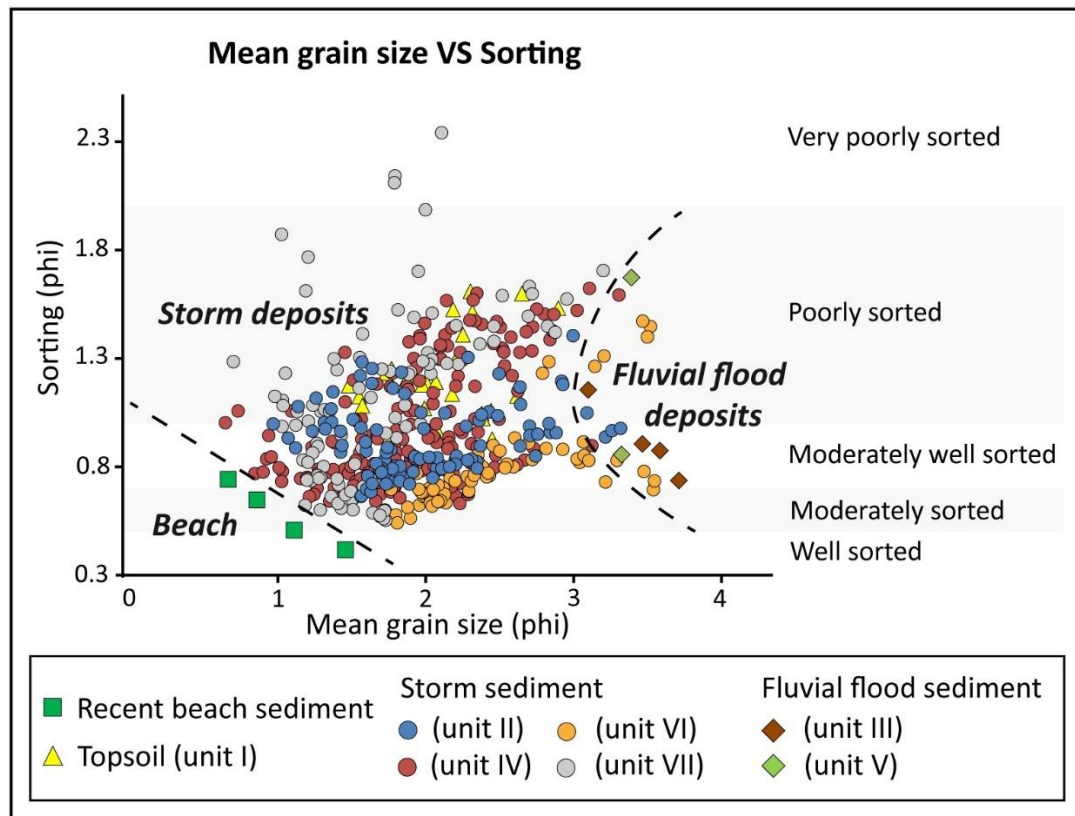


Figure 20 Plotting statistical values of the mean grain size versus sorting. The number of sediments plotted is as follows: recent beach ($n = 4$), Unit I ($n = 27$), Unit II ($n = 97$), Unit III ($n = 4$), Unit IV ($n = 177$), Unit V ($n = 2$), Unit VI ($n = 69$), and Unit VII ($n = 94$). The dashed line divides the zone of a statistical distribution pattern of beach sediment, storm sediment, and fluvial flood sediment (Kongsen et al., 2021b).

5.2.4 Relevance of grain size parameter for classification

Mean grain size, sorting, skewness, and kurtosis were used to characterize each unit in the cores (Units I-VII) and shore-normal process samples (recent beach sediment). These grain parameters have also been analyzed by others in sediments from various zones of coastal environments, such as beaches, dunes, berms, and rivers, which are affected by significantly different natural dynamic processes (e.g., Folk and Ward, 1957; Mason and Folk, 1958; Friedman, 1961, 1967; Bagnold, 1963).

The scatter plot of the mean grain size against the sorting showed the differentiation of beach sediment, storm sediments, and fluvial flood sediments quite clearly (Figure 20). Other plots that demonstrated a trend are presented in Figure 21.

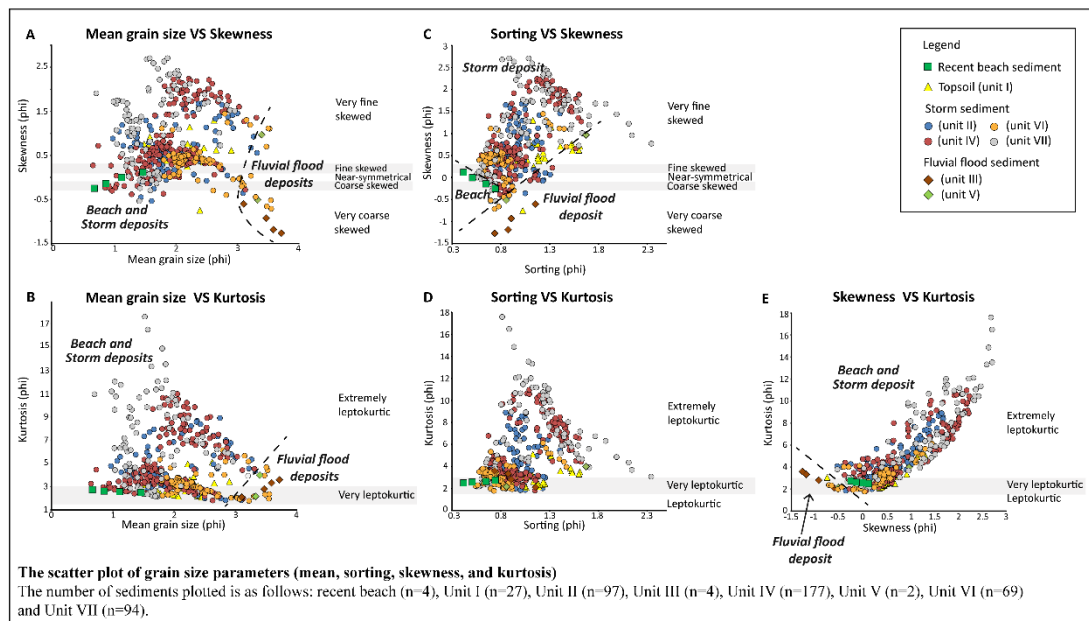


Figure 21 Plotting statistical values of the mean grain size vs skewness (A), mean grain size vs kurtosis (B), sorting vs skewness (C), sorting vs kurtosis (D), and skewness vs kurtosis (E). The dashed line in (A) and (B) divides the zone of a statistical distribution trend of beach and storm sediment from fluvial flood sediment. Next, the dashed line in (C) divides the zone of a statistical distribution trend of beach sediment, storm sediment, and fluvial flood sediment. Finally, the dashed line in (E) divides the zone of a statistical distribution trend of beach and storm sediment from fluvial sediment (Kongsen et al., 2021b).

When comparing the mean grain size and sorting (Figure 20), the recent beach sediments had coarse to medium sand and were moderate to well-sorted, while the storm sediments had medium to very fine sand and were moderate to moderately well sorted, although some parts were poorly sorted. The topsoil sediment (Unit I) seemed to be distributed in similar patterns to the storm sediment (Units II, IV, and

VII), which implied that a storm deposited the topsoil. In Units III and V, fluvial flood deposits sediments had very fine sand and tended to have lower skewness phi values and higher mean grain size phi values than the storm sediments (Units II, IV, VI, and VII), shore-normal beach, and topsoil sediment (Unit I) (Figures 20-21; Tables 4 and 5).

Comparisons between the grain size distribution curves and plotted grain size parameters (Figures 20-21) revealed that the majority of storm sediments were transported from beaches. This is based on the mixing and overlapping in the plots, which is consistent with the grain size distribution curves of the recent beach sediment. Furthermore, reworking and redepositing of the preexistent storm layers were also identified in Unit II of core VN2. It is also possible that both units were reworked and redeposited during the next storm event (Williams, 2011). Topsoil sediments had predominantly bimodal distributions, while storm sediments in Unit II exhibited a unimodal distribution. However, it is reasonable to assume the topsoil sediments of Unit I were part of the storm sediments in Unit II because of their similar grain size distribution curves, which both indicated medium to fine sand. Thus, the very fine sand in the topsoil sediment possibly originated from transportation during rainfall. All of this is also demonstrated by the similarity in physical properties (composition, roundness, and sphericity) of storm deposits, topsoil sediments, and recent beach sediments (Tables 4-5).

The comparison of grain size distribution curves (Figure 17) revealed that there was no finer-grained sediment (silt and clay) in the recent beach and storm deposits, especially in Units II, VI, and VI. Note that the grain size distribution curves of the silt and clay in the storm sediment of Unit VII are the distribution curves of MRCs. The absence of silt-sized and/or clay-sized sediments in the storm deposits is common, especially in surf zones and/or breaker zones, because most grains smaller than 0.140 mm remain suspended or are washed away by waves (Friedman, 1967). Usually, fine-grained particles smaller than 0.150 mm ($>2.75 \phi$) influenced by oscillatory water movement are swept up by waves, dispersed in the water column, and then transported offshore (Bagnold, 1963; Ingle, 1966). However, finer-grained sediments in the range of silt and clay were found in the grain size distribution curves of the fluvial flood sediments (Units III and V; Figure 17). This supports the difference in the grain size distribution curves between the storm and fluvial sediments.

5.2.5 Age of depositional events

In principle, the Hoa Duan barrier would have accumulated from the transportation of longshore currents, of which we do not know the exact age or origin point. Based on the OSL dating (Table 6; see the location of the sample point in Figure 2C) of sediments from ST2 at 50-cm depth from the surface, the depositional age of the sand barrier can be estimated. Sample ST2 was the oldest and was deposited around 520 ± 25 years ago, while the OSL dates of the nearby ST3

and ST7 at 50 cm depth and ST8 and ST8-1 at 30 m and 50 cm depth, respectively, have ages of 350 ± 25 , 350 ± 50 , 340 ± 60 , and 300 ± 50 years, respectively. We can conclude that the barrier in this area has been accumulating for a long time, starting earlier than 520 ± 25 years ago, then stopping somewhere between 350 ± 50 and 300 ± 50 years ago. This assumption matches a historical French map, which confirms the existence of this barrier and lagoon in the late seventeenth century (Schweyer, 2018; Tana, 2019). However, it is peculiar that OSL dating of the investigated transect (ST4, ST5, and ST6) returned ages younger than other locations: modern, modern, and 130 ± 10 yr, respectively, which is similar to the modern age of ST1 (see the location of the sample point in Figure 2C). With the difference in the OSL ages in this area, we discuss more on the issues of the evolution of the barrier formation, the disastrous events (both storm and fluvial flood), and the historical data in see section “Dynamic and Evolution of the Hoa Duan Sand Barrier”.

5.2.6 Dynamic and evolution of the Hoa Duan sand barrier

The closing and opening of the Hoa Duan inlet tended to rework the sand barrier sediments. The morphological change in the Hoa Duan barrier was chronologically observed in the Google Earth Timelapse (Figure 22). Based on Lam et al. (2007), in 1952, the barrier formation here tended to grow gradually from southeast to northwest direction. The location of the Thuan An inlet was different and then from its present location because it was blocked from the sand body of

the barrier (Figure 22A). Similarly, comparing the location of the study area from 1952 to 1999, the shape of the Hoa Duan barrier was narrower than in the present. The satellite images indicate that the Hoa Duan barrier (study area) was relatively stable between 1952 and 1999 before a strong fluvial flood event in November 1999. In 2000, the satellite image showed the Hoa Duan barrier had been affected by the fluvial flood in November 1999, resulting in a dramatic morphological change that breached and scoured the sediment of the barrier seawards, contributing to an ephemeral inlet. After that, the Hoa Duan barrier recovered during 2000-2003.

In terms of the recovery process, the observable recovery of the Hoa Duan barrier was relatively rapid, being filled up with sand materials within 3 years after the destructive flood of November 1999. Before the flood, the Hoa Duan barrier was a stable barrier formation with sediment accumulation in the northwest direction, as shown in Figure 22A. After the flood in November 1999, breaching of the Hoa Duan barrier until it became an ephemeral inlet (Hoa Duan inlet), which created the large accommodation space suitable for the rapid rate of deposition (Choowong et al., 2009) by trapping the sediment materials of the northwestward longshore current and depositing it laterally and vertically within the Hoa Duan inlet. Later, the closing of the Hoa Duan inlet occurred in 2001, and the rate of the deposition then seems to have decreased from 2001 to 2003 due to the reduction of accommodation space, whereas the beach zone remained stable. In 2003, the accommodation space greatly decreased and the barrier formation almost returned to the normal state, but

the shape of the barrier had become wider than it was in 1999 before the flood event. The Hoa Duan barrier has remained stable until the present day.

There have been 37 tropical storms and 26 typhoons recorded in central Vietnam from 1951 to 2019 (Table 7), and so it is possible that increasing barrier sedimentation, as observed from the crest of the barrier height up to 2-m amlt (Figure 22E), might have been generated from storm waves that created the upward deposition of sediments (Otvos, 2000; Snedden et al., 2011; Nott, 2015; Tamura et al., 2017) under the overwash regime (Sallenger, 2000). Although it is relatively difficult to confirm the depositional process for the whole barrier and the known flood and storm event due to the complexity of its formation and the lack of reliable records, the OSL dates of ST4, ST5, and ST6 at a 40-cm depth from the surface can serve as a cutoff point and indicate 130±10 years ago to present. Thus, more than 130±10 years ago, there were two storms (Units VI and VII) and one fluvial flood (Unit V) that deposited sediment on the barrier, and there were two storms (Units IV and II) and one fluvial flood (Unit III), depositing from 130±10 years ago to present. The presence of sedimentary layers from prior natural hazard events in this sand barrier emphasized the necessity for coastal communities to initiate adapting measures in order to mitigate the loss from upcoming natural hazards.

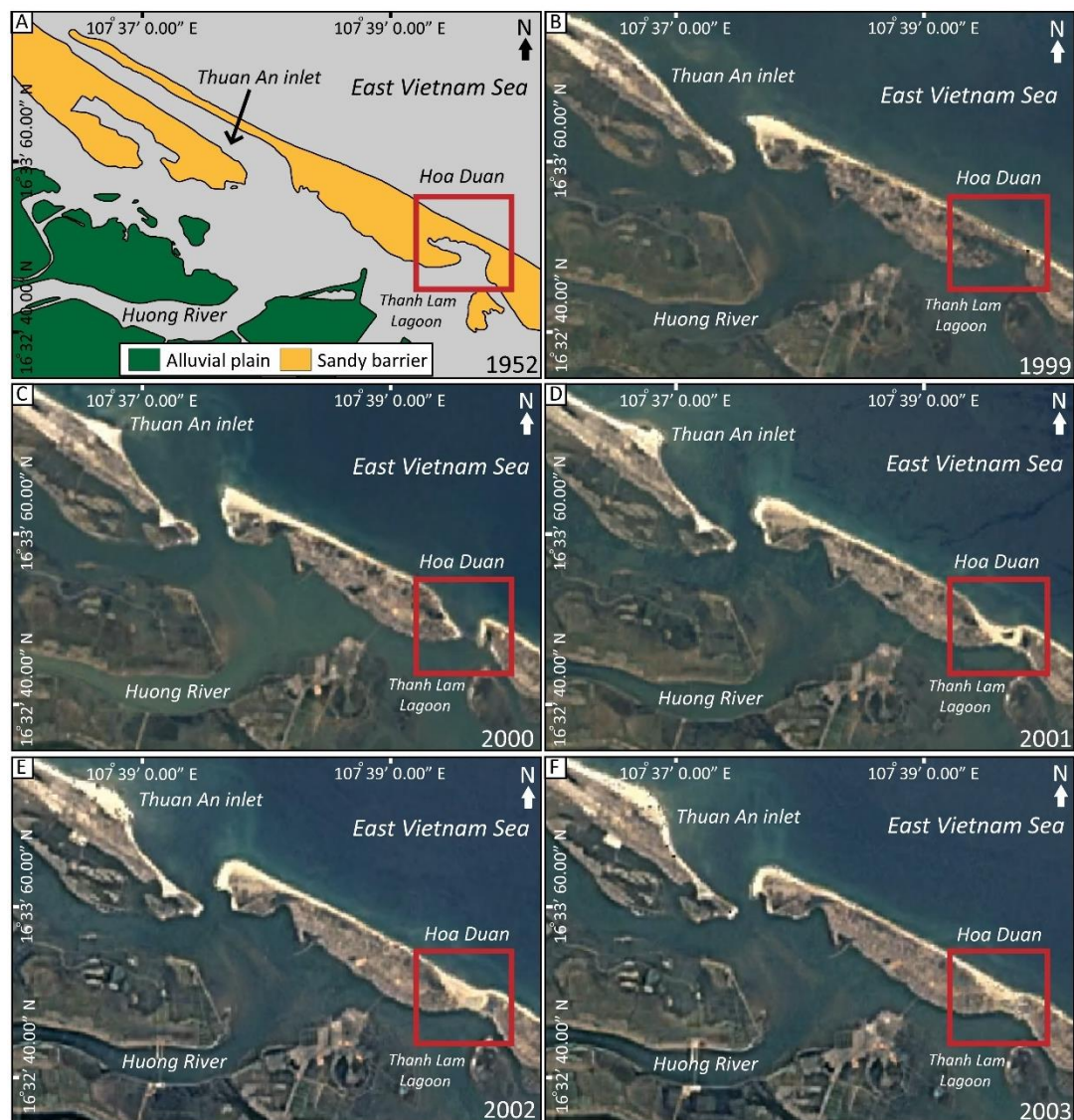


Figure 22 The episodic satellite imageries accessed through the Google Earth Timelapse showing the morphological change of the study area (Hoa Duan barrier) and the adjacent area (Thuan An inlet). (A) the morphology of the study area and Thuan An inlet in 1952 (modified from Lam et al., 2007), (B) The morphology of barrier formation before the flood in November 1999, (C) breaching of the Hoa Duan barrier after the Flood in November 1999 created the large accommodation space of trapping sediment materials from northwestward longshore current, (D), (E) and (F) recovering of Hoa Duan barrier that sand sediments were progressively filled up in 2001, 2002 and 2003, respectively. Red rectangular represents the study area in Hoa Duan barrier (Kongsen et al., 2021b).

Table 7 Lists of tropical storm and typhoon tracks occurred chronologically in central Vietnam during 1951 to 2019 (Kongsen et al., 2021b).

Number	Name	Type	Year	Number	Name	Type	Year
1	Louise	Typhoon	1951	33	Georgia	Tropical storm	1986
2	Trix	Typhoon	1952	34	Betty	Typhoon	1987
3	Wilma	Typhoon	1952	35	Cecil	Typhoon	1989
4	Nancy	Tropical storm	1954	36	Angela	Typhoon	1989
6	Tilda	Typhoon	1964	37	Dan	Typhoon	1989
7	Bille	Tropical storm	1964	38	Becky	Typhoon	1990
8	Clara	Typhoon	1964	39	Fred	Tropical storm	1991
9	Tilda	Typhoon	1964	40	Lewis	Tropical storm	1993
10	Nadine	Tropical storm	1965	41	Winona	Tropical storm	1993
11	Polly	Tropical storm	1965	42	Luke	Tropical storm	1994
12	Pasty	Tropical storm	1967	43	Lois	Tropical storm	1995
13	Rose	Tropical storm	1968	44	Willie	Tropical storm	1996
14	Tess	Tropical storm	1969	45	Fritz	Tropical storm	1997
15	Doris	Typhoon	1969	46	Eve**	Tropical storm	1999
16	Kate	Typhoon	1970	47	Kaemi	Tropical storm	2000
17	Harriet	Typhoon	1971	48	Wokong	Typhoon	2000
18	Kim	Tropical storm	1971	49	Usagi	Tropical storm	2001
19	Della	Typhoon	1971	50	Koni	Tropical storm	2003
20	Elsie	Typhoon	1972	51	Vicente	Tropical storm	2005
21	Flossie	Typhoon	1972	52	Damrey	Typhoon	2005
22	Lorna	Typhoon	1972	53	Xangsane	Typhoon	2006
23	Faye	Tropical storm	1974	54	Lekima	Typhoon	2007
24	Carla	Tropical storm	1977	55	Mekkhala	Tropical storm	2008
25	Kit	Tropical storm	1978	56	Nock-Ten	Tropical storm	2011
26	Alice	Tropical storm	1979	57	Wutip	Typhoon	2013
27	Ruth	Tropical storm	1980	58	Vamco	Tropical storm	2015
28	Sarah	Tropical storm	1983	59	Talas	Tropical storm	2017
29	Vernon	Tropical storm	1984	60	Sonca	Tropical storm	2017
30	Agnes	Typhoon	1984	61	Doksuri	Typhoon	2017
31	Cecil**	Typhoon	1985	62	Bebinca	Tropical storm	2018
32	Andy**	Typhoon	1985	63	Podul	Tropical storm	2019

**Typhoon and tropical storm which strike Thua Thien Hue directly and caused the severe damages to properties and lives.

5.3 Comparison between the sedimentary characteristics of storms in Laem Son, Thailand and Hoa Duan, Vietnam

From both study areas, it is completely clear there are many factors affected the process of the storm occurrence and deposition such as geological and geographical location, the storm frequency, size and intensity of storm, direction of storm track, time of storm occurrence, source of sediment material, topographical configuration, surge height, preservation potential and coastal geomorphology.

Laem Son area is situated in the southern part of Thailand, which is associated with the Andaman Sea (Figure 1), whereas Hoa Duan area in the central part of Vietnam is related to the South China Sea (Figure 3). Although these two areas are similarly located close the open sea, the influence of storm occurred in both areas is different. Based on the stratigraphy of both areas, only one layer of storm deposit was discovered from Laem Son area, while four layers of storm was found in Hoa Duan area. This is because the movement direction of storm tracks plays a role. Usually, storms generated in the Andaman Sea and the South China Sea move their tracks in the similar direction which are from east to west. Therefore, the number of storm deposits found from Hoa Duan area is higher than Laem Son area because Hoa Duan area is directly impacted from the movement direction of storm tracks generated in the South China Sea (from east to west). However, the location of Laem Son is in the opposite of storm track direction. Not only Laem Son area, but

also throughout the coastline of southern Thailand in the Andaman sea side are difficult to find the storm deposit. Only some rare case of extreme storm can impact Laem Son area as an exemplary severe storm event of Cyclone Nargis impacted Myanmar in 2007. This event is attributed to be the anomalous direction of storm track which moved from west to east.

In terms of the sedimentary structures and the sediment characteristics between Laem Son and Hoa Duan areas (Table 8), the storm sediments found from Laem Son area ranged from fine- to very fine-grained sand (2.4 to 3.08 phi), while the storm sediments from Hoa Duan are in ranges of coarse- to very fine-grained sand (0.65 to 3.55 phi). Moreover, the sediment structures appeared in the storm sediment layer of Hoa Duan area display the detail of the sedimentary evidence clearer than Laem Son such as sharp top and bottom contacts, lamination, cross lamination, mud rip-up clasts, mud laminae and the wedge shape profile, while the storm layer of Laem Son show sharp erosional top contact, lamination and shell fragment layer. This is because the sources of transportation of storm layers in Hoa Duan area originated from several sources which are different in grain sizes such as river, lagoon, beach ridge, beach and sea floor, while Laem Son area is lesser. Various sediments in Laem Son area (including storm and tsunami sediments) are very similar in grain size which imply the sediment source themselves in the area.

Table 8 Comparison of and the sedimentary characteristics of the storm sediments discovered from the area of Laem Son, Thailand and the area of Hoa Duan, Vietnam.

Lists	Laem Son	Hoa Duan
References	This study	This study (Kongsen et al., 2021b)
Location	Andaman Sea, Thailand	South China Sea, Vietnam
Geomorphology	Sandy beach, ridge and swale	Sandy beach, ridge, barrier island, lagoon, river and alluvial plain
Elevation	0.8 - 2.4	0.9 - 2.5
Storm layer number	1	4
Sphericity	Low to high	Low to high
Roundness	Sub-angular to rounded	Very angular to well-rounded
Mean (phi)	2.4 - 3.08	0.64 - 3.55
Mean	Fine to very fine sand	Coarse to very fine sand
Sorting (phi)	0.44 - 1.24	0.54 - 2.34
Sorting	Well sorted to poorly sorted	Moderately well-sorted to poorly sorted
Skewness (phi)	-1.49 - 0.28	-0.71 - 2.7
Skewness	Very coarse-skewed, coarse-skewed, near-symmetrical, fine-skewed	Very coarse-skewed, coarse-skewed, near-symmetrical, fine-skewed and very fine-skewed
Kurtosis (phi)	2.27 - 5.98	1.83 - 17.58
Kurtosis	Very leptokurtic to extremely leptokurtic	Very leptokurtic to extremely leptokurtic
Modality	Unimodal distribution	Multimodal distribution
Organic matter (%)	0.67 - 5.75	0.09 - 3.89
Carbonate content (%)	0.71 - 17.57	0.01 - 1.33
Marine fossil and microfossil	Ostracods, foraminifers, bivalve, and spicule	Ostracods and foraminifers
Grading	Normal and reverse	Normal and reverse
Sedimentary structures	Sharp top contact, shell fragment layer, lamination	Sharp erosional top and bottom contacts, mud rip-up clasts, lamination, cross lamination, wedge sharp profile
Depositional age	>350 yr	> 130±10 yr and during 130±10 yr to present

5.4 The difference of K, Th and U from OSL dating

According to Tables 3 and 7, the potassium, uranium and thorium values of both Hoa Duan area, Thua Thien Hue, Vietnam and Laem Son National Park area, Ranong, Thailand obtained from dating are different. Obviously, the values of Th and U from Hoa Duan area, Thua Thien Hue, Vietnam displays values much lower than

the area of Laem Son National Park. This indicates the original source of sand sediments deposited along the beach of both areas. Based on the geological locations of both areas, Laem Son area is backed by many granitic rock mountains, whereas the granitic source in Hoa Duan area is much farther than Laem Son area. Because when the granitic rock decomposed, it provides not only quartz and felspar which are the original source of sand, but also clay as well. Hence, that is why the values of Th and U in Laem Son area is much higher than Hoa Duan area in all OSL samples.



CHAPTER 6

CONCLUSION

In this thesis the sediments obtained from the area of Laem Son National Park, Ranong, Thailand and Hoa Duan area, Thua Thien Hue, Vietnam are used to analyze the frequency of past high energy events such as tsunamis and extreme storms. This can be challenging in coastal areas where all preserved deposits have similar sedimentological characteristics. The challenge is that in the coastal areas where contain the similar characteristic of the sediments such as the sediment type and grain size, it is relatively difficult to identify and differentiate the type of the coastal deposits. In this study, the coastal area of Laem Son National Park, Andaman Sea, southern Thailand served as the suitable place to study the types of the coastal deposits using the multi-proxy data on stratigraphy, physical characteristic, grain size analysis, loss on ignition, remains of marine organisms and OSL dating.

Our findings suggest that the coastal area of Laem Son National Park mainly consisted of eight sediment types including the normal recent beach, monsoon-driven storm surges sediments (MSS), topsoil (Unit I), the 2004 Indian Ocean Tsunami (Unit II), old surface before 2004 Indian Ocean Tsunami (Unit III), upper backshore zone (Unit IV), upper foreshore zone (Unit V), and storm deposits (Unit VI). Every coastal sediment which was discovered here has shown the similar characteristics of grain size in the range of fine- to very fine-grained sand, but difference in physical

properties (composition, roundness and sphericity), the statistical values of grain size parameters (mean grain size, sorting, skewness and kurtosis), remains of marine organisms and the percentage of organic matter and carbonate contents. Based on Laem Son stratigraphy, two layers of high energy deposits were discovered including 2004 Indian Ocean Tsunami and paleo-storm. 2004 Indian Ocean Tsunami layer was classified from slight lamination, sharp erosional lower contact with the old surface before 2004 Indian Ocean Tsunami, the absence of remains of marine organisms, a high amount of organic matter and a low amount of carbonate. On the other hand, the paleo-storm layer was identified based on lamination, shell fragments, a high amount of organic matter and carbonate. Our OSL dating results suggests that the layer of the paleo-storm event which is located beneath the beach ridge layer was found at the age older than 350 years. The beach ridge formation here starts forming somewhere during the age older than 350 years to 35 ± 10 years which is the time of developing topsoil layer until the 2004 Indian Ocean Tsunami event deposited and preserved in the Laem Son area.

Sedimentary records of past storm surges and fluvial flood events found on the Hoa Duan barrier island revealed the episodic natural hazard events at the Thua Thien Hue province, central Vietnam. Four layers of storm deposits and two layers of fluvial flood deposits from three cores were recognized. Sedimentary characteristics, grain size statistic parameters, and OSL dating were used to define the storm surge and fluvial flood events in the past centuries. Storm sediments were characterized

by having coarser grain sizes, with a low organic and carbonate content, containing sedimentary structures, including parallel and inclined landward lamination, multiple sets of normal and reverse grading, mud rip-up clasts, and sharp and erosional contacts (both top and bottom), with finer-grained layers. Conversely, fluvial flood deposits contained only fine to very-fine sand, strikingly high organic and carbonate contents, and only sharp erosional top and bottom contacts with coarser-grained layers. Comparisons between grain size distribution curves of the storm and fluvial sediments indicated that they both had a unimodal distribution but differed in sediment size. Comparing grain size parameters (mean, sorting, skewness, and kurtosis) revealed the clearest differentiation between storms and fluvial floods is the plot of mean grain size against sorting. These sedimentological analogs can also be used as a diagnostic key for storm deposits and fluvial flood deposits in places with similar geomorphological conditions. Based on the OSL results, we suggest that before 130 ± 10 years ago, two storms (Units VI and VII) and one fluvial flood (Unit V) deposited sediment on the barrier, and, from 130 ± 10 years ago to the present, deposits were made by two storms (Units II and IV) and one fluvial flood (Unit III). These sedimentary records indicate natural events that affected people and property locally and in the wider region. Although no tsunami deposits have been recognized in this study site, the characteristic of storms and flood deposits from this analysis, more or less, confirms the frequency of these two catastrophic events. A diagnostic sedimentary key of these two hazards can help improve the understanding of the

geomorphological evolution of the studied site and other parts of this coastal region to remind the coastal community to prepare well for future coastal hazards.





จุฬาลงกรณ์มหาวิทยาลัย
CHULALONGKORN UNIVERSITY

REFERENCES

- Allen, J. R. L. (1984). "Parallel lamination developed from upper-stage plane beds: A model based on the larger coherent structures of the turbulent boundary layer." Sedimentary Geology **39**: 227–242.
- Avramidis, P., Bekiari, V., Kontopoulos, N., Kokidis, N. (2013). "Shallow coastal lagoon sediment characteristics and water physicochemical parameters – Myrtari lagoon, Mediterranean Sea, western Greece." Fresenius Environmental Bulletin **22**: 1628-1635.
- Bagnold, R. A. (1963). Mechanics of marine sedimentation. The Sea: Ideas and Observations on Progress. M. L. Hill. New York, NY, Interscience. **3**: 507-528.
- Beckman, M., An, L. V., Bao, L. Q. (2002). Living with the Floods: Coping and Adaptation Strategies of Households and Local institutions in Central Vietnam. Stockholm, Stockholm Environmental Institution.
- Bell, R., Cowan, H., Dalziell, E., Evans, V., O’Leary, M., Rush, B., Yule. L. (2005). "Surveys of impacts on the Andaman coast, southern Thailand following the great Sumatra-Andaman earthquake and tsunami of December 26, 2004." The Bulletin of the New Zealand Society for Earthquake Engineering **38**: 124-148.

- Berner, R. A. (1968). "Calcium carbonate concentrations formed by the decomposition of organic matter." Science **159**: 195-197.
- Bevacqua, A., Yu, D., Zhang, Y. (2018). "Coastal vulnerability: Evolving concepts in understanding vulnerable people and places." Environmental Science & Policy **82**: 19-29.
- Blott, S. J., Pye, K. (2001). "GRADISTAT: a grain size distribution and statistics package for the analysis of unconsolidated sediment." Earth Surface Processes and Landforms **26**: 1237-1248.
- Brady, N. C., Weil, R. R. (1999). The Nature and Properties of Soils. Upper Saddle River NJ, Prentice-Hall, Inc.
- Bridge, J. S. (1978). Planar and parallel lamination. Encyclopedia of Sediments and Sedimentary Rocks. G. V. Middleton, Church, M.J., Coniglio, M., Hardie, L.A., Longstaffe, F.J. . Berlin, Springer.
- Bridge, J. S. (1984). "Large-scale facies sequences in alluvial overbank environments." Journal of Sedimentary Petrology **54**: 583-588.
- Brill, D., Klasen, N., Bruckner, H., Jankaew, K., Scheffers, A., Kelletat, D., and Scheffers, S. (2012). "OSL dating of tsunami deposits from Phra Thong Island, Thailand." Quaternary Geochronology **10**: 224-229.

- Cadigan, R. A. (1961). "Geologic interpretation of grain-size distribution measurements of Colorado Plateau sedimentary rock." Journal of Geology **69**(2): 121-144.
- Chaimanee, N., Tathong, T. (2005). The post-tsunami survey for coastal damage assessment along the Andaman Sea coast, Southern Thailand. Scientific Forum on the Tsunami: Its Impact and Recovery. Asian Institute Technology, Thailand, A Regional Symposium.
- Cheel, C. R. (1990). "Horizontal lamination and the sequence of bed phases and stratification under upper-flow-regime conditions." Sedimentology **37**: 517-529.
- Choowong, M., Murakoshi, N., Hisada, K.I., Charoentitirat, T., Charusiri, P., Phantuwongraj, S., Wongkok, P., Choowong, A., Subsayjun, R., Chutakositkanon, V., Jankaew, K., Kanjanapayont, P. (2008). "Flow conditions of the 2004 Indian Ocean tsunami in Thailand, inferred from capping bedforms and sedimentary structures." Terra Nova **20**(2): 141-149.
- Choowong, M., Murakoshi, N., Hisada, K.I., Charusiri, P., Daorerk, V., Charoentitirat, T., Chutakositkanon, V., Jankaew, K., Kanjanapayont, P. (2007). "Erosion and Deposition by the 2004 Indian Ocean Tsunami in Phuket and Phang-nga Provinces, Thailand." Journal of Coastal Research **23**(5): 1270-1276.
- Choowong, M., Phantuwongraj, S., Charoentitirat, T., Chutakositkanon, V., Yumuang, S., Charusiri, P. (2009). "Beach recovery after 2004 Indian Ocean tsunami from

Phang-nga, Thailand." Geomorphology **104**(3-4): 134-142.

Cooper, J. A. G. (1989). "Fairweather versus flood sedimentation in Mhlanga Lagoon, Natal: implications for environmental management." South African Journal of Geology **92**: 279-294.

Cui, L., Ge, Z., Yuan, L., Zhang, L. (2015). "Vulnerability assessment of the coastal wetlands in the Yangtze Estuary, China to sea-level rise." Estuarine, Coastal and Shelf Science **156**: 42-51.

Dastgheib, A., Reyns, J., Thammasittirong, S., Weesakul, S., Thatcher, M., Ranasinghe, R. (2016). "Variation in the Wave Climate and Sediment Transport Due to Climate Change along the Coast of Vietnam." Journal of Marine Science and Engineering **86**: 1-20.

Day, J. W. J., Cable, J. E., Lane, R. R., Kemp, G. P. (2016). "Sediment deposition at the Caernarvon crevasse during the Great Mississippi Flood of 1927: Implications for coastal restoration." Water **38**: 1-12.

Degering, D., Degering, A. (2020). "Change is the only constant – time-dependent dose rates in luminescence dating." Quaternary Geochronology **58**: 1-14.

Donnelly, J. P. (2005). "Evidence of past intense tropical cyclones from back barrier Salt Pond sediment: a case study from Isla de Culebrita Puerto Rico, USA." Journal

of Coastal Research **42**: 201-210.

Donnelly, J. P., Roll, S., Wengren, M., Butler, J., Lederer, R., Webb, I. I. I. (2001).

"Sedimentary evidence of intense hurricane strikes from New Jersey." Geology **29**: 615-618.

Elsner, J. B. (2007). "Tempests in time." Nature **44**: 647-649.

Fagherazzi, S., Du, X. (2007). "Tsunamigenic incisions produced by the December 2004 earthquake along the coasts of Thailand, Indonesia and Sri Lanka." Geomorphology **99**: 120-129.

Feldens, P., Schwarzer, K., Sakuna, D., Szczuciński, W., Sompongchaiyakul, P. (2012).

"Sediment Distribution on the inner continental shelf off Khao Lak (Thailand) after the 2004 Indian Ocean tsunami." Earth, Planets and Space **64**: 875-887.

Feldens, P., Schwarzer, K., Szczuciński, W., Statterger, K., Sakuna, D., Sompongchaiyakul,

P. (2009). "Impact of 2004 tsunami on seafloor morphology and offshore sediments, Pakarang Cape, Thailand." Polish Journal of Environmental Studies **18**: 63-68.

Fielding, C. R. (2006). "Upper flow regime sheet, lenses, and scour fills: extending the range of architect elements for fluvial sediment bodies." Sedimentary Geology **190**: 227-240.

- Folk, R. L., Ward, W.C. (1957). "Brazos River bar: A study in the significance of grain size parameters." Journal of Sedimentary Petrology **27**(1): 3-26.
- Friedman, G. M. (1961). "Distinction between dune, beach, and river sands from their textural characteristics." Journal of Sedimentary Petrology **31**: 514-529.
- Friedman, G. M. (1967). "Dynamic processes and statistical parameters compared for size frequency distribution." Journal of Sedimentary Petrology **37**(2): 327-354.
- Fritz, H. M., Blount, C.D., Thwin, S., Thu, M.K., Chan, N. (2010). Cyclone Nargis Storm Surge Flooding in Myanmar's Ayeyarwady River Delta. Indian Ocean Tropical Cyclones and Climate Change. Y. Charabi. Dordrecht, Springer: 295-303.
- Fritz, W. J., Moore, J.N. (1988). Basics of physical stratigraphy and sedimentology. New York, the United States of America, John Wiley.
- Fujino, S., Naruse, H., Matsumoto, D., Jarupongsakul, T., Sphawajruksakul, A., Sakakura, N. (2009). "Stratigraphic evidence for pre-2004 tsunamis in southwestern Thailand." Marine Geology **262**: 25-28.
- Galbraith, R. F., Robert, R.G., Lasleft, G.M., Yoshida, H., Olley, J.M. (1999). "Optical dating of single and multiple grains of quartz from Jinmium rock shelter, northern Australia: Part I, experimental design and statistical models." Archaeometry **41**: 339-364.

- Gornitz, V. (1991). "Global coastal hazards from future sea level rise." Palaeogeography, Palaeoclimatology, Palaeoecology **89**: 379-398.
- Goslin, J., Clemmensen, L. B. (2017). "Proxy records of Holocene storm events in coastal barrier systems: Storm-wave induced markers." Quaternary Science Reviews **174**: 80-119.
- Hawkes, A., Bird, M., Cowie, S., Grundy-Warr, C., Horton, B.P., Hwai, A.T.S., Law, L., Macgregor, C., Nott, J., Ong, J.E., Rigg, J., Robinson, R., Tan-Mullins, M., Sa., T.T., Yasin, Z., Aik, L.W. (2007). "Sediments deposited by the 2004 Indian Ocean Tsunami along the Malaysia-Thailand Peninsula." Marine Geology **242**(1-3): 169-190.
- Heiri, O., Lotter, A.F., Lemcke, G. (2001). "Loss on ignition as a method for estimating organic and carbonate content in sediments: reproducibility and comparability of results." Journal of Paleolimnology **25**: 101-110.
- Hemer, M., Fan, Y., Mori, N., Semedo, A., Wang, X. L. (2013). "Projected changes in wave climate from a multi-model ensemble." Nature Climate Change **3**: 471-476.
- Hirai, Y., Lap, N. V., Oanh, T. T. K. (2008). "Assessment of Impacts of Sea Level Rise on Tam Giang-Cau Hai Lagoon Area Based on a Geomorphological Survey Map." Regional Views **21**: 1-8.

IFRC (2001). World Disaster Report 2001: Focus on Recover. Geneva, IFRC: 1-248.

Imamura, F., To, D. V. (1997). "Flood and Typhoon Disasters in Viet Nam in the Half Century Since 1950." Natural Hazards **15**: 7-87.

Ingle, J. C. (1966). The movement of beach sand. New York, NY, Elsevier.

IPCC (2014). Summary for policymakers. In: . Climate Change 2014 - Impacts, Adaptation, and Vulnerability: Part A: Global and Sectoral Aspects Contribution of Working Group II to the Fifth Assessment Report of the Intergovernmental Panel on Climate Change. V. R. Barros, Field, C.B., Dokken, D.J., Mastrandrea, M.D., Mach, K.J., Bilir, T.E., Chatterjee, M., Ebi, K.L., Estrada, Y.O., Genova, R.C., Girma, B., Kissel, E.S., Levy, A.N., MacCracken, S., Mastrandrea, P.R., White, L.L. Cambridge, Cambridge University Press: 1-32.

Jankaew, K., Atwater, B.F., Sawai, Y., Choowong, M., Charoentitirat, T, Martin, E., Prendergast, A. (2008). "Medieval forewarning of the 2004 Indian Ocean Tsunami in Thailand." Nature **455**: 1228-1231.

Karlsson, J. M., Skelton, A., Sandén, M., Ioualalen, M., Kaewbanjak, N., Pophet, N., Asavanant, J., von Matern, A. (2009). "Reconstructions of the coastal impact of the 2004 Indian Ocean tsunami in the Khao Lak area, Thailand." Journal of Geophysical Research **14**: 1-14.

- Kendall, M. A., Paterson, G.L.J., Aryuthaka, C., Nimsantijaroen, S., Kongkaeow, W., Whanpetch, N. (2006). "Impact of the 2004 tsunami on intertidal sediment and rocky shore assemblages in Ranong and Phangnga provinces, Thailand." The Phuket Marine Biological Center Research Bulletin **67**: 63-75.
- Khan, N. S., Horton, B. P., McKee, K. L., Jerolmack, D., Falcini, F., Enache, M. D., Vane, C. H. (2013). "Tracking sedimentation from the historic A.D. 2011 Mississippi River flood in the deltaic wetlands of Louisiana." Geology **41**: 391-394.
- Kitamura, A., Ito, M., Ikuta, R., Ikeda, M. (2018). "Using molluscan assemblages from paleotsunami deposits to evaluate the influence of topography on the magnitude of late Holocene mega-tsunamis on Ishigaki Island, Japan." Progress in Earth and Planetary Science **5**(1): 1-10.
- Kleinen, J. (2002). "Historical perspectives on typhoons and tropical storms in the natural and socio-economic system of Nam Dinh (Vietnam)." Journal of Asian Earth Sciences **29**: 523-531.
- Kongsen, S., Phantuwongraj, S., Choowong, A., Chawchai, S., Chaiwongsaen, N., Fuengfu, S., Vu, D.T., Tuan, D.Q., Preusser, F. (2021). "Barrier Island Sediments Reveal Storm Surge and Fluvial Flood Events in the Past Centuries at Thua Thien Hue, Central Vietnam." Frontiers in Ecology and Evolution **9**: 1-22.
- Kongsen, S., Phantuwongraj, S., Choowong, M. (2021). "Distinguishing Late Holocene

storm deposit from shore-normal beach sediments from the Gulf of Thailand."

Frontiers in Earth Science **9**: 1-18.

Kontopoulos, N., Bouzos, N. (2011). "The sedimentology of the modern lagoons in the Western Paloponnesus." The Bulletin of the Geological Society of Greece **44**: 1-18.

Kortekaas, S., Dawson, A.G. (2007). "Distinguishing tsunami and storm deposits: An example from Martinhal, SW Portugal." Sedimentary Geology **200**: 208-221.

Krumbein, W. C., Pettijohn, F.J. (1983). Manual of sedimentary petrography. New York, NY, Appleton-Century-Crofts.

Kumar, V. S., Babu, V.R., Babu, M.T., Dhinakaran, G., Rajamanickam, G.V. (2008). "Assessment of Storm Surge Disaster Potential for the Andaman Islands." Journal of Coastal Research **24**: 171-177.

Lam, N. T., Stive, M. J. F., Verhagen, H. J., Wang, Z. B. (2007). Morphodynamics of Hue tidal inlets, Vietnam. Asian and Pacific Coast 2007. Nanjing, China.

Larson, M., Hung, N. M., Hanson, H., Sundstrom, A., Sodervall, E. (2014). Impacts of Typhoons on the Vietnamese Coastline: A Case Study of Hai Hau Beach and Ly Hoa Beach. Coastal Disasters and Climate Change in Vietnam: Engineering and Planning Perspectives. N. D. Thao, Takagi, H., Esteban, M. London, Elsevier.

Lay, T., Kanamori, H., Ammon, C.J., Nettles, M., Ward, S.N., Aster, R.C., Beck, S.L., Bilek, S.L., Brudzinski, M.R., Butler, R., DeShon, H.R., Ekstöröm, G., Satake, K., Sipkin, S. (2005). "The Great Sumatra-Andaman Earthquake of 26 December 2004." Science **308**: 1127-1133.

Leatherman, S. P., Williams, A. T. (1983). "Vertical sedimentation units in a barrier island washover fan." Earth Surface Processes and Landforms **8**: 141-150.

Lee, C.-S., Lin, Y.-L., Cheung, K. K. W. (2006). "Tropical Cyclone Formation in the South China Sea Associated with the Mei-Yu Front." Monthly Weather Review **134**: 2670-2687.

Liu, K. B. (2004). Paleotempestology: Geographic Solutions to Hurricane Hazard Assessment and Risk Prediction. WorldMinds: Geographical Perspectives on 100 Problems. D. Janelle, Warf, B., Hansen, K. Dordrecht, Springer.

Liu, K. B., Fearn, M. L. (1993). "Lake-sediment record of late Holocene hurricane activities from coastal Alabama." Geology **21**: 793-796.

Liu, K. B., Fearn, M. L. (2000). Holocene history of catastrophic hurricane landfalls along the Gulf of Mexico coast reconstructed from coastal lake and marsh sediments. Current stresses and potential vulnerabilities: implications of global change for the Gulf Coast Region of the United States. Z. H. Ning, Abdollahi, K. K. . Baton

Rouge, Gulf Coast Region Climate Change Council and Franklin press: 38-47.

Liu, K. B., Fearn, M. L. (2000). "Reconstruction of prehistoric landfall frequencies of catastrophic hurricanes in northwestern Florida from lake sediment records." Quaternary Research **54**: 238-245.

Lucrezi, S., Schlacher, T. A., Walker, S. (2009). "Monitoring human impacts on sandy shore ecosystems: a test of ghost crabs (*Ocypode* spp.) as biological indicators on an urban beach." Environmental Monitoring and Assessment **152**: 413-424.

Luijendijk, A., Hagenaars, G., Ranasinghe, R., Baarr, F., Donchyts, G., Aarninkhof, S. (2018). "The State of the World's Beaches." Scientific Reports **8**(1): 1-11.

Maanan, M., Rueff, H., Adouk, N., Zourarah, B., Rhinane, H. (2018). "Assess the human and environmental vulnerability for coastal hazard by using a multi-criteria decision analysis." Human and Ecological Risk Assessment **24**: 1642-1658.

Mason, C. C., Folk, R. L. (1958). "Differentiation of beach, dune, and aeolian flat environments by size analysis, Mustang Island, Texas." Journal of Sedimentary Petrology **28**: 211-226.

Masselink, G., Heteren, S. (2014). "Response of wave-dominated and mixed-energy barriers to storms." Marine Geology **352**: 321-347.

Mathers, S., Zalasiewicz, J. (1999). "Holocene Sedimentary Architecture of the Red River

Delta, Vietnam." Journal of Coastal Research **15**: 314-325.

Matsumoto, D., Sawai, Y., Yamada, M., Namegaya, Y., Shinozaki, T., Tekeda, D., Fujino, S., Tanigawa, K., Nakamura, A., Pilarczyk, J. E. (2016). "Erosion and sedimentation during the September 2015 flooding of the Kinu River, central Japan." Scientific Reports **6**: 1-10.

McBride, E. F. (1971). Mathematical treatment of size distribution data. Procedures in sedimentary petrology. R. F. Carver. New York, NY, Willey Interscience: 109-127.

McGranahan, G., Balk, D., Anderson, B. (2007). "The rising tide: assessing the risks of climate change and human settlements in low elevation coastal zones." Environment and Urbanization **19**: 17-37.

McGregor, G. R. (1995). "The tropical cyclone hazard over the South China Sea 1970-1989: Annual spatial and temporal characteristics." Applied Geography **15**(1): 35-52.

Mcphaden, M. J., Foltz, G.R., Lee, T., Murty, V.S.N., Ravichandran, M., Veechi, G.A., Vialard, J., Wiggert, J.D., Yu, L. (2009). Ocean-atmosphere interactions during cyclone Nargis. Eos, Transactions American Geophysical Union. **90**: 53-60.

Monecke, A., Finger, W., Klarer, D., Kongko, W., McAdoo, B.G., Moore, A.L., Sudrajat, S.U. (2008). "A 1,000-year sediment record of tsunami recurrence in northern

Sumatra." Nature **455**: 1232-1234.

Morton, R. A., Gelfenbaum, G., Jaffe, E.B. (2007). "Physical criteria for distinguishing sandy tsunami and storm deposits using modern examples." Sedimentary Geology **200**(3-4): 184-207.

Morton, R. A., Sallenger, A. H. Jr. (2003). "Morphological impacts of extreme storms on Sandy Beaches and Barriers." Journal of Coastal Research **19**: 560-576.

Murray, A. S., Wintle, A.G. (2000). "Dating quartz using an improved single-aliquot regenerative-dose (SAR) protocol." Radiation Measurements **32**(1): 57-73.

Nanayama, F., Shigeno, K., Satake, K., Shimokawa, K., Koitabashi, S., Miyasaka, S., Ishii, M. (2000). "Sedimentary differences between the 1993 Hokkaido-nansei-oki tsunami and the 1959 Miyakojima typhoon at Taisei, southwestern Hokkaido, northern Japan." Sedimentary Geology **135**(1-4): 255-264.

Nerem, R. S., Beckley, B. D., Fasullo, J. T., Hamlington, B. D., Masters, D., Mitchum, G. T. (2018). "Climate-change-driven accelerated sea-level rise detected in the altimeter era." Proceedings of the National Academy of Sciences **115**: 2022-2025.

Nga, P. H., Takara, K., Van, N. C. (2018). "Integrated approach to analyze the total flood risk for agriculture: The significance of intangible damages – A case study in

Central Vietnam." International Journal of Disaster Risk Reduction **31**: 862-872.

Nghiem, T. L., Stive, M. J. F., Verhagen, H. J., Wang, Z. B. (2007). Morphodynamics of Hue tidal inlets, Vietnam. Proceedings of the Fourth International Conference on Asian and Pacific Coasts, Nanjing, China Ocean Press.

Nguyen, H. N., Duong, Q. N. (2015). Situation of erosion, accretion in Thua Thien Hue province and countermeasure. Vietnam-Japan Workshop on Estuaries, Coasts and Rivers 2015. Hoi An: 2-7.

Nguyen, P. H., Bui, Q. C., Nguyen, X. D. (2012). "Investigation of earthquake tsunami source, capable of affecting Vietnamese coast." Natural Hazards **64**: 311-327.

Nott, J. F. (2015). Chapter 5 – Palaeostorm Surges and inundations. Coastal and Marine Hazard, Risk, and Disaster. J. F. Shroder, Ellis, J. T., Sherman, D. J. Amsterdam, Elsevier: 129-152.

Otvos, E. G. (2000). "Beach ridges – definitions and significance." Geomorphology **32**: 83-108.

Owens, P. N., Batalla, R. J., Collins, A. J., Gomez, B., Hicks, D. M., Horowitz, A. J., Kondolf, G. M., Marden, M., Page, M. J., Peacock, D. H., Petticrew, E. L., Salomons, W., Trustrum, N. A. (2005). "Fine-grained sediment in river systems: environmental significance and management issues." River Research and Applications **21**: 693-

717.

Pentakota, S., Vivek, S., Rao, K.S. (2018). "Role of Andaman Sea in the intensification of cyclones over Bay of Bengal." Natural Hazards **91**: 1113-1125.

Phantuwongraj, S., Choowong, M. (2012). "Tsunami versus storm deposits from Thailand." Natural Hazards **63**: 31-50.

Phantuwongraj, S., Choowong, M., Chutakositkanon, V. (2008). Possible storm deposits from Surat Thani and Nakhon Si Thammarat provinces, the southern peninsular Thailand. Proceedings of the international symposium on geoscience resources and environments of Asian terranes, Bangkok, Thailand.

Phantuwongraj, S., Choowong, M., Nanayama, F., Hisada, K-I., Charusiri, P., Chutakositkanon, V., Pailoplee, S., Chabangbon, A. (2013). "Coastal geomorphic conditions and styles of storm surge washover deposits from Southern Thailand." Geomorphology **192**: 43-58.

Powers, W. C. (1953). "A new roundness scale for sedimentary particle." Journal of Sedimentary Petrology **23**(2): 117-119.

Prendergast, A. L., Cupper, M.L., Jankaew, K., Sawai, Y. (2012). "Indian Ocean tsunami recurrence from optical dating of tsunami sand sheets in Thailand." Marine Geology **295-298**: 20-27.

- Prescott, J. R., Hutton, J. T. (1994). "Cosmic ray distributions to dose rates for luminescence and ESR dating: large depths and long-term variations." Radiation Measurements **23**: 497-500.
- Rogozhin, E. A. (2016). "Traces of Ancient Tsunamis in the Coastal Parts of South China Sea." Izvestiya, Atmospheric and Oceanic Physics **52**: 683-696.
- Rosenthal, Y., Holbourn, A.E., Kulhanek, D.K., Aiello, I.W., Babila, T.L., Bayon, G., Beaufort, L., Bova, S.C., Chun, J.-H., Dang, H., Drury, A.J., Dunkley Jones, T., Eichler, P.P.B., Fernando, A.G.S., Gibson, K., Hatfield, R.G., Johnson, D.L., Kumagai, Y., Li, T., Linsley, B.K., Meinicke, N., Mountain, G.S., Opdyke, B.N., Pearson, P.N., Poole, C.R., Ravelo, A.C., Sagawa, T., Schmitt, A., Wurtzel, J.B., Xu, J., Yamamoto, M. and Zhang, Y.G. (2018). Expedition 363 methods. Proceedings of the International Ocean Discovery Program 363 (College Station, TX).
- Rothwell, R. G. (1989). Minerals and Mineraloids in Marine Sediments: An Optical Identification Guide. London, Elsevier.
- Rubin, D. M., Nelson, J. M., Topping, D. J. (1998). "Relation of inversely graded deposits to suspended-sediment grain-size evolution during the 1996 flood experiment in Grand Canyon." Geology **26**: 99-102.
- Sakuna-Schwartz, D., Feldens, P., Schwarzer, K., Khokiattiwong, S., Stattegger, K. (2015). "Internal structure of event layers preserved on the Andaman Sea continental

shelf, Thailand: tsunami vs. storm and flash-flood deposits." Natural Hazards and Earth System Sciences **15**: 1181-1189.

Sakuna, D., W. Szczuciński, P. Feldens, K. Schwarzer., S. Khokiattiwong. (2012). "Sedimentary deposits left by the 2004 Indian Ocean tsunami on the inner continental shelf offshore of Khao Lak, Andaman Sea (Thailand)." Earth, Planets and Space **64**: 931-943.

Sallenger, J. A. H. (2000). "Strom impact scale for barrier island." Journal of Coastal Research **16**: 890-895.

Satake, K., Aung, T.T., Sawai, Y., Okamura, Y., Win, K.S., Swe, W., Swe, C., Swe, T.L., Tun, S.T., Soe, M.M., Oo, T.Z., Zaw, S.H. (2006). "Tsunami height and damage along the Myanmar coast from the December 2004 Sumatra-Andaman earthquake." Earth, Planets and Space **58**: 243-252.

Schweyer, A. V. (2018). Exploitation of a historical geographic information system (GIS) in the Thua Thiên-Hue and Quang Tri provinces, Central Vietnam. Selected Papers from the Second SEAMEO SPAFA International Conference on Southeast Asian Archaeology. N. H. Tan. Bangkok, SEAMEO SPAFA: 227-2352.

Sedgwick, P. E., Davis, R. A. (2003). "Stratigraphy of washover deposits in Florida: implications for recognition in the stratigraphic record." Marine Geology **200**: 31-

48.

Snedden, J. W., Tillman, R. W., Culver, S. J. (2011). "Genesis and Evolution of a Mid-Shelf, Storm-Built Sand Ridge, New Jersey Continental Shelf, U.S.A." Journal of Sedimentary Research **81**: 534-552.

Somsa-Ard, N., Pailoplee, S. (2013). "Seismic Hazard Analysis for Myanmar." Journal of Earthquake and Tsunami **7**(4): 1-14.

Stein, S., Okal, E.A. (2005). "Speed and size of the Sumatra earthquake." Nature **434**: 581-582.

Sudharam, Y., Murthy, T.V.R., Somayajulu, Y.K. (2006). "Estimation of tropical cyclone heat potential in the Bay of Bengal and its role in the genesis and intensification of storms." Indian Journal of Geo-Marine Sciences **35**(2): 135-138.

Suppasri, A., Muhari, A., Ranasinghe, P., Mas, E., Shuto, N, Imamura, F., Koshimura, S. (2012). "Damage and reconstruction after the 2004 Indian Ocean tsunami and the 2011 Great East Japan tsunami." Journal of Natural Disaster Science **34**(1): 19-39.

Tamura, T., Nicholas, W. A., Oliver, T. S. N., Brooke, B. P. (2017). "Coarse-sand beach ridges at Cowley Beach, north-eastern Australia: Their formative processes and potential as records of tropical cyclone history." Sedimentology **65**: 721-744.

- Tana, L. (2019). The Changing Landscape of the Former Linyi in the Provinces of Quang Tri and Thua Thiên-Hue. NSC Working Paper. Singapore, ISEAS – Yusof Ishak Institute.
- Thuy, N. B., Kim, S., Chien, D. D., Dang, V. H., Hole, L. R. (2017). "Assessment of storm surge along the coast of central Vietnam." Journal of Coastal Research **33**: 518-530.
- Trieu, C. D., Dung, L. V., Bach, M. X., Hung, P. N., Trong, C. D., Tuan, T. A., Quang, P. T., Hien, P. T., Cuong, N. D. (2017). "Some preliminary results of paleo-tsunami study in the coastal region of the Nghe An province, Vietnam." **17**: 108-114.
- Tuttle, M. P., Ruffman, A., Anderson, T., Jeter, H. (2004). "Distinguishing tsunami and storm deposits in eastern North America: The 1929 Grand Banks tsunami versus the 1991 Halloween storm." Seismological Research Letters **75**(1): 117-131.
- Vousdoukas, M. I., Ranasinghe, R., Mentaschi, L., Plomaritis, T. A., Athanasiou, P., Lujendijk, A., Feyen, L. (2020). "Sandy coastlines under threat of erosion." Nature Climate Change **10**: 260-263.
- Vu, T. T., Ranzi, R. (2017). "Flood risk assessment and coping capacity of floods in central Vietnam." Journal of Hydro-environment Research **14**: 44-60.
- Wang, G., Su, J., Ding, Y., Chen, D. (2007). "Tropical cyclone genesis over the south China

sea." Journal of Marine Systems **68**: 318-326.

Webster, P. J. (2008). "Myanmar's deadly daffodil." Nature Geoscience **1**(8): 488-490.

Wentworth, C. K. (1922). "A scale of grade and class terms for clastic sediments." The Journal of Geology **30**: 377-392.

Williams, H., Hoang, L. V., Elliott, P., Nguyen, H. H., Manh, H. (2019). "A Tentative Record of Mid-Holocene Sea-Level Highstand and Barrier Overwash from Cam River Mount, Vietnam." Journal of Coastal Research **35**: 852-860.

Williams, H. F. L. (2010). "Storm surge deposition by Hurricane Ike on the McFadden National Wildlife Refuge, Texas: implication for paleotempestology studies." Journal of Foraminiferal Research **40**: 210-219.

Williams, H. F. L. (2011). "Stratigraphic record of Hurricanes Audrey, Rita and Ike in the Chenier Plain of southwest Louisiana." Journal of Coastal Research **64**: 1921-1926.

Williams, H. F. L. (2013). "600-year sedimentary archive of hurricane strikes in a prograding beach ridge plain, southwestern Louisiana." Marine Geology **336**: 170-183.

Williams, H. F. L., Choowong, M., Phantuongraj, S., Surakiatchai, P., Thongkhao, T., Kongsen, S., Simon, E. (2016). "Geologic records of Holocene typhoon strikes on

the Gulf of Thailand coast." Marine Geology **372**: 66-78.

Yamada, M., Fujino, S., Goff, J., Chague-Goff, C. (2016). "Large-scale erosion and overbank deposition caused by the July 2013 flood of the Abu River, Yamaguchi City, Japan." Island Arc **25**: 386-399.

Yamashita, S., Nakajo, T., Nishida, N., Naruse, H. (2011). "Characteristics and depositional pattern of fluvial-flooding event at 2009 in the Kushida River Delta, Ise bay, central Japan." Journal of the Sedimentological Society of Japan **70**(81-92).

Yao, Q., Liu, K. B., Williams, H., Joshi, S., Bianchette, T. A., Ryu, J., Dietz, M. (2019). "Hurricane Harvey Storm Sedimentation in the San Bernard National Wildlife Refuge, Texas: Fluvial Versus Storm Surge Deposition." Estuaries and Coasts **43**(5): 971-983.

Yoshida, H., Yamamoto, K., Minami, M., Katsuta, N., Sin-ichi, S., Metcalfe, R. (2018). "Generalized conditions of spherical carbonate concretion formation around decaying organic matter in early diagenesis." Scientific Reports **8**: 1-10.

Zavala, C., Pan, S. (2018). "Hyperpycnal flows and hyperpycnites: Origin and distinctive characteristics." Lithologic Reservoirs **30**: 1-27.

Zhu, C., Zheng, C., Ma, C., Sun, Z., Zhu, G., Wang, H., Gao, H., Wang, P., Huang, R. (2005). "Identifying paleoflood deposits archived in Zhongba Site, the Three Gorges

reservoir region of the Yangtze River, China." Chinese Science Bulletin **50**: 2493-2504.





จุฬาลงกรณ์มหาวิทยาลัย
CHULALONGKORN UNIVERSITY

VITA

NAME Stapana Kongsen

DATE OF BIRTH 03 May 1991

PLACE OF BIRTH Sattahip, Chonburi, Thailand

INSTITUTIONS ATTENDED Singsamut School (High school)
Burapha University (B.Sc)
Chulalongkorn University (M.Sc)

HOME ADDRESS 43/26 M.6 Sattahip, Sattahip, Chonburi, Thailand 20180

PUBLICATION Harry William, Montri Choowong, Sumet Phantuwongraj, Peerasit Surakietchai, Thanakrit Thongkhao, Stapana Kongsen, Eric Simon. 2016. Geologic records of Holocene typhoon strikes on the Gulf of Thailand coast. *Marine Geology*, Vol. 372, 66-78.

Peerasit Surakietchai, Montri Choowong, Punya Charusiri, Thasinee Charoentitirat, Sakonwan Chawchai, Santi Pailoplee, Akkaneewut Chabangbon, Sumet Phantuwongraj, Vichai Chutakositkanon, Stapana Kongsen, Parisa Nimnate, Raphael Bissen. 2018. Paleographic Reconstruction and History of the Sea Level Change at Sam Roi Yot National Park, Gulf of Thailand. *Tropical Natural History*, Vol. 18(2), 112-134.

Stapana Kongsen, Sumet Phantuwongraj, Montri Choowong. 2021. Characteristics of ancient storm from southern peninsular, Gulf of Thailand: Interpretation based on sedimentary and sedimentological evidences and OSL-based chronology. *Frontier in Earth Science*, Vol. 9, 1-18

Stapana Kongsen, Sumet Phantuwongraj, Montri Choowong, Sakonvan Chawchai, Nikhom Chaiwongsaen, Supawich Fuengfu, Doan Thi Anh Vu, Dinh Quoc Tuan and Frank Preusser. 2021. Barrier Island Sediments Reveal Storm Surge and Fluvial Flood Events in the Past Centuries at Thua Thien Hue, Central Vietnam. *Frontier in Ecology and Evolution*, Vol. 9, 1-22.

Stapana Kongsen, Sumet Phantuwongraj, Montri Choowong, Sakonvan Chawchai, Sirawat Udomsak, Chanista Chansom, Chanakan Ketthong, Peerasit Surakietchai, Johannes M. Miodic and Frank Preusser. 2022. Multi-proxy approach to identify the origin of high energy coastal deposits from Laem Son National Park, Andaman Sea of Thailand. *Quaternary International*, Vol. 625, 82-95.

The 90th Anniversary Ratchadapisek Somphot Endowment Fund of Chulalongkorn University

AWARD RECEIVED

จุฬาลงกรณ์มหาวิทยาลัย
CHULALONGKORN UNIVERSITY
 The Royal Golden Jubilee Ph.D. program (Grant No. PHD/0198/2560) (3.G.CU/60/B.1)